Cartography M.Sc.

Master thesis

Mapping Vegetation Dynamics from Remote Sensing Time Series

Edwin Hilary Amegashie

2020

Mapping Vegetation Dynamics from Remote Sensing Time Series

submitted for the academic degree of Master of Science (M.Sc.)
conducted at the Department of Civil, Geo and Environmental Engineering
Technical University of Munich

Author:	Edwin Hilary Amegashie
Study course:	Cartography M.Sc.
Supervisor:	Dr. Ekaterina Chuprikova (TUM)
Reviewer:	Dr.rer.nat Nikolas Prechtel (TUD)

Chair of the Thesis
Assessment Board: Prof. Dr. Liqiu Meng

Date of submission: 31.03.2020

Statement of Authorship

Herewith I declare that I am the sole author of the submitted Master's thesis entitled:

"Mapping Vegetation Dynamics from Remote Sensing Time Series"

I have fully referenced the ideas and work of others, whether published or unpublished. Literal or analogous citations are clearly marked as such.

Munich, 31.03.2020 Edwin Hilary Amegashie

ACKNOWLEDGEMENT

To God be the Glory! Great things He has done! I thank God Almighty for giving me life, wisdom, great health and strength to do this work. I would like to thank my supervisor Dr. Ekaterina Chuprikova for her selfless and invaluable support, constructive criticisms, motivation and constant encouragement which have greatly shaped the quality of this work. I would also like to extend my sincere appreciation to my external reviewer, Dr. Nikolas Prechtel for his immense contributions. I would like to extend my heartfelt gratitude to the programme coordinator, Miss Juliane Cron for her selfless support.

With a cheerful heart, I dedicate this piece of work first to God Almighty, my supervisors, my parents *Mr. Richard Besah Amegashie* (of blessed memory) and *Madam Vivian Abla Gokah*, my brother Mr. DPK Amegashie (**UG**), my sisters *Faustina Amegashie, Valerie Doe and Henrietta Agboado*, my uncle WO1 (Rtd) *T.K Amegashie* (of blessed memory), my siblings *Edith Amelia, Bernice, Nicholas, Oliver* and my cousins *Linus, Selasi, Maxwell, Gilbert, Edem*, my niece *Akorfa, Rev. Fr. Prosper Mensah*, and my friend *Julius Nyonyo* for their immense support and motivation throughout my studies. A special appreciation goes to Miss Sharon Selasie Ametorwo for the constant encouragement and motivation. I thank all friends and the entire 2017 cohort of ERASMUS Mundus Cartography programme especially *Mr. Mohammed Elsayed* and *Miss Elizabeth Sarah Palmer* for their support, thank you all for your tolerance during my studies! Akpe na Mawu!!

LIST OF ABBREVIATIONS

AVHRR- Advanced Very High Resolution

CHIRPS- Climate Hazards Group Infrared Precipitation

DVI- Difference Vegetation Index

EVI- Enhanced Vegetation Index

ET- Evapotranspiration

FAPAR- Fraction of Absorbed Photosynthetically Active Radiation

FVC – Fraction Vegetation cover

GARI- Green Atmospherically Resistant Index

GEE- Google Earth Engine

GHGs- Greenhouse Gases

GPR- Green Precipitation Index

IPCC- Intergovernmental Panel on Climate Change

LULC- Land Use Land Cover

LAI- Leaf Area Index

MODIS- Moderate Resolution Imaging Spectroradiometer

NOAA- National Oceanic and Atmospheric Administration

NDVI – Normalized Difference Vegetation Index

NIR- Near Infrared

NPP- Net Primary Productivity

PCC- Pearson Correlation Coefficients

PET- Potential Evapotranspiration

PVI- Perpendicular Vegetation Index

RVI- Ration Vegetation Index

SAVI- Soil Adjusted Vegetation Index

WDVI- Wide Dynamic Vegetation Index

Abstract

Extreme climate variability has become a worldwide phenomenon. While developed countries put preventive measures in place to deal with the impact of climate change, most of the developing countries in Sub- Saharan Africa bear the full brunt of the changing environment. In Arid and Semi-Arid areas, where water scarcity limits most activities such as agriculture, livestock, and household chores, the majority of the citizens' lives depend on agriculture for livelihood. Thus, it causes substantial stress for the local communities. This thesis, therefore, focuses on mapping vegetation dynamics from remote sensing time series data in the Republic of Sudan, in order to analyse and visualize the past events, e.g., drought and their impact on vegetation of the selected case studies from different dimensions. Disaggregating the years into seasons, with a focus on 2015 and 2017 rainy seasons, seasonal integral results computed by the Pearson correlation coefficients showed a strong positive correlation between NDVI, soil moisture and evapotranspiration. Mean annual NDVI graphs show a general increasing trend in vegetation. For the long term, breakpoints and seasonal trajectories, low standard deviations were recorded across the case studies. A cross correlation graph to determine the lag in response between NDVI, soil moisture and evapotranspiration on monthly basis show no significant lags. Vegetation dynamics have been visualized using "small multiple" static maps in order to depict trends, changes and dynamics of vegetation change. The maps show the spatio-temporal dynamics of vegetation, where high NDVI values were generally recorded from July to September.

Keywords: mapping, vegetation dynamics, NDVI, soil moisture, evapotranspiration, mean, correlation, standard deviation, lag

Table of Content

1. Introduction 13
   1.1. Motivation 14
   1.2. Problem statement 15
   1.3. Research objectives and questions 16
   1.4. Research scope and proposed solution 17
   1.5. Research limitations 19
2. Foundations and Related work 21
   2.1. Climate variables 21
   2.2. Remote sensing for vegetation studies 22
   2.3. Vegetation indices 23
   2.4. Controlling factors and NDVI 26
3. Data and Case Study 30
   3.1. Study Area 30
      3.1.1. Hot desert climate (BWh) 31
      3.1.2. Hot semi-arid climate (BSh) 32
      3.1.3. Tropical savannah climate (Aw) 33
   3.2. Datasets 34
      3.2.1. MODIS NDVI (Terra or Aqua Image Collections) 34
      3.2.2. Evapotranspiration 36
      3.2.3. Soil Moisture 37
4. Methodology 39
   4.1. Data Acquisition 39
   4.2. Pre- processing 40
   4.3. Data modelling and implementation 44
5. Visualization vegetation dynamics 50
   5.1. Visualizing space and time 51

5.2. Visualizing change in space and time 51
5.3. Prototypes for visualizing vegetation dynamics 58
5.3.1. Trend 59
5.3.2. Change 61
5.3.3. Dynamics 61
6. Results and Discussion 63
6.1. Hot desert climate (BWh) 63
6.1.1. BWhI 63
6.1.2. BWhII 69
6.1.3. BWhIII 75
6.2. Hot semi-arid climate (BSh) 80
6.2.1. BShI 80
6.2.2. BShII 85
6.2.3. BShIII 91
6.3. Tropical savannah climate (Aw) 96
6.3.1. AwI 96
6.3.2. AwII 100
6.3.3. AwIII 104
7. Conclusion and Outlook 110

List of Figures

Figure 1: Google Earth Engine Interface 19
Figure 2: Climate Map of Sudan and Case Studies 31
Figure 3: An Example of Cloudy MODIS Image 35
Figure 4: Schematic depiction of data acquisition in GEE 40
Figure 5: Schematic depiction of pre-processing 42
Figure 6: Linear trending of NDVI 43
Figure 7: Detrended NDVI time series 43
Figure 8: Harmonic model showing actual and fitted NDVI values 46
Figure 9: Schematic depiction of the implementation process 49
Figure 10: A schematic depiction of the proposed state of the art visualization 57
Figure 11: Line chart showing NDVI values 60
Figure 12: Area chart for visualizing trend 60
Figure 13: An example of Isopleth map for visualizing change in vegetation 61
Figure 14: Screenshot of animation for depicting vegetation dynamics 62
Figure 15: Mean annual NDVI values and linear regression line at BWhI 65
Figure 16: Cross correlation between monthly mean NDVI and Soil moisture 66
Figure 17: Cross correlation between monthly mean NDVI and evapotranspiration 67
Figure 18: Yearly static maps of vegetation dynamics in BWhI 68
Figure 19: Mean annual NDVI values and linear regression line at BWhII 71
Figure 20: Cross correlation between monthly mean NDVI and soil moisture at BWhII 72
Figure 21: Cross correlation between monthly mean NDVI and evapotranspiration at BWhII 73
Figure 22: Monthly static maps of vegetation dynamics at BWhII 74
Figure 23: Mean annual NDVI and linear regression at BWhIII 76
Figure 24: Cross correlation between mean monthly NDVI and soil moisture at BWhIII 77
Figure 25: Cross correlation between monthly mean NDVI and evapotranspiration at BWhIII 78
Figure 26: Yearly static maps of vegetation dynamics in BWhIII 79
Figure 27: Mean annual NDVI and linear regression at BShI 81
Figure 28: Cross correlation between monthly mean NDVI and soil moisture at BShI 82
Figure 29: Cross correlation between monthly mean NDVI and evapotranspiration at BShI 82
Figure 30: Monthly vegetation dynamics at BShI, 2015 (May - October) 84
Figure 31: Monthly vegetation dynamics at BShI, 2017 (May - October) 85
Figure 32: Mean annual NDVI and linear regression at BShII 87
Figure 33: Cross correlation between monthly mean NDVI and soil moisture in BShII 88
Figure 34: Cross correlation between mean monthly NDVI and evapotranspiration 88

Figure 35: Yearly static maps of vegetation dynamics in BShII 90
Figure 36: Mean Annual NDVI and linear regression at BShII 92
Figure 37: Cross correlation between mean monthly NDVI and soil moisture at BShIII 93
Figure 38: Cross correlation between mean monthly NDVI and evapotranspiration at BShIII 93
Figure 39: Monthly vegetation dynamics at BShIII, 2015 (May-October) 94
Figure 40: Monthly vegetation dynamics at BShIII, 2017 (May-October) 95
Figure 41: Mean annual NDVI and linear regression at AwI 97
Figure 42: Cross correlation between mean monthly NDVI and soil moisture at AwI 98
Figure 43: Cross correlation between mean monthly NDVI and evapotranspiration at AwI 98
Figure 44: Yearly static maps of vegetation dynamics in AwI 99
Figure 45: Mean annual NDVI and linear regression at AwII 101
Figure 46: Cross correlation between mean monthly NDVI and soil moisture at AwII 102
Figure 47: Cross correlation between mean monthly NDVI and evapotranspiration at AwII 102
Figure 48: Monthly vegetation dynamics at AwII, 2015 (May-October) 103
Figure 49: Monthly vegetation dynamics at AwII, 2017 (May-October) 104
Figure 50: Mean annual NDVI and linear regression at AwIII 105
Figure 51: Cross correlation between mean monthly NDVI and soil moisture at AwIII 107
Figure 52: Cross correlation between mean monthly NDVI and evapotranspiration at AwIII 108
Figure 53: Yearly static maps of vegetation dynamics in AwIII 109

List of Tables

Table 1: Layers of MODIS Vegetation Index 36
Table 2: Layers MODIS Evapotranspiration 37
Table 3: Layers of Root zone soil moisture (*estimated) 37
Table 4: Layers of NASA-USDA soil moisture (*estimated) 38
Table 5: Statistical values for BWhI 65
Table 6: Statistical values at BWhII 71
Table 7: Statistical values at BWhIII 77
Table 8: Statistical values at BShI 81
Table 9: Statistical values at BShII 87
Table 10: Statistical values at BShIII 92
Table 11: Statistical values at AwI 97
Table 12: Statistical values at AwII 101
Table 13: Statistical values at AwIII 106

1. Introduction

In recent years, remote sensing datasets have proved to be efficient and indispensable in a range of applications. Distinguishing these diverse fields of applications have been demonstrated in several studies such as land degradation monitoring (Abdel-Kader, 2019), assessing the impact of droughts (West, Quinn, & Horswell, 2019), forest inventory (Hou et al., 2019; Latifi & Heurich, 2019), wildfire monitoring (Lippitt, Stow, & Riggan, 2016; Szpakowski & Jensen, 2019), ecosystems services assessment and environmental impact assessments (Dawson, Cutler, & Brown, 2016; Vargas, Willemen, & Hein, 2019), flood hazard and risk assessment(Rahman & Di, 2017), understanding the impact of climate change on agriculture (Siddig, Stepanyan, Wiebelt, Grethe, & Zhu, 2020), land use and land cover changes(Raziq, Xu, & Li, 2016; Hua, 2017), and of particular interest, mapping vegetation dynamics (Mohammadi, Costelloe, & Ryu, 2017; Reddy & Prasad, 2018) and exploring its trends, spatial and temporal dimensions.

Monitoring vegetation dynamics is crucial as it plays a significant role in regulating water-energy balance and sequestering carbon dioxide, one of the main GHGs (greenhouse gases) accelerating climate change. Invariably, the dynamics of local vegetation phenology is a significant indicator of environmental change (Reed et al., 1994; Fensholt and Proud, 2012; Begue et al., 2014). In Sub-Saharan Africa, vegetation loss is on the rise, probably due to excessive deforestation (Brandt et al., 2017). Dominant plant species (terrestrial ecosystems) are on the brink of extinction, which will further exacerbate the impact of climate change. This adverse effect becomes severe in water-limited climatic environments such as arid and semi-arid regions. The Republic of Sudan, amidst other socio-economic challenges, is losing its vegetative cover at an alarming rate partly due to the increasing population with a ripple effect of high demand for land use well as the intrinsic impacts of climate change. It is, therefore, relevant to monitor vegetation dynamics to take proactive steps in reducing further vegetation loss in Sudan. Against this backdrop, using remote sensing datasets to map vegetation

dynamics is crucial since it is cost and time effective, readily available compared to in situ observations and other national datasets that are difficult to get in developing countries for research.

1.1. Motivation

Climate change is a global phenomenon with its attendant consequences. This change is characterized by increasing heat waves, irregular rainfall patterns, rising sea levels, drought, desertification, floods, and diminishing flora and fauna in various ecosystems. Extreme short-term weather events, intra-seasonal and inter-decadal variability occur against a backdrop of longer-term climatic changes (Easterling et al., 2000), to which systems display complex responses (Schurman et al., 2018; Von Buttlar et al., 2018). This has created imbalances in various ecosystems at global, regional, national, and local levels.

It is, therefore, of high relevance to foster the knowledge on how vegetation types respond to different climatic conditions such as precipitation, evapotranspiration and temperature over time. Similarly, the anthropogenic infractions on the environment are increasing at an alarming rate. These infractions are mainly caused by changes in land use patterns driven by population growth and resource exploitation, as well as the destruction of vegetation cover, which in effect influences climatic conditions. Vegetation plays an essential role in maintaining natural ecosystems by which plants act as Carbon sinks in sequestering Carbon dioxide from the atmosphere. However, plant growth depends on climate variables such as soil moisture, evapotranspiration, precipitation, temperature, as well as land use changes to some extent. In this regard, mapping vegetation dynamics in this era of global climate change needs to be addressed, particularly in regions where vegetation loss is on the increase. The issue is usually exacerbated when in developing countries, research regarding vegetation loss is minimal. To this end, soil moisture, evapotranspiration, precipitation and its interrelationships with vegetation in regions with variable climatic conditions have taken a centre stage in developmental discussions. This is because, in these regions, limitations to water have negative

impacts on plants growth; an important indicator of rapid environmental change. This has necessitated the study regarding vegetation changes in the Republic of Sudan, using remote sensing time series.

1.2. Problem statement

Our environment is continuously changing. Global climate change resulting in droughts, irregular rainfall patterns, and increasing temperatures across major ecosystems have increased over the years. Plant communities have been adversely affected due to their sensitivity to environmental elements (Yue et al., 2010) "Vegetation cover change is gaining popularity as a key determinant of global environmental change" (Rees, Condit, Crawley, Pacala, & Tilman, 2001); hence, vegetation dynamics have been identified to be of primary importance in the global change of terrestrial ecosystems (Eugster et al., 2000; Suzuki, Masuda, & G. Dye, 2007). Several studies have been conducted regarding the nexus between climate variables and vegetation changes. Yan et al., (2017), for example, studied the relationship between the dynamic change of vegetation cover and driving forces in Nanxiong Basin, China. W. Zhao et al., (2017), also conducted a study on climatic factors driving vegetation declines in the 2005 and 2010 Amazon droughts. Other researchers looked at how vegetation responds to climate with a certain time lag (Huiling, Xiaobing, Yun, Lingmei, & Zhongfei, 2010; Saatchi et al., 2013; D. Wu et al., 2015; Assal, Anderson, & Sibold, 2016). However, it suffices to note that these studies have been conducted in geographical units that receive a significant amount of rainfall. As a result, little has been done in semi-arid and arid regions where rainfall amounts are minimal and temperatures are excessively high, thereby presenting adverse conditions to plants' life exacerbated by anthropogenic infractions. Putting the study area, the Republic of Sudan, into context, the literature regarding the quantitative relationship between vegetation and meteorological conditions is sparse. Also, most of the studies conducted relied on in-situ observations although Remote sensing data holds many prospects for mapping vegetation dynamics with a high degree of accuracy (Weng, 2001; Rimal, 2011; Olokeogun, Iyiola, &

Iyiola, 2014; Appiah, Schröder, Forkuo, & Bugri, 2015; Raziq et al., 2016). It is against this background that the study seeks to address this yawning gap in the Republic of Sudan, which presents a unified and typical example with different climate zones where water scarcity limits vegetation growth, agriculture, livestock, and household chores by using remote sensing data available in a cloud computing environment. In this context, the study seeks to map vegetation dynamics against its controlling factors; soil moisture, evapotranspiration, and precipitation.

1.3. Research objectives and questions

This sub-section elucidates the objectives underlying the study. It does so by identifying and disaggregating the main goal into specific objectives as well as their corresponding research questions. The main aim of the thesis is to map vegetation dynamics from remote sensing time series by leveraging on cartographic principles to visualize the spatio-temporal changes in vegetation over a given area. Vegetation dynamics will be studied not on a plant level but in terms of the vitality dynamics of larger plant associations as far as observable by optical medium resolution space sensors. The time range covered will roughly be from the year 2005 in cognizance with other controlling factors for about 10 to 15 years. The thesis will specifically address the following objectives;

1. To determine and analyse the quantitative changes in vegetation over time against controlling factors (soil-moisture, evapotranspiration, and precipitation) based on the representative case studies.
2. To map vegetation dynamics based on the spatio-temporal extent of various representative case studies as observed from remote sensing time series.
3. To identify and analyse the trends and patterns of vegetation dynamics based on the representative case studies.

The corresponding research questions following the research objectives that will be addressed in this thesis are as follows;

1. How can controlling factors influence vegetation changes over time?
2. How can vegetation dynamics be cartographically represented within the spatio-temporal extent of various representative case studies?
3. How different are the trends and patterns of vegetation dynamics within the various study areas (representative case studies)?

1.4. Research scope and proposed solution

The focus of the research is geographically in the Republic of Sudan, a region with varied climatic conditions. However, due to the large expanse of the country, there will be spatial aggregations resulting in clusters of areas that will serve as a reference point for exploring the questions of spatial relations. The study will focus on the relationship between meteorological conditions and vegetation changes over time-based on remote sensing data. It is worthwhile noting that these spatial clusters will help to do an informed analysis. A clear distinction regarding irrigated and rain-fed areas will be made to understand their relationship to climatic factors. To analyse the strength of correlation between soil moisture, evapotranspiration, precipitation, and vegetation, suitable mathematical approaches will be used; mean, standard deviation and Pearson correlation coefficient. Besides, this thesis will provide a prototypical series of maps and graphics that represent the vegetation dynamics over the area of interest. As stated earlier, there is a general deficiency in the usage of Remote sensing data coupled with cloud computing in advancing vegetation research in the Republic of Sudan. "Cloud-computing resources enable efficient image processing on otherwise computationally intensive tasks, such as with the classification of large volumes of image data, and particularly when using advanced machine learning algorithm. Google Earth Engine, a cloud-based platform for geospatial analysis, aptly addresses that need" (Gorelick et al., 2017).

The proposed solution utilizes the Google Earth Engine (GEE) platform for conducting studies on vegetation dynamics, as this platform allows researchers to analyse all the datasets needed. All a user required to access the portal is a Google user account and an active internet connection. After, the JavaScript code editor can be accessed, which in effect enhances the direct data retrieval permitting users to test and develop algorithm and preview results in real-time interactively. Ultimately, there are other exciting features about the platform that makes it useful from different dimensions. Firstly, GEE stores satellite imagery with nearly 600 datasets from about 50 distinguished datasets providers obtained from 30 satellites such as PROBA-V, AVHRR, GSMAP, MODIS, and TRMM. Secondly, GEE organizes and makes it available for scientists and researchers for global-scale data mining, scientific analysis, and visualization of geospatial datasets. Below is figure 1 which shows the interface of Google Earth Engine environment.

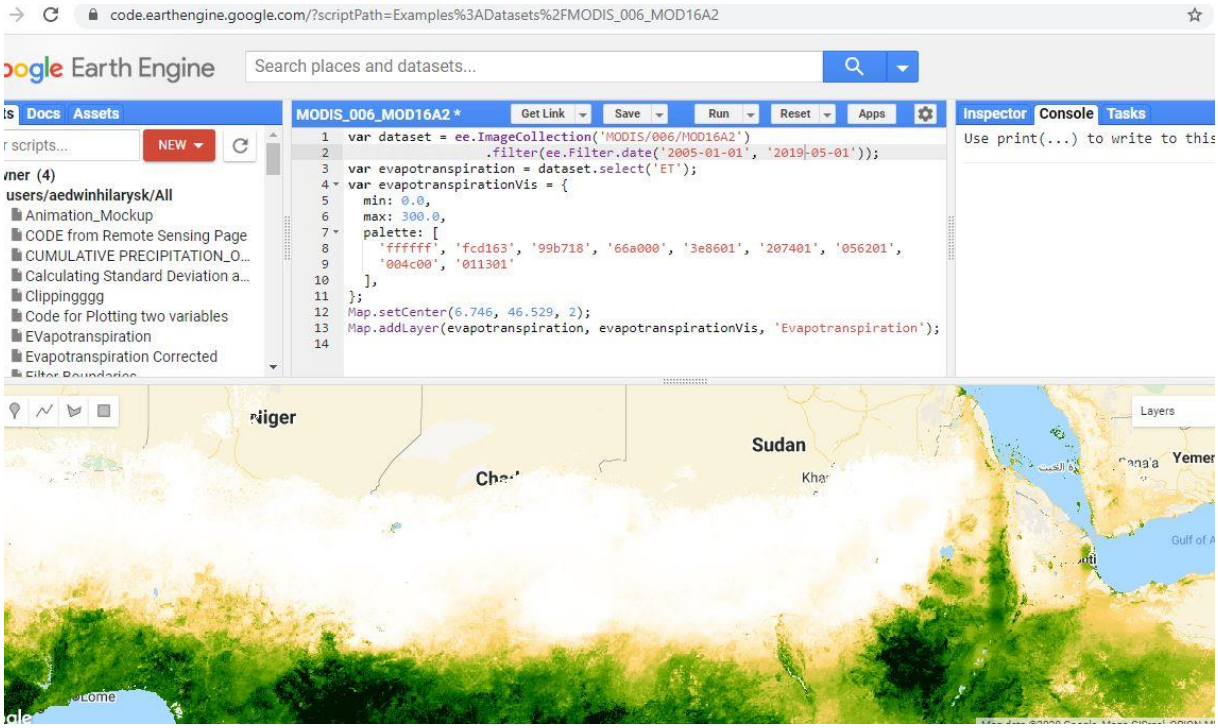

Figure 1: Google Earth Engine Interface

1.5. Research limitations

Although this Master thesis seeks to explore the various dimensions of vegetation dynamics; spatio-temporal representation of quantitative changes in order to address the knowledge gap, further work that goes beyond the available time is necessary. Some of the concepts will form the basis or directions for future research, where they will be addressed in an in-depth manner. This is because of time constraints and the complexity if all the dimensions, for example a specialization on specific plant species and a regional refinement of the historical meteorological records are to be examined at once. In this regard, the study addressed not the species-specific response to climatic conditions; thus, it did not highlight which particular species of plants withstand adverse climatic conditions or not. Similarly, the

focus of the analysis was done on the basis of representative case studies representing the various climate types not the whole country. The selection of these representative case studies was based on an exploratory approach to identify areas with vegetation cover. From a similar perspective, the study did not analyse the controlling effects of precipitation and temperature as well as land use and land cover changes on vegetation dynamics.

2. Foundations and Related work

2.1. Climate variables

According to Intergovernmental Panel on Climate Change (IPCC), Fourth Assessment Report by Solomon, S. et al., (2007), climate change refers to "a change in the state of the climate that can be identified using, for example, statistical tests as changes in the mean and or the variability of its properties, and that persists for an extended period, typically decades or longer. It refers to any change in climate over time, whether due to natural variability or as a result of human activity." Climate variables play a significant role in influencing vegetation changes either in the short term or long term. For the purposes of this thesis, evapotranspiration (meteorological condition), and soil moisture (hydrological factor) have been discussed.

Evapotranspiration

Evapotranspiration involves two main processes: evaporation and transpiration. Evaporation occurs when water in its liquid state is converted to water vapour and removed from the evaporating surface. It usually takes place on surfaces such as lakes, rivers, soils, and wet vegetation. Evaporation and transpiration occur concurrently, which makes it difficult to differentiate the two processes. Apart from the water availability in the topsoil, the evaporation from a cultivated soil is primarily calculated by the fraction of the solar radiation incident on the soil surface. This fraction diminishes over the growing season as the crop (vegetation) develops, and the canopy covers the majority of the ground area (FAO, 2020)

Soil Moisture

Soil moisture is one of the main variables in determining the vitality of land surface ecosystems and cultivated fields. It is an inevitable component of the "three-phase system" of the soil, which consists of air, moisture, and soil minerals (Bangalore, 2004; Craig, 2005). Soil

moisture depicts the amount of water available in the pores between soil particles. The amount of water held in the upper 10cm of the soil is referred to as surface soil moisture, whiles the moisture within the upper 200cm of the soil available to plants is called root zone soil moisture (NASA, n.d.). Soil moisture impacts geological, ecological, biological, and hydrological behaviours (Campbell, 1974; HILLEL, 1980; Fang & Daniels, 2006) of the soil. In addition, it plays a major role pertaining to plants growth, functioning of the natural ecosystems and biodiversity (Robinson et al., 2008). Application of adequate and timely moisture for irrigation based on soil-moisture-plant environment is crucial in the agriculture sector (Howell, 2001; Falloon, Jones, Ades, & Paul, 2011).

2.2. Remote sensing for vegetation studies

Using remote sensing for monitoring vegetation change has advanced over the years, although monitoring vegetation change is a challenge since it is continuously changing. However, remotely sensed time series are mostly efficient. The Intergovernmental Panel on Climate Change (IPCC) report by Solomon, S. et al., (2007), underscores the need to assess climate change impacts on vegetation dynamics through repeated, long term, and accurate satellite measurements.

Remote sensing techniques are therefore needed over a range of scales to effectively capture and quantify the significant spatio-temporal dimensions of vegetation change. According to Bruzzone, Smits, & Tilton (2003), the advancement of unique techniques for the analysis of multi-temporal data are complicated in the remote sensing domain. Nevertheless, remote sensing techniques and datasets provide useful means for global vegetation mapping (Boyd & Danson, 2005). As a result, there is considerable interest in using remotely sensed time series to map vegetation change, which is relatively easy compared to field observations. Among the methods significant for monitoring vegetation change in remote sensing, spectral vegetation indices (VIs) are the most prominent. Practically, spectral vegetation indices are calculated as

the ratio of two wavebands to contrast an absorbing feature with a reflective reference feature, and ultimately the status, biogeochemical composition, and structure of the vegetation is revealed by the spectral reflectance signatures (Ustin, Roberts, Gamon, Asner, & Green, 2004).

2.3. Vegetation indices

Vegetation indices commonly involve a ratio and, or a linear combination of the Red and Near-infrared (NIR) wavelengths of the electromagnetic spectrum (Huete, Justice, & Liu, 1994). According to Townshend, Justice, Li, Gurney, & McManus, (1991) and Roy, (1997), vegetation indices are essential for the scientific community in a range of fields such as detecting changes, calculate fractional vegetation cover, biomass and leaf area index (LAI). As a result, vegetation indices in remote sensing have formed the basis of a scientific approach for monitoring vegetation dynamics at various scales, e.g. seasonal, inter-annual, and inter-decadal variations. In 1969, Jordan proposed a vegetation index (VI) called Ratio Vegetation Index (RVI) based on the assumption that leaves absorb comparatively more red than infrared light; RVI can be mathematically expressed as:

$$\mathbf{RVI} = \mathbf{R / NIR}$$

where NIR is the Near-infrared band reflectance, and R is Red band reflectance. The RVI is frequently used for green biomass calculations and monitoring, especially in high-density vegetation areas. Nonetheless, when the vegetation cover is less dense, about 50% of vegetation coverage, RVI becomes sensitive to atmospheric effects, and its representation of biomass is weak, therefore limiting its applicability.

Similarly, Richardson & Wiegand (1977), developed the Perpendicular Vegetation Index (PVI), which is a simulation of the Green Vegetation Index (GVI) in R and NIR two-dimensional data. The spectral response from the soil is presented as a slash in the NIR−R coordinate system. The effect can be described as the soil shows a high spectral reflectance in the NIR and R bands. The distance between the point of reflectivity (R, NIR) and the soil line is defined as the Perpendicular Vegetation Index.

Another widely used vegetation index is the Leaf Area Index (LAI). Leaf Area Index is used to explain the potential surface area available for leaf gas exchange between the terrestrial biosphere and the atmosphere (Cowling & Field, 2003). LAI is a useful parameter controlling a lot of bio-physical processes of the vegetation, such as the interception of sunlight and rainfall, transpiration, photosynthesis, carbon and nutrient cycles. Although the Leaf Area Index has been useful, it is limited since it is species specific and not readily robust when it cuts across a variety of species with different canopies and leaf structures (Boegh et al., 2002; Broge & Mortensen, 2002; Xiao et al., 2002;Colombo, Bellingeri, Fasolini, & Marino, 2003). Enhanced Vegetation Index (EVI) is another widely used spectral vegetation index. The main advantage of EVI is that, it is more sensitive to differences in densely vegetated areas and better accounts for atmospheric influences.

A study conducted by Viña, Gitelson, Nguy-Robertson, & Peng (2011), compared the effectiveness of different vegetation indices. Among those used were the Normalized Difference Vegetation Index (NDVI), Enhanced Vegetation Index (EVI), the Green Atmospherically Resistant Vegetation Index (GARI), the Wide Dynamic Range Vegetation Index (WDRVI) and the Simple Ratio (SR). A sensitivity analysis revealed that EVI and WDRVI had higher sensitivities. According to Gago et al., (2015), assessing vegetation status is typically based on the Normalized Difference Vegetation Index. This is because, in low biomass environments, NDVI is the most preferred vegetation index for assessing vegetation status. Along with the different techniques, other factors like soil moisture, humidity, precipitation, and temperature are analysed to support studies in vegetation dynamics. Consequently, NDVI appeared to the preferred vegetation index for monitoring vegetation status and dynamics. After considering the advantages and limitations of applicability regarding the diverse nature of the study area, NDVI is considered to be most appropriate in achieving useful results.

Normalized Difference Vegetation Index (NDVI)

Normalized Difference Vegetation Index (NDVI) is one of the most widely used vegetation indices to determine the health conditions of vegetation. It is a measure of how visible light is absorbed and infrared light reflected by plants in the electromagnetic spectrum. (NASA, n.d. a)

Principally, NDVI based time series are primary to the remote sensing of vegetation growth and also in deriving statistical observations related to vegetation dynamics (Hall-Beyer, 2003; Pettorelli et al., 2005). To quantitatively assess the vegetation, the difference between Near-infrared and Red-light spectral reflectance is used to arrive at a value. The NDVI values range from -1 to +1, although there is no clear distinction for each type of land cover. Similarly, an NDVI value close to +1 (0.8 - 0.9) likely represents dense green vegetation.

Mathematically, the NDVI value can be derived using the ratio: **NDVI= (NIR – R) / (NIR + R)**

where, NIR is Near-Infrared and R is Red light from the visible spectrum.

Generally, NDVI assessment has become an established way to calculate healthy vegetation in the scientific domain based several NDVI products derived over the years from different sensors that readily support extensive time-series analyses. Nonetheless, in other to detect vegetation dynamics over time based on optical data, e.g., MODIS, atmospheric correction must be performed. Atmospheric corrections include cloud masking to remove cloudy pixels and linear interpolation to account for the cloudy pixels.

NDVI time series are normally variable. In most instances, these series are characterized by patterns like seasonality, trends and localized sudden changes (De Beurs & Henebry, 2005). Remote sensing techniques based on time series analysis are normally used to depict vegetation changes (Bradley, Jacob, Hermance, & Mustard, 2007), and at the same time, taking care of the varying processes.

The vegetation growth can be characterized by calculating “NDVI metrics” such as the date of green-up, magnitude of maximum NDVI, time-related integration of NDVI, duration of the

growing season, and amount of NDVI change (Borak, Lambin, & Strahler, 2000; Hall-Beyer, 2003; De Beurs & Henebry, 2005). NDVI time series can be used to obtain the parameters mentioned above. Furthermore, the inter-annual changes of vegetation dynamics can also reveal significant information on the response of vegetation to climatic conditions such as sparse rainfall patterns and increasing temperature.

2.4. Controlling factors and NDVI

Soil moisture is widely used to quantify the amount of water available in the soil, and is arguably the key element in understanding the climate-soil-vegetation system both in time and in space (Rodriguez-Iturbe, 2000; Laio, Porporato, Ridolfi, & Rodriguez-Iturbe, 2002) However, soil water balance also plays a major intermediate role between seasonal changes and plant water usage. According to Nicolai-Shaw, Zscheischler, Hirschi, Gudmundsson, & Seneviratne (2017), assessing the correlation between soil moisture and vegetation dynamics is key in water-limited environments such as arid and semi-arid regions where the greenness-precipitation ratio (GPR); the amount of net primary productivity per unit rainfall, has been largely used to quantify vegetation growth and productivity. Thus, the study area for this thesis serves as a unique testbed for exploring and understanding the relationship between soil moisture and plants' growth.

According to Song, Wesely, Coulter, & Brandes (2000), in vegetated ecosystems, root-zone soil moisture serves as a linkage between surface phenology and underground water storages which robustly influences surface water stability and energy segregation due to evapotranspiration. T. Chen, de Jeu, Liu, van der Werf, & Dolman (2014), found strong positive correlations, especially between soil moisture and NDVI. It was observed that vegetation responds to changes in soil moisture gradients from arid to moist conditions and affirmed the possibility to use satellite soil moisture data to monitor vegetation dynamics. In

the temporal extent, the relationship becomes stronger where soil moisture and NDVI exhibits coherent trend changes.

Evidence of recent studies with regards to vegetation changes on the one hand and the relationship between these vegetation changes and controlling factors (drivers) is necessary to provide insight and serve as the basis for the methodological approaches.

Measho et al., (2019), conducted a time series spatio-temporal analysis of vegetation dynamics in Eritrea spanning 18 years. Results of the linear regression model indicated that about 57.1% of the areas covered demonstrated a decreasing annual NDVI trend along the South-Western Eritrea. Similarly, results of mean annual precipitation and mean vegetation index revealed a strong positive correlation between NDVI and precipitation with the Pearson correlation coefficient (PCC), averaging around 0.84. Of the areas sampled as test sites, 87.16% show a positive correlation between NDVI and precipitation during the growing season (39.34%, $p < 0.05$). Based on the results, the study concluded that decreasing trends of vegetation with spatial heterogeneity is as a result of rainfall variability. In a related research, W. Zhao et al., (2017), applied multiple linear regression to investigate factors responsible for the 2005 and 2010 Amazon droughts. It was found that the Amazonian vegetation greenness responded to precipitation, radiation, and temperature with time-lag effects averaging at intervals of 0±4, 0±6 and 0±9 months, respectively.

On the overarching impact of soil moisture on vegetation, Ahmed, Else, Eklundh, Ardö, & Seaquist (2017), conducted a study on the dynamic response of NDVI to soil moisture variations in the Sahel region. The strength of correlation between NDVI and soil moisture was tested by a windowed cross-correlation at different time lags. Thus, a significant positive trend in NDVI was found in central and western Sahel with the affinity for high correlation values with shorter lags were recorded when soil moisture is correlated with the same month as NDVI ("lag0"). On the vegetation types, grassland and cropland were found to respond with "lag0". The relationship between soil moisture and NDVI is further explored by X. Wang, Xie, Guan,

& Zhou (2007), with an emphasis on the reaction of NDVI to root-zone soil moisture. The study found a statistically significant correlation between soil moisture and NDVI at different soil depths ranging from 5cm to 20cm. It was further indicated that there is more time lag of 10 days compared to 5 days for NDVI to respond to soil moisture variation in humid regions than in semi-arid regions; equally the response of grass to variations in soil moisture in semi-arid environments is mostly instantaneous.

Land cover and land use changes (LULC) equally play crucial roles in vegetation dynamics. Land-use and land-cover (LULC) change is a multifaceted socio-economic and ecological issue that requires a vivid understanding of the relationship and interaction between the environment and human-induced activities (Spalding, 2017; Handavu, Chirwa, & Syampungani, 2019; Xiang, Song, & Li, 2019). Recently, land-use change has intensified biodiversity, climate change and ecosystem service losses in the global spectrum since the growing population has put an enviable pressure on natural resources which has also altered hydrological conditions with its corresponding biophysical effects (Meyfroidt, P., van Noordwijk, M., Minang, P., Dewi, S., Lambin, 2011). According to Beygi Heidarlou, Banj Shafiei, Erfanian, Tayyebi, & Alijanpour (2019); T. Xu, Gao, & Li (2019), the information or data on reliable land extents, spatial and temporal distribution, and rate of land use and land dynamics constitute the indispensable pre-requisite components for implementing natural resource management, planning and strategies in developing a thorough understanding, monitoring changes in the environment and to predict future driving forces and pathways of land-use changes.

H. Chen, Liu, Ding, & Huang (2018), conducted a research in “Western Songnen plain using phenology-based residual trend analysis of NDVI time series”. The results based on inter-annual variability of SOS and EOS indicate an erratic and significant fluctuation of SOS, particularly between 2002 and 2004. In a separate study on human-induced vegetation change

along the Mekong River Basin, Na-U-Dom, Mo, & García (2017), used Mann–Whitney U test for a paired test for arriving at mixed results. Along the Mekong Delta in Vietnam as well as north-east Thailand, high anthropogenic infractions on croplands were recorded, but it rather improved cropland greenness. However, the spatial extents of the basin in Laos and Myanmar showed low human activities but with significant land degradation on the forest ecosystems. In another instance, while vegetation has depicted a strong decreasing NDVI trend over 10 years in high human activities areas except for cropland, the evergreen forest was found to be highly-sensitive to even the least degree of human activities.

3. Data and Case Study

3.1. Study Area

To obtain empirical results of vegetation changes based on the remote sensing time series, there is the need to situate the study within a geographical boundary. In this case, the Republic of Sudan is the overall study area because the country is undergoing rapid vegetation loss, yet research in that domain is effectively lacking. However, the high availability and quality of remote sensing datasets, in particular MODIS dataset, make the study on vegetation dynamics possible. Due to the large extent of the country, test sites, or representative case studies have been delineated based on climate classification as distinguished by Koeppen-Geiger. Figure 2 shows the climate classification of Sudan with the various representative case studies.

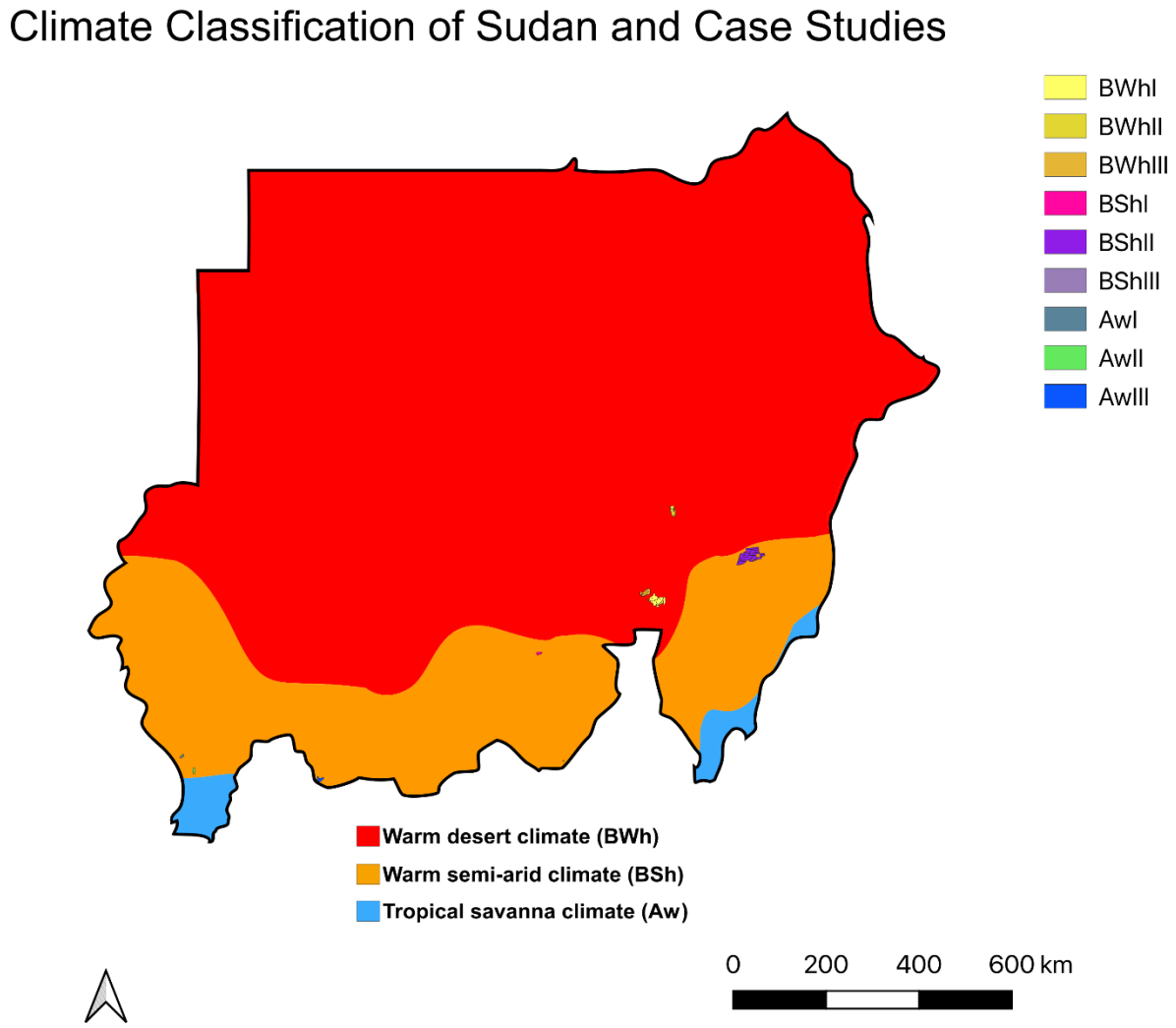

Figure 2: Climate Map of Sudan and Case Studies

3.1.1. Hot desert climate (BWh)

The hot desert climate covers more than two-thirds of the country's total land area. The different climate variables used to characterise this climate zone are the amount of precipitation (rainfall) received and average temperature throughout the year. With regard to this climate zone, some areas such as **Khartoum, Omdurman, Nyala and Kassala** are prominent.

Khartoum, for instance records nearly "no rainfall" throughout the year. The mean yearly temperature is 29.6°C while the annual rainfall is 135 mm. There is a variation of 62 mm precipitation between the driest month of January and the wettest months, of which precipitation reaches its highest in August. Similarly, the difference in yearly temperature is about 10.8 °C with the warmest month of May recording an average temperature of 34.1°C (Climate-Data.org, 2020). Similar to Khartoum is **Kassala** which records almost the same mean yearly temperature of about 29.2°C. Although rainfall here is scarce throughout the year, the annual precipitation is around 264mm of which most is concentrated in August, averaging 91 mm. On average, the highest temperature of about 33.4 °C is recorded in May (Climate-Data.org, 2020a).

As evidenced by the two main climate variables: temperature and precipitation, vegetation dynamics in this climate zone will be highly seasonal. To get empirical results, three test sites, or representative case studies have been delineated. However, due to the severity of temperature and scarcity of rainfall, which inhibits the thriving of natural vegetation, areas delineated in this zone are within irrigated schemes. These representative case studies are named **BWhI, BWhII and BWhIII**, respectively, which are situated across the climate zone with different area coverages. **BWhI** covers an area of about 561.33km², **BWhII** 191.99km² and **BWhIII** 214.95km², respectively. Figure 2 gives an overview of the representative case studies.

3.1.2. Hot semi-arid climate (BSh)

The hot semi-arid climate zone shares similar characteristics with the hot desert climate (BWh). In terms of area, this zone covers the second-largest area and extends southwards from the boundary of the hot desert climate zone. Precipitation in this zone is relatively high and lasts longer compared to the largest climate zone. Among some of the areas covered by the hot semi-arid climate zone are Al-Qadarif, Sennar, Geneina and the Nuba Mountains of South Kordafon surrounded by settlements such as Kitrah, Dalami, Abu Kershola and Umm Hitan.

Taking Al-Qadarif, for example, the amount of precipitation recorded annually is about 576 mm although slight showers are experienced throughout the year partly due to the effect of the local steppe climate.

In this climate zone, the rainy season spans 6 months, starting from May until October, with the torrential rains occurring between June and September. The average temperature in Al-Qadarif is 28.6°C (Climate-Data.org, 2020b). Sennar, on the other hand, has comparable climatic conditions as Al-Qadarif. Whereas the yearly precipitation is 432 mm, both precipitation and temperature vary by 150 mm and 7.6 °C, respectively (Climate-Data.org, 2019). In an attempt to represent vegetation dynamics as a characteristic of the climatic conditions, three main test sites have been delineated across the climate zone. These representative case studies have been carefully digitized to cover only plant species as depicted by satellite imagery. Of these three sites, one area is on the Nuba mountains, and the other is near Al- Qadarif, and the remaining test site is situated between the two digitized sites. Within this study, the test sites will be called **BShI (Nuba mountains)**, **BShII (Al-Qadarif)** and **BShIII** respectively. The area covered by BShI (Nuba mountains) is 58.77km², BShII (Al-Qadarif) is 110.70km² and BShIII is 2.58km².

3.1.3. Tropical savannah climate (Aw)

The tropical savannah climate of Sudan is more or less like "dotted patches" of grass across a rainforest. In occupies the least area with reference to the total land area of the country. This climate zone can be clearly distinguished in the south-west and east corners of the country as a boundary between Sudan and South Sudan. Regardless of the total area covered, three test sites have been digitized for the purposes of obtaining empirical results regarding vegetation dynamics. These representative case studies are named AwI covering about 41.74km², AwII 52.81km² and AwIII 91.54km² accordingly. Climatic conditions in the tropical savannah climate section are vividly distinguished by the amount of precipitation received throughout

the year. Al Kurumuk, for instance, receives approximately 933 mm of rainfall each year with an average temperature of 27.5 °C. Precipitation in this climate zone spans 6 months, from May to October although April and November also receive some amount of rainfall. While precipitation throughout the year varies by 210 mm, temperature varies by 6.4°C accordingly (Cliamte-Data.org, 2018). The representative case studies for this climate zone are in figure 2.

3.2. Datasets

3.2.1. MODIS NDVI (Terra or Aqua Image Collections)

As a proxy for vegetation index, NDVI is used in this master's thesis. Remote sensing datasets, as the name implies, are obtained from the Earth's surface based on observations from sensors on-board satellites. The actual NDVI dataset for this research is provided by Moderate Resolution Imaging Spectroradiometer (MODIS) on the Terra Instrument (satellite). Although MODIS is best for observing large-scale changes in the biosphere due to its far-reaching 2,330-km wide viewing swath recorded in 36 discrete spectral bands, it is an optical sensor. Due to its optical nature, when the sensor is monitoring changes on the land surface, the results obtained are mostly interfered with by weather conditions, in this case clouds. It is, therefore, necessary to do atmospheric correction (cloud masking) or pre-processing on the dataset (NDVI) before using it for further analysis in order to obtain cloud-free results. Figure 3 shows an image of a cloudy MODIS collection.

Figure 3: An Example of Cloudy MODIS Image

Source: (NASA, 2005)

"The Terra Moderate Resolution Imaging Spectroradiometer (MODIS) Vegetation indices (MODIS/006/MOD13Q1) Version 6 data are generated every 16 days at 250 meters (m) spatial resolution as a Level 3 product. The MOD13Q1product provides two primary vegetation layers. The first is the Normalized Difference Vegetation Index (NDVI), which is referred to as the continuity index to the existing National Oceanic and Atmospheric Administration-Advanced Very High-Resolution Radiometer (NOAA-AVHRR) derived NDVI" (Didan, 2015). The second vegetation layer is the Enhanced Vegetation Index (EVI), which has high sensitivity over dense vegetation. The algorithm chooses the best available pixel value from all the acquisitions within the 16 days period. Low clouds, low view angle, and the highest vegetation index value (NDVI/ EVI) is the criteria used. In addition to the vegetation and the two quality layers, the HDF file have MODIS reflectance bands 1 (red), 2 (near-infrared), 3 (blue), and 7 (mid-infrared), as well as four observation layers (Didan, 2015).

Resolution	Acquisition period	Units	Valid range	Scale factor	Description
250m	16 days	NDVI	-2000to 10000	0.0001	NDVI
250m	16 days	EVI	-2000 to 1000	0.0001	EVI
250m	16 days	Bit field	0 to 65534	N/A	VI quality indicators
250m	16 days	N/A	0 to 10000	0.0001	Surface reflectance band 1
250m	16 days	N/A	0 to 10000	0.0001	Surface reflectance band 2
250m	16 days	N/A	0 to 10000	0.0001	Surface reflectance band 3
250m	16 days	N/A	0 to 10000	0.0001	Surface reflectance band 7
250m	16 days	Degree	0 to 18000	0.01	View zenith angle of VI pixel
250m	16 days	Degree	0 to 18000	0.01	Sun zenith angle of VI pixel
250m	16 days	Degree	-18000 to 18000	0.01	Relative azimuth angle of VI pixel
250m	16 days	Julian day	1 to 366	N/A	Day of year VI pixel
250m	16 days	Rank	0 to 3	N/A	Quality reliability of VI pixel

Table 1: Layers of MODIS Vegetation Index

Source: (USGS.gov, 2020)

3.2.2. Evapotranspiration

"The MOD16A2 version 6 evapotranspiration is an 8-day composite dataset produced at 500meter (m) pixel resolution based on the Sinusoidal Coordinate System. The algorithm used for the MOD16 data product collection is based on the logic of the Penman-Monteith equation, which includes inputs of daily meteorological reanalysis data". The two pixel values for the evapotranspiration layers: ET and PET are the sum of all eight days within the composite period. Also, the pixel values for the two Latent Heat layers (LE and PLE) are the average of all eight days within the composite period (Running, S., Mu, Q., Zhao, 2017).

Resolution	Acquisition period	Units	Valid range	Scale factor	Description
500m	8 days	kg/m²/8day	-32767 to 32700	0.1	Total evapotranspiration
500m	8 days	J/m²/day	-32767 to 32700	10000	Average latent heat flux
500m	8 days	kg/m²/8day	-32767 to 32700	0.1	Total potential evapotranspiration
500m	8 days	J/m²/day	-32767 to 32700	10000	Average potential latent heat flux
500m	8 days	Bit field	0 to 254	N/A	Evapotranspiration quality control flags

Table 2: Layers MODIS Evapotranspiration

Source: (USGS, 2020)

3.2.3. Soil Moisture

For the soil moisture dataset, two categories are used: root zone soil moisture for the entire duration of the study, and subsurface soil moisture for the temporal (seasonal) computations or analysis.

(i)

The root zone soil moisture is derived from a larger set called Global Land Data Assimilation System (GLDAS), which combines satellite and ground-based observation products. “It uses advance land surface modelling and data assimilation techniques to generate optimal fields of land surface states and fluxes”. Table 3 shows a short version of the soil moisture dataset captured in the larger collection.

Name	Units	Range	Description
RootMoist_inst	kg/m^2	2 to 949.6*	Root zone soil moisture
SoilMoi0-10cm_inst	kg/m^2	1.99 to 47.59*	Soil moisture
SoilMoi10-40cm_inst	kg/m^2	5.99 to142.8*	Soil moisture
SoilMoi40-100cm_inst	kg/m^2	11.99 to 285.6*	Soil moisture
SoilMoi1100-200cm_inst	kg/m^2	20 to 476*	Soil moisture

*Table 3: Layers of Root zone soil moisture (*estimated)*

Source: (NASA, 2020)

(ii)

The NASA-USDA Global soil moisture provides soil moisture dataset at a spatial resolution of 0.25°x0.25° across the globe. These datasets include surface and subsurface soil moisture (mm), soil moisture profile (%), and surface and subsurface soil moisture anomalies" (NASA, 2020). It covers the period from 2010 until present. The final product of this soil moisture dataset is obtained by combining observations from the Soil Moisture Ocean Salinity (SMOS) into a modified layer. To assimilate the datasets for the final product, 1-D ensemble Kalman Filter approach have been applied (NASA, 2020). The layers of this soil moisture are provided in table 4.

Name	Description	Units	Value range
Ssm	Surface soil moisture	mm	0 to25.39*
Susm	Subsurface soil moisture	mm	0 to 274.6*
Smp	Soil moisture profile	fraction	0-1*
Ssma	Subsurface soil moisture	-	-4 to 4*
Ssma	Surface soil moisture anomaly	-	-4 to 4*

*Table 4: Layers of NASA-USDA soil moisture (*estimated)*

Source: (NASA, 2020)

4. Methodology

4.1. Data Acquisition

MacEachren (1995), asserted that how good and efficient spatial dynamics are extracted and empirically depicted essentially rests on several factors. Some of these factors are elements related to data acquisition, such as the duration considered, the temporal resolution contained by that duration, and the spatial extent and resolution since detecting meaningful patterns, trends and cycles are keenly influenced by these aspects. For the purpose of this thesis, remotely sensed time-series datasets have been used.

The primary and necessary remote sensing datasets are hosted in Google's Cloud Computing platform known as the Google Earth Engine. The mentioned datasets are available at GEE platform and can be searched through the data catalogue by using tags like weather, climate and land cover. The GEE provides a user-friendly environment. Besides, each dataset has a ready-to-use code samples attached to it. All that is needed is to click on the "Open in Code Editor" button that is located below the code snippets, and the code will subsequently open in Earth Engine Code Editor and with a click on "Run", the dataset can be explored. With the in-built capabilities, algorithms and the available datasets, the Google Earth Engine offers a well-organized framework for researching vegetation dynamics by relying on Remote Sensing data supplemented by cloud computing. Below is a schematic depiction of data acquisition in the Google Earth Engine environment (GEE), as shown figure 4.

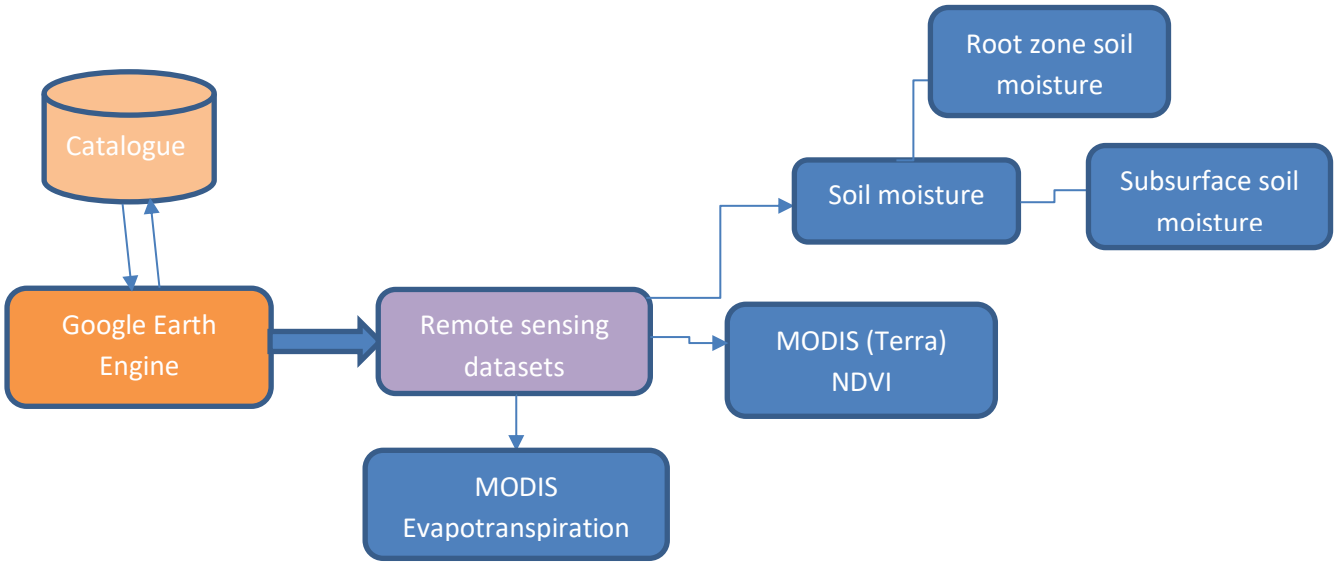

Figure 4: Schematic depiction of data acquisition in GEE

4.2. Pre- processing

Although the producers regularly pre-process satellite datasets before they are made public to different users, quality issues still remain a challenge. A chunk of optical remote sensing datasets, LANDSAT, AVHRR, SPOT and MODIS are influenced by unfavourable conditions that need to be corrected. The necessity of pre-processing remote sensing (vegetation indices) datasets has been demonstrated in various studies. For example, Dong, Id, Qin, & Wan (2019), used MODIS NDVI quality control flags (QC) to remove clouds and snow pixels from the spectral vegetation reflectance as well as model correction to adjust angle constraints; Choudhary, Shi, Singh, & Corgne (2019), in a related study, conducted radiometric and geometric corrections, and re-projected the datasets into a single world geodetic system. It was followed by filtering to remove noise, then data vectorization, interpolation, image enhancement and subsequent accurate band combination; Fatikhunnada, Solahudin, Buono, Kato, & Boro (2020), during pre-processing, used linear interpolation to reconstruct and standardize vegetation index time series. FFT and Wavelet transform were used for noise

filtering in order to retain seasonal cropping signals; Bin et al., (2019), equally used RPC coefficient for geometric correction in the ENVI software and radiometric calibration respectively.

From the above studies, pre-processing or smoothing techniques can be outlined as: (i) atmospheric correction (noise reduction)-cloud and snow masking (ii) geometric-corrections; (iii) mosaicking images (iv) computing and reconstructing NDVI time series, and (v) layer stacking. Noise reduction or smoothing, therefore, is a fundamental and important procedure before further implementation. However, the pre-processing steps that will be used in the context of this study are cloud masking (noise reduction) to remove cloudy pixels, and linear interpolation for gap-filling or to account for missing pixel values as proven in other studies such as (Fensholt, Rasmussen, Theis, & Mbow, 2009; Maneta et al., 2018 and R. Wang et al., 2020).

Linear trending and de-trending

Linear trending of vegetation time series is essential in undertaking significant analysis related to changes over time. Easdale, Bruzzone, Mapfumo, & Tittonell (2018), used simple linear regression to estimate the linear trend in inter-annual NDVI over time by aggregating 16 day NDVI composite into annual NDVI integrals. Results from the regression analysis show a decreasing trend characterized by significant negative slope, an increasing trend identified by significant positive slope, and no trend. In a related study, Pang, Wang, & Yang (2017), applied the frequently used least squares linear trend to calculate the trends in precipitation, temperature, and NDVI over time. Other studies emphasized the significance of using linear regression in detecting seasonal or temporal changes in a time series analysis (de Jong, Verbesselt, Schaepman, & de Bruin, 2012; Fensholt & Proud, 2012), while Schucknecht, Erasmi, Niemeyer, & Matschullat (2013), used the ordinary least square regression to calculate a linear trend.

De-trending, on the other hand, is necessary for time series analysis. Its effectiveness has been demonstrated in vegetation studies; for example, X. Guo, Zhang, Yuan, Zhao, & Xue (2015), used de-trended fluctuation analysis to decouple the temporal behaviour of vegetation time series from a long term (range) time series. The analysis from the de-trending technique unveiled insights of temporal vegetation dynamics distinguished from long term trends. The significance of de-trending has been corroborated by L. Zhao, Dai, & Dong (2018), where multiple regression with NDVI was linearly de-trended to get rid of trends and to compute the impact of each climatic factor on vegetation changes. From the above examples, it is implicitly clear that linear trending and de-trending are important in analysing vegetation time series.

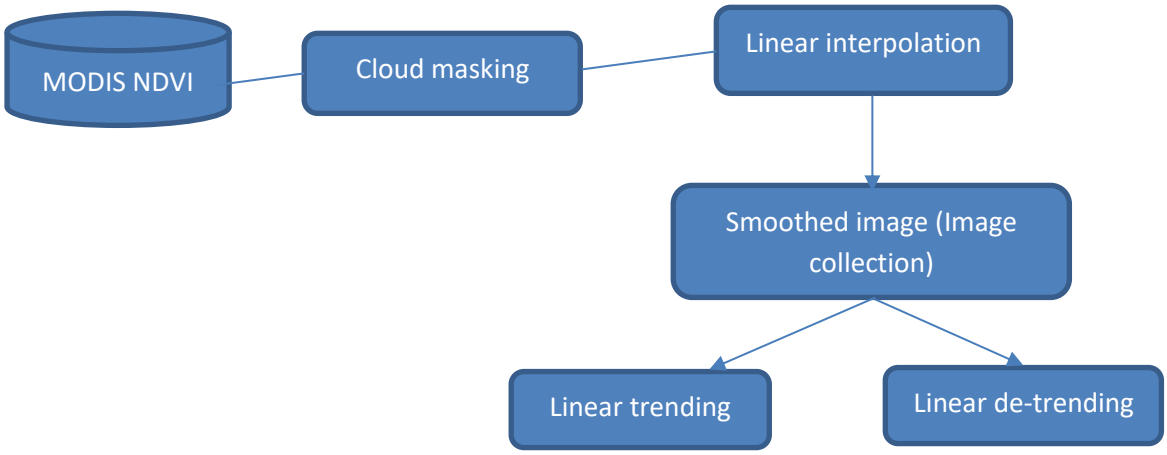

Figure 5: Schematic depiction of pre-processing

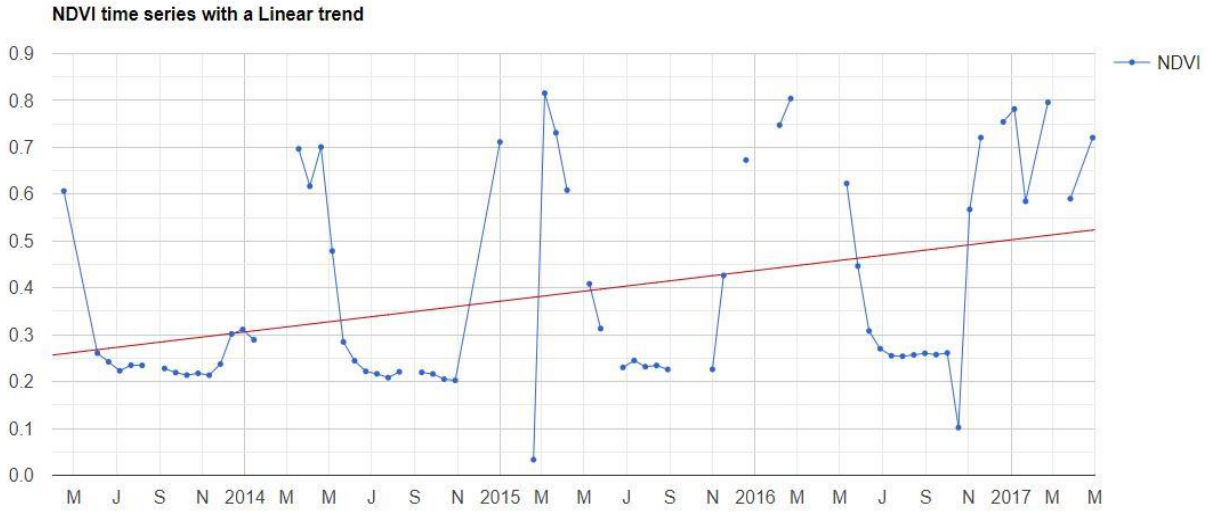

Figure 6: Linear trending of NDVI

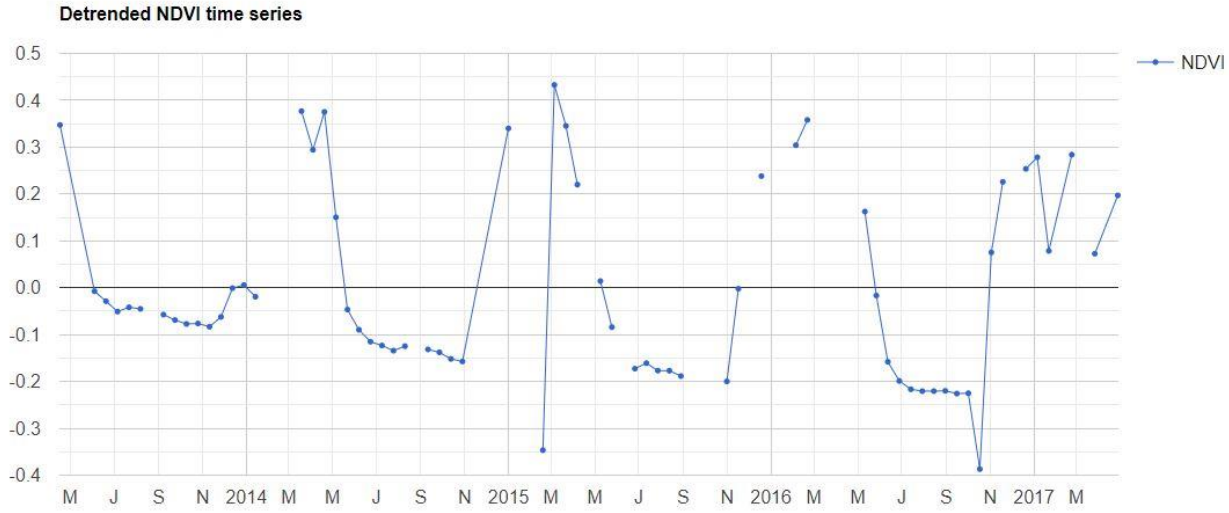

Figure 7: Detrended NDVI time series

4.3. Data modelling and implementation

There exist different data modelling approaches applicable to vegetation time series modelling. For instance, Cai, Jönsson, Jin, & Eklundh (2017), compared the performance of five data modelling (smoothing) methods; "Savitzky-Golay fitting (SG), locally weighted regression scatterplot smoothing (LO), spline smoothing (SP), asymmetric Gaussian function fitting (AG), and double logistic function fitting (DL)"(pp 20-22) in reconstructing NDVI time series and simulating vegetation phenology. Zhai, Zhang, Zhang, & Li (2018), asserted that cloud and cloud shadows normally characterize optical remote sensing images. This by extension, hinders the capacity of earth observation by optical sensors to be entirely cloud-free. As a result of the obstacles mentioned above, using remote sensing datasets for applications including vegetation monitoring (Lu, Coops, & Hermosilla, 2017), change detection (Zhu, 2017) and particularly for quantitative analysis (Zhai et al., 2018) can result in severe problems. Therefore, data modelling preceding implementation is necessary since the datasets are obtained in a continuum; "time series" with fluctuations and frequent changes which are non-negligible.

In most cases, the type of noise presented in an NDVI data set strongly influences the approach to reducing noise, particularly when focussing on seasonality and spatio-temporal data representation (Hird and McDermid, 2009; Julien and Sobrino, 2010). Most of the interval-fixed composite of LANDSAT-NDVI, AVHRR-NDVI or MODIS-VI products are standardized for the users with their complete processing and production system. However, majority of the local filtering (smoothing) or modelling methods require representation of a time-series that is continuous and evenly spaced (Bradley et al., 2007; Eklundh and Jönsson, 2011; Zhu et al., 2012).

Examples of modelling techniques used in vegetation studies are; statistical model for estimating mid-day NDVI (Wheeler & Dietze, 2019); flexible fourier transform (FFT) model in forecasting soya bean yield (C. Xu & Katchova, 2019); time-delay neural network(TDNN)

for predicting NDVI in arid and semi-arid regions (T. Wu, Fu, Feng, & Bai, 2019); using historical data for predicting NDVI based on crop growth model (Berger, Ettlin, Quincke, & Rodríguez-bocca, 2018), and harmonic regression of Landsat time series (Wilson, Knight, & McRoberts, 2018). However, for the purposes of this study, harmonic modelling will be adopted since it works best for time series data (Padhee & Dutta, 2019), and has the capability of capturing actual temporal dynamics "trends" (Yang, Luo, Huang, Wu & Sun, 2019). A linear trending and de-trending, preceding the harmonic modelling of MODIS NDVI will be undertaken in order to estimate the general trend of NDVI over time prior to computing the harmonics.

Harmonic modelling

The effectiveness of Harmonic modelling in vegetation time series analysis has been well demonstrated (Wilson, Knight, & McRoberts, 2018; Landmann, Eidmann, Cornish, Franke, & Siebert, 2019; Roy & Yan, 2020). Not only is the harmonic modelling applicable to vegetation indices derived from specific satellites such as LADNSAT, AVHRR or SPOT NDVI, but its application to MODIS NDVI time series is also a common approach in academia. For example, the performance of harmonic analysis in reconstructing global MODIS NDVI time series (Zhou, Jia, & Menenti, 2015), estimation of dynamic parameters of MODIS NDVI time series (Chakraborty, Banerjee, Gupta, Papandreou-suppappola, & Christensen, 2017), spatio-temporal reconstruction of MODIS NDVI based on time series harmonic analysis (Padhee & Dutta, 2019), and land-cover monitoring based on time series satellite images (Jung & Lee, 2019)

Harmonic modelling (analysis) has proved to be one of the best performing techniques in monitoring vegetation dynamics (Kostadinov et al., 2017). It is computed as the sum of cosine waves and an additive component. Alternatively, it can be expressed in terms of time series as

the sum of sinusoids at different frequencies (Shumway and Stoffer, 2017). Every single wave is known as a harmonic term and is identified by its amplitude (height of the maximum), frequency (number of cycles), and phase (delay from time zero). An important aspect of the harmonic model is its inherent capability to estimate seasonality devoid of noise which usually characterizes time series data, and to predict the phenological behaviour (trends and patterns) of NDVI over time. Below is figure 8 showing the harmonic modelling of actual NDVI and fitted values.

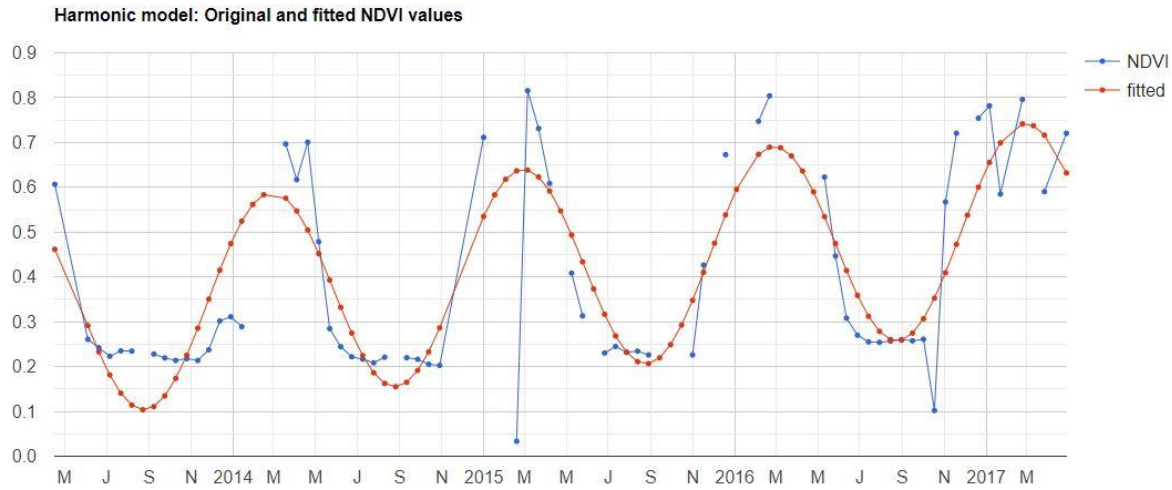

Figure 8: Harmonic model showing actual and fitted NDVI values

Case introduction for seasonality

As indicated earlier, sub-setting and analysing vegetation dynamics on seasonal parameters is crucial for differentiating intra-annual and inter-annual vegetation change. This importance of seasonal dependent analysis has been indicated by Zhang, Brandt, Tong, Tian, & Fensholt, (2017), where a distinction between start of season (SOS) and end of season (EOS),

heavy rainfall events and days of rainfall were made. A strong correlation between rainfall and vegetation was found during the growing season. Similarly, the spline cubic function was used to investigate the seasonal pattern in vegetation changes (Sharma, Ueranantasun, Tongkumchum, Campus, & Rd, 2018). Situating the study in the context of Sudan, two rainy seasons can be distinguished. A shorter period of about three months(July-September), which occurs in the Hot desert climate (BWh) and a longer period of six months(May- October) which that takes place in the Hot semi-arid climate (BSh) and Tropical savannah climate (Aw) respectively. The seasonal analysis, therefore, will be modelled based on this trajectory.

Sdn = $Sn_1 + Sn_2$,

where Sn_1 is the first rainy season from May to October,

Sn_2 the second rainy season from July to September.

Implementation

Calculating the statistical or quantitative changes in vegetation, in fulfilment of the first objective of this thesis is based on the methodologies described above. NDVI mean have been calculated in three folds; monthly mean NDVI throughout a given year (seasonal), the mean annual NDVI calculated for three break points of five years: 2005-2009, 2010-2014, and 2015-2019 as well as that of the entire study period of 15 years (2005-2019). Secondly, the standard deviation of NDVI for the entire period, breakpoints, and on seasonal basis have been computed. A third quantitative indicator that closely intertwines with the third objective is linear regression, which is to estimate the linear trend of NDVI over time. The linear regression as depicted by the regression line has been fitted for the entire duration of the study.

Determining the relationship between two variables; an independent and dependent variable is also necessary in this thesis. For determining the relationship, Pearson correlation

is the most preferred because is less sensitive to noise and is resistant to outliers, therefore, can handle the fluctuations in time series data by providing the strength and directions of linear relationship between two variables. Computing the Pearson correlation between NDVI and other controlling factors; soil moisture and evapotranspiration will be done for the long term, break points and on seasonal basis. Similarly, a cross correlation between NDVI and soil moisture, as well as between NDVI and evapotranspiration, have been calculated. This is to determine the lag (delay) in the response of NDVI to soil moisture and evapotranspiration.

Furthermore, mapping vegetation dynamics in this context has to do with the representation of changes over time, where NDVI is used as a proxy for vegetation. The specific case introduction will be a focus on the spatio-temporal extent, although the changes as observed over the entire time span will be taken into consideration. The spatio-temporal extent in this context will take into account the seasonality (temporal dimension) based on the rainy seasons of the various climate zones; the representative case studies as the spatial dimensions. Since this objective follows closely from the quantitative changes, the mapping will take into account yearly representations, and for the seasonality: monthly maps will be produced spanning the rainy seasons as described in the preceding paragraph. The seasonality will focus on two years, 2015 and 2017 where severe droughts were reported in Sudan. In figure 9, the schematic depiction of the implementation has been provided.

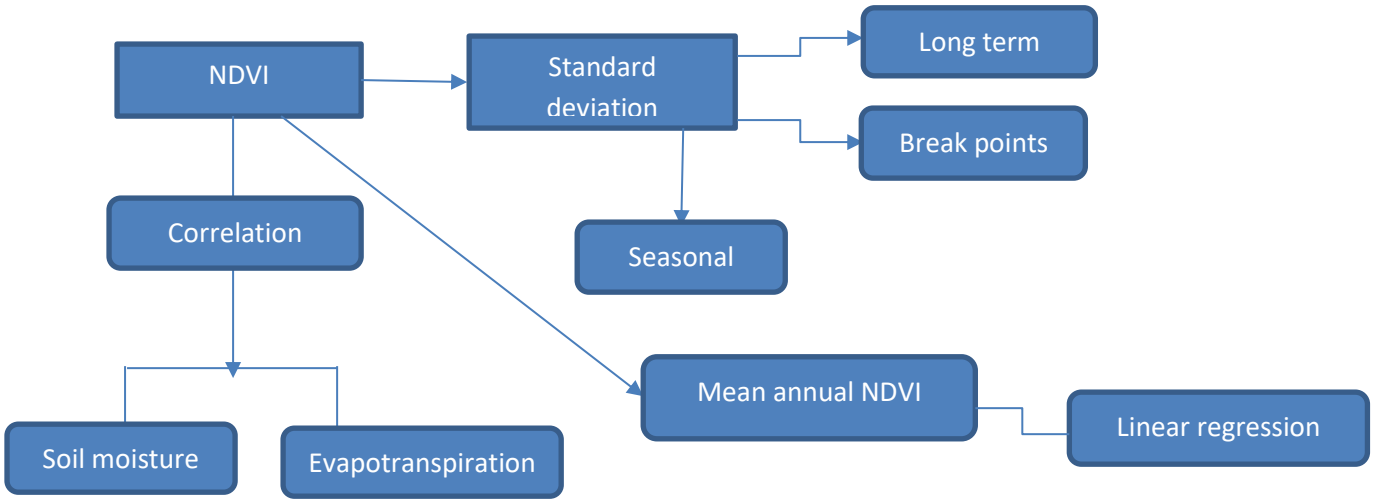

Figure 9: Schematic depiction of the implementation process

5. Visualization vegetation dynamics

The concept of visualization has been extensively discussed across several disciplines, e.g. geoscience (Graser, Schmidt, Roth, & Brändle, 2019), medicine (Yang & Chen, 2019), cognitive science (Y. S. Kim, Walls, Krafft, & Hullman, 2019), and business analytics (Jia, Wang, Lei, Zhao, & Guan, 2014). Data visualization techniques integrate digital technologies, algorithms and cognitive aspects to make data comprehensible. The spatial data visualization approaches, along with traditional methods of data representation (e.g., tables, diagrams, charts), can support discovery and allow users to undertake both qualitative and quantitative data analysis.

As explained by MacEachren and Kraak (2001), geovisualization incorporates methodologies from scientific visualization, cartography, image examination, information visualization, exploratory data analysis and geographic information systems to provide theory, techniques, and tools for the visual exploration, analysis, fusion and presentation of geospatial data. Multiple representations in displaying geospatial datasets in different ways within the geovisualization environment place maps on a higher level to stimulate visual reasoning around geospatial patterns, connections, and trends.

5.1. Visualizing space and time

Time is an essential component in visualizing or mapping changes in spatial-temporal data. In general, two temporal primitives: time point or time interval are the most common to display time visually (Aigner, Miksch, Müller, Schumann, & Tominski, 2007). Time intervals are mostly used to investigate how events occur in time or how a series of events are overlapped at a given location, whether changes are gradual or abrupt. Regardless of the primitive selected for time visualization, the core aim of it is to compare and contrast data at diverse points in time, observe and detect changes, trends, and patterns in the dataset that has been visualized. Spatio-temporal information can be visualized using various techniques. For instance, animated flow visualization (Van Wijk, 2002), which are created from streamline images based on data abstraction and iconic representations; Time wheel (Tominski, Abello, & Schumann, 2004), an axes-based visualization of multivariate data with a focus on temporal dependencies and helix glyphs on maps (Tominski, Schulze-Wollgast, & Schumann, 2005), which emphasizes cyclic patterns in spatio-temporal dimensions

5.2. Visualizing change in space and time

Change is ubiquitous and inherent in a dynamic world. Within the context of geovisualization, changes can be identified in both spatial and temporal domains. Spatial dynamics and spatial changes over time are significant inquiries among geospatial data visualization practitioners, academics, and researchers. Within geovisualization, representing spatial dynamics is of key interest since it enables the user to trace, analyse, and visualize the variations in a spatial phenomenon. Change in the context of geovisualization explains the differences in the spatial and/ or thematic appearances of geographical phenomena over a given timeframe. For this discussion, the change will be distinguished and explained in the spatial and temporal domains.

Within the spatial domain, various attributes can characterize or represent changes. For instance, C. A. Blok (2005), proposed concepts of **appearance (disappearance), mutation and movement.**

Appearance or disappearance describes the real changes with regards to the occurrence of an original phenomenon or the dying of a current phenomenon, e.g. tornado, flood and bushfire.

Changes in the state of a prevailing phenomenon, for instance, land cover changes (e.g., from forest to a cultivated area), can be described by mutation. Therefore, Mutation describes the alteration, which affects the thematic feature constituents of a prevailing phenomenon. To provide enough details, C. A. Blok (2005), distinguished two sub-categories; Mutation at the nominal level of measurement and Mutation at higher than nominal level of measurement.

Movement explains variations in the spatial location and/or the geometry of a phenomenon. Within the context of geovisualization, two sub-divisions of movement has been distinguished as movement along trajectory and boundary shift (C. A. Blok, 2005).

- Movement along a trajectory describes a movement through which the entire phenomenon changes its location. This type of movement usually follows a certain path; it can, therefore, be presumed that movement does not happen instantaneously but rather over a period of time where some continuation is involved. Alongside the route, the geometric features of the phenomenon may change.
- Boundary shift, on the other hand, refers to movement, where at least part of the phenomenon retains its position yet expands to cover other areas occupied by a prevailing phenomenon, such as a desert encroachment to areas with vegetation cover, or an area with a high vegetation index. These types of movement may take place at a particular time or gradually occurs over an extended timeframe.

In the temporal domain, characterizing the dynamic nature of geospatial phenomena revolves around unique concepts that help to describe the inherent changes over time. These characteristics according to C. A. Blok (2005), include;

- Moment time, which explains the date or the position in a time of a change in the spatial domain.
- Sequence similarly describes the order of periods in a sequence of changes in the spatial environment.
- Duration, on the other hand, refers to the length of time involved in a change and/or the time between changes in the spatial domain. This could be stated in absolute or comparative terms such as total number of time units or views such as short or lengthy respectively
- Pace talks about to the degree of change over a given time frame and can be stated in terms such as slow or quick; or at increasing or diminishing or persistent frequency of change (Maceachren, 1995).
- Frequency refers to the total number of times that a specific phase recurs in a sequence of changes in the spatial domain.

Detecting change within the spatial and temporal domains have been explained in the preceding paragraphs with their unique characteristic concepts. However, merging the two concepts is crucial to this study in order to describe changes in dynamic geospatial data vividly. Aside from supporting the effective detection and analysis of changes in dynamic geospatial data, variations over comparatively long periods entail the integration of distinct changes into a generally spatio-temporal domain to clearly see patterns of change. In this regard, two separate perspectives, namely circle, and trend, described below incorporate changes in spatio-temporal patterns over longer series.

- The cycle describes the periodical re-appearance to an earlier state or condition (Muehrcke & Muehrcke, 1992). Cycles are rather common in the physical environment; for instance, daily or seasonal cycles in atmospheric developments and seasonal, bi-annual cycles in vegetation dynamics are relatively common. But additional phenomena, such as locust invasion, erosion could display cyclic patterns.
- The trend, on the other hand, explains the arranged but non-cyclical pattern (Muehrcke & Muehrcke, 1992). It is the overall direction or propensity of development over a period of time. A couple of distinguished examples are rate of recurrence of cyclones.

Static and animated maps for visualizing change in geospatial context

Over the years, there have been a large number of studies concerning the visualisation of spatio-temporal data (Andrienko, Andrienko, & Gatalsky, 2000; Ott and Swiaczny, 2001; D. Guo, Chen, MacEachren, & Liao, 2006; Roth, 2011; Ramakrishna, Chang, & Maheswaran, 2013; Sun, Liu, Wu, Liang, & Qu, 2014; David & J M Tauro, 2015; Wang et al., 2016; Kim et al., 2018). O'Sullivan & Unwin (2010), asserted that aside from the visualization of geospatial data to enhance research findings, the field of geovisualization has changed the traditional role of cartography by integrating spatial data into the analysis. Several techniques for mapping spatio-temporal data have been documented due to the dynamics of a natural phenomenon for patterns and relationships (Alan, 2001), and to expedite thinking, understanding, and knowledge creation around geospatial data (Lorensen, 2004).

While experimenting with alternative methodologies for the representation and exploration of spatio-temporal data, Andrienko, Andrienko, & Gatalsky (2003), proposed two concepts to illustrate visualizations, while the first concept depicts identification tasks with a focus on spatial objects or locations at a given instant, the other deals with determining the time moment(s) when definite features of objects or locations occur. Static map and animation were used in solving tasks related to the first concept, while a time-series graph was used in the second concept. It was found that time-series graph easily enables one to conclude at what time moments the characteristic value for a given entity was the highest or the lowest and similarly when the highest or the lowest value among all entities was reached. Putting this study into perspective, one of the objectives is to map spatio-temporal data with regards to vegetation dynamics from a remotely sensed time series.

Mapping and visualizing geospatial dynamics is exceedingly process-oriented hence dominated by various techniques and state-of-the-art technologies with unique functionalities depending on the purpose and context. Although there is more to geovisualization than the

progress of cartographic knowledge in various aspects, Johnston (1981) & De Koninck (2012), emphatically stated that within geovisualization, patterns in a map are vital although most concepts with regards to geospatial data mostly deal with spatial patterns. The pattern, according to C. Blok, Köbben, Cheng, & Kuterema (1999), refers to a collection of perceptual elements such as symbols and pixels in space and/or in time, which form an object. The role of patterns in exploring geo-data are varied. Among the various interests normally pursued are the existence of patterns in the data, the characteristics of the patterns, interactions, and dissimilarities or correspondences in patterns.

Static maps mostly offer the opportunity to present results of interpretations of data usually in change maps, anomaly maps or multi-temporal colour composites. This approach enhances spatial reasoning, and it can be combined with further functionality, such as interaction with pixels or objects and values retrieval over time. Although static maps by their nature are restricted in the extent of data that can be presented, and the variety of time units that can be shown, Adrienko & Andrienko (2011); Kessler (2011), ensuing from Monmonier's typologies for cartographic representation mentioned single static maps and series of static maps among others as a way of representing spatio-temporal data.

Single static maps exist in a variety of ways, such as change maps, anomaly maps, and density maps (Scheepens et al., 2011). Still, they are not suitable when handling complex data that spans multiple time periods. With regard to this limitation and owing to the sheer nature of the study, and in particular, fulfilling the objective of mapping changes in vegetation dynamics over longer time periods, multiple static maps will be the most efficient. Multiple static maps are preferred over single static maps due to possibility for several depictions of the same information, or multiple parts of the same area through which changes can be represented in a cleaner and effective manner. Juxtaposing of different time slices over the same area, for instance, can further elucidate temporal patterns that have been represented. Similarly, multiple static maps are efficient when handling seasonal data since small multiple representations can

help to identify differences between the seasons and allow users to scan between the seasonal depictions. With these advantages of multiple static maps, it is deemed efficient for representing spatio-temporal data compared to dynamic visualization (animation), which is usually concerned with displaying sequential information about micro-steps of changes**.**

Hence, **this study will focus on using multiple static maps for mapping vegetation dynamics. The thesis adopts the workflow presented in figure 10.**

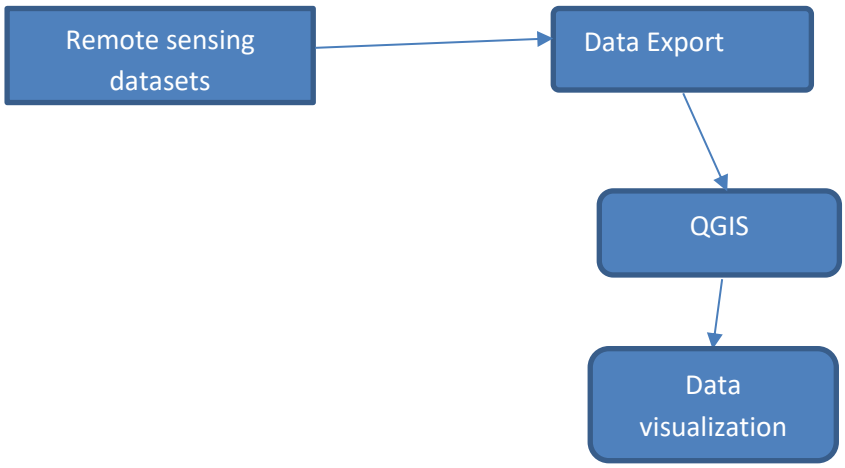

Figure 10: A schematic depiction of the proposed state of the art visualization

Summary

How well spatial dynamics are rendered depends, among other things, on factors related to data acquisition, such as "the period considered and the temporal resolution within that period, spatial extent and resolution since seeing patterns, trends, cycles and other spatio-temporal aspects of geospatial data" (Maceachren, 1995). This chapter, therefore, provided an overview of concepts related to visualization, various visualization techniques, and characteristics of change in the spatial and temporal domain. An in-depth discussion on two "front runners" regarding visualization; animation and static maps. As stated earlier, this study will focus on small multiples (static maps) for the visualization of vegetation dynamics.

5.3. Prototypes for visualizing vegetation dynamics

Techniques for data visualization are endless. A study conducted by Gulati & Sharma (2020), depicts data visualization techniques based on models and taxonomy. This work highlighted simple techniques such as scatter plots and stacked bar graph to more advanced means of visualization including box and whisker plots, heat Map, gantt chart and tree map. In a related study focusing on generating insights through data visualization and analysis, other means of data visualization were introduced such pacman visualization and clustered projections (Nestorov, Jukić, Jukić, Sharma, & Rossi, 2019). The studies above clearly show that the field of visualization is continuously evolving and been revamped by new visualization techniques. It is against this background that this sub-section provides a protoype of other visualization techniques aside static maps that can be used to visualize vegetation dynamics over time. However, in the context of this thesis, the prototype of visualization techniques have been segregated to address specific aspects of mapping vegetation dynamics. These are visualizing trends, change and dynamics.

5.3.1. Trend

Exploring trends in time series datasets is key in understanding dynamics. Trends in datasets reveal whether there is an increase (upward trend), decrease (downward trend) or no trend which implies stationarity in the dataset. These trends sometimes can be used to predict the future occurrences in the dataset. While specific techniques exist for the visualization of trends, no single technique has an overall advantage. Ultimately, this prototype is centred on two techniques for the purposes of visualizing trends in vegetation dynamics; line and area charts. Line charts are simple to use in representing the trajectory in a dataset. Yunhai, Wang, Han, Zhu, Deussen, & Chen (2018), stated that line graphs are the most preferred options for the visualization of a time series data. This is due to the fact that the slopes; up and down in line graphs help to perceive trends and patterns effectively compared to scatter plots. Area charts, on the other hand, are effective in visualizing trend. Inherently, they are perfect when depicting an overall trend where time-series relationship is shown. Likewise, area charts can intrinsically show volume of trend over time. Yunhai Wang et al., (2018), indicated the importance of using charts, and by extension area charts in visualizing and analysing complex data, and presenting quantitative information to reinforce understanding. Figure 11 and 12 depict line and area charts respectively.

Line chart

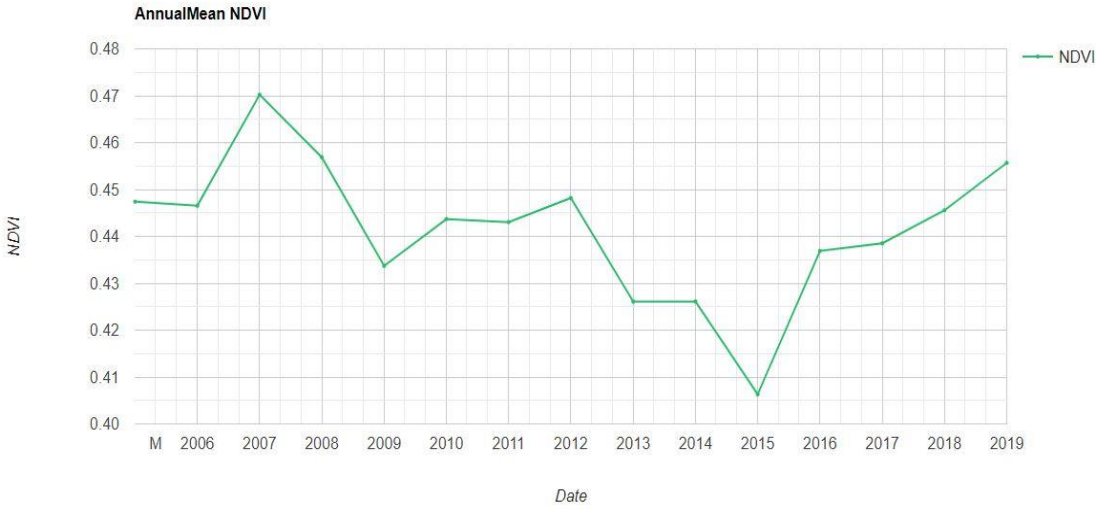

Figure 11: Line chart showing NDVI values

Area chart

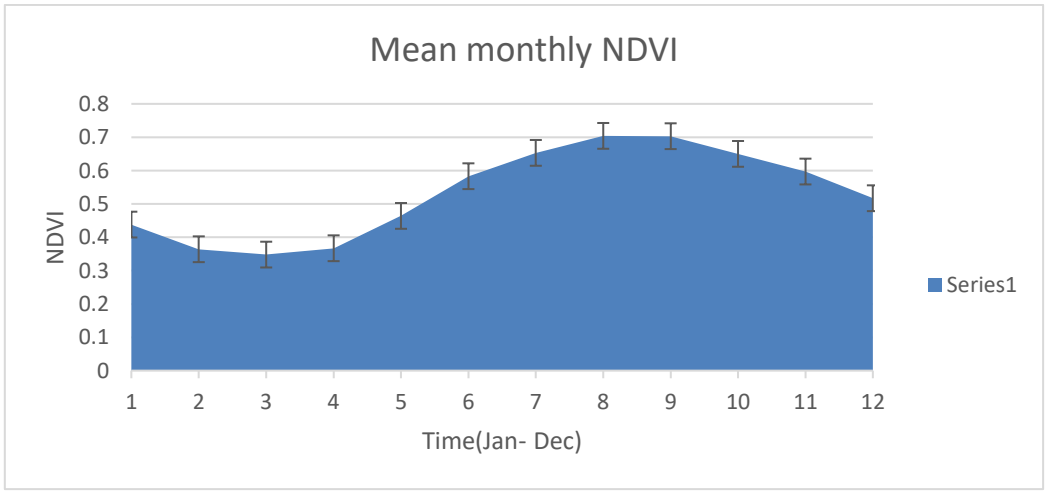

Figure 12: Area chart for visualizing trend

5.3.2. Change

Isopleth map is a visualization technique that aptly suits the visualization of change. It is mostly suited for a data with a continuous distribution. As a result, visualizing change in vegetation can be depicted by an isopleth map. Below is an example isopleth map shown by figure 13.

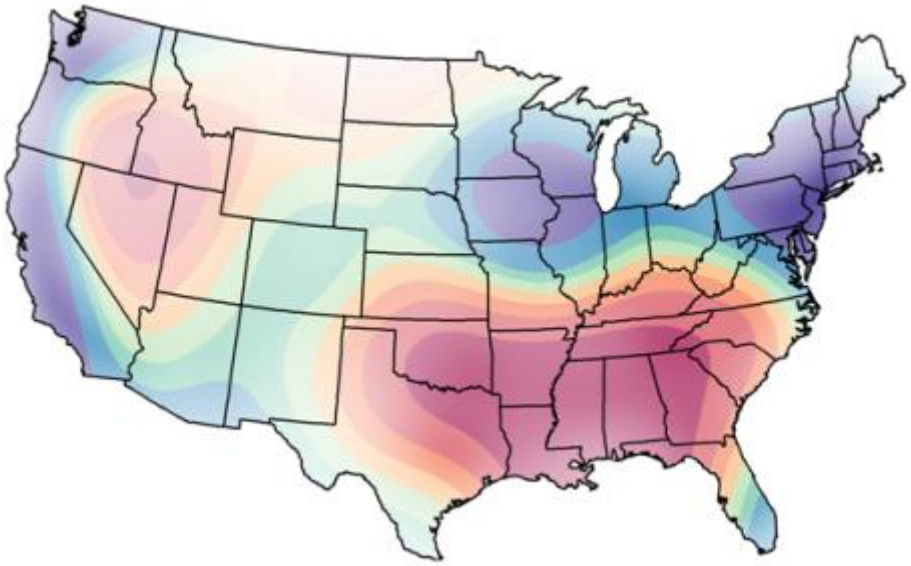

Figure 13: An example of Isopleth map for visualizing change in vegetation

Source: (Bing.com, 2020)

5.3.3. Dynamics

Animation is a visualization technique in representing dynamics that can efficiently serve as an alternative for "small multiple" static maps. Kan & Kan (2017), stated that although animating vegetation dynamics is laborious and tedious work because of its complicated geometry, 2D harmonic based simulation of vegetation dynamics is crucial. This is because it reveals the sequential processes of natural-looking vegetation changes over time. Ultimately, animation shows the details of changes and enables the user to interact with the process of

animation in order to get details. Yunzhe Wang, Baciu, & Li (2019), indicated that using animation to visualize dynamics is an important technique to show comprehensible transformations by which snapshots depict various segments of a change over time. From the advantages of using animation to visualize dynamics, it can therefore help to interact with various layers of a spatio-temporal data accurately and at the same time being a user-friendly. Figure 14 below is a screenshot of animation of a vegetation change over time.

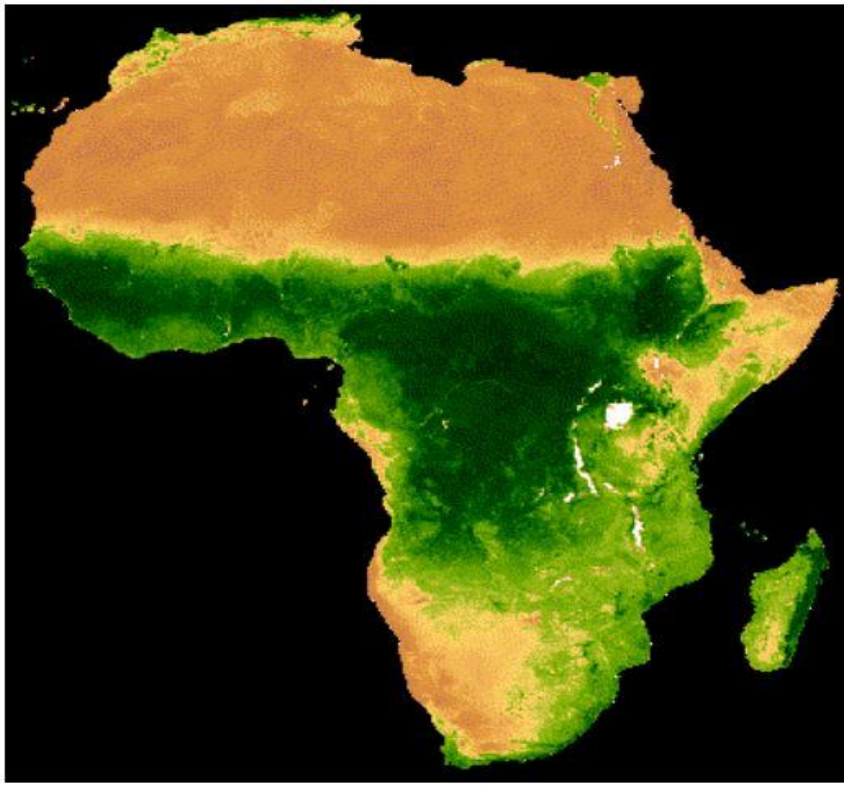

(Engine, 2020)

Figure 14: Screenshot of animation for depicting vegetation dynamics

6. Results and Discussion

6.1. Hot desert climate (BWh)

6.1.1. BWhI

Quantitative changes in vegetation

As shown in figure 15, the mean inter-annual NDVI from 2005 to 2019 follows an erratic trend. From figure 15, no monotonic trend can be found. Rather, from one mean annual NDVI to the other, a "hump curve" is formed in most cases. From figure 15, these trends can be observed; decreasing- increasing, gentle increase and a gradual decreasing trends. For the long term, the standard deviation of the dataset is 0.01 which implies that all the NDVI values within the stipulated period are clustered around the mean such that there is not enough difference between the values recorded. The highest NDVI value recorded was 0.4 in 2014 while the lowest was 0. 3 recorded in 2009. The standard deviation in the NDVI dataset for the long term is the same for the various breakpoints as indicated in table 5. Although the standard deviation for 2012 season is 0.05, it is not high compared to all the values recorded. Interestingly, the linear regression line across the NDVI values depicts an overall increasing trend because the NDVI values are not entirely different from each other except for an outlier recorded in the year 2009.

Correlation

Assessing the relationship between NDVI and other controlling factors especially soil moisture and evapotranspiration is vital in monitoring and mapping vegetation dynamics. In the context of this thesis, the correlation was determined based on the Pearson correlation coefficients. For the long term, there was a weak positive correlation of 0.24 between NDVI and soil moisture. This correlation coefficient, although it is positive, it is also insignificant. However, for the break points, an uphill positive correlation was recorded for two periods; r= 0.69 and 0.55 for 2005-2009 and 2010-2014, respectively. However, there is a significant negative correlation of r = -0.64 for the period from 2015-2019.

This negative correlation gives a different twist for the relationship between NDVI and soil moisture during the period. This can be attributed to the fact that for 2015 and 2017, there was severe drought in the republic of Sudan, which subsequently have ripple effect on the other years hence a negative correlation. Consequently, temperature in the hot climate zone is excessively high and will be exacerbated by drought resulting in the negative correlation. On seasonal basis, the correlation between NDVI and soil moisture is positively significant. Out of the three seasons sampled, only 2012 season has a correlation coefficient of 0.65, while the remaining two seasons of 2015 and 2017 recorded significant positive correlation of 0.93 and 0.88, respectively.

The relationship between NDVI and evapotranspiration, as estimated by Pearson correlation coefficient (PCC) depicts positive correlation for the long term, break points as well as for the seasons. From table 5, there is a strong positive correlation of 0.69 between NDVI and evapotranspiration for the long term. While all the break points recorded positive correlation, the period from 2005-2009 and 2015-2019 depicted significantly strong positive correlations of 0.91 and 0.82 while the period from 2010-2014 has correlation of 0.68 identical to that of the long term. For the seasonal trajectories, there was a perfect or strong significant positive correlation between NDVI and evapotranspiration. For the three seasons, the range of correlation is between 0.90 and 0.96. This range of correlation coefficient depicts a strong positive relationship between the two variables, NDVI and evapotranspiration.

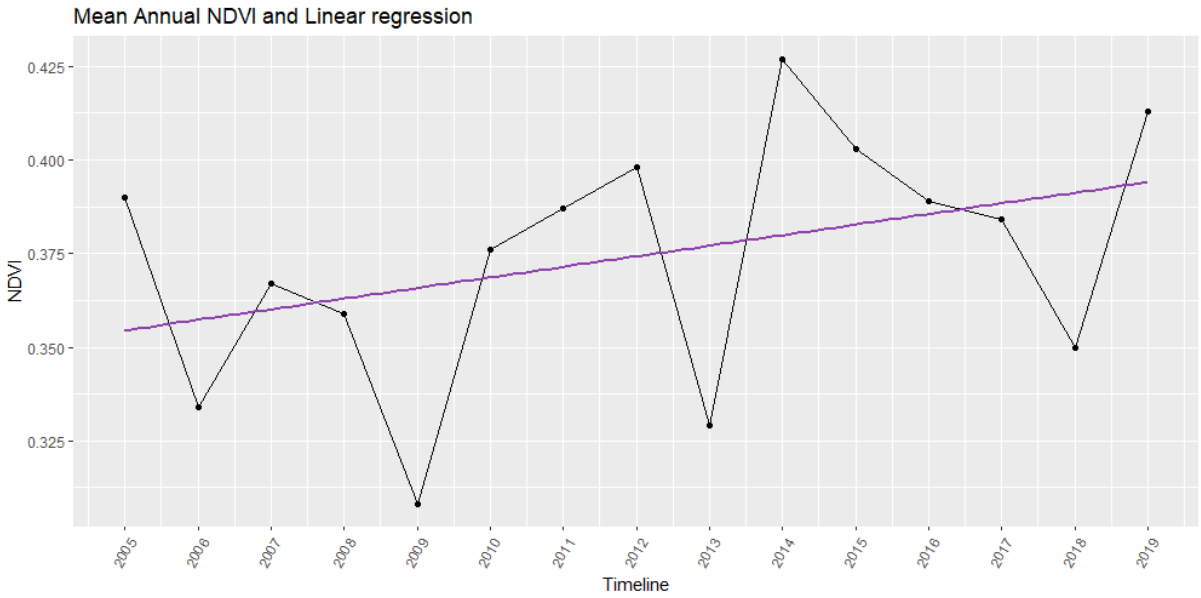

Figure 15: Mean annual NDVI values and linear regression line at BWhI

	Long term	Break Points			Seasonal		
	2005 - 2019	2005-2009	2010 -2014	2015-2019	2012	2015	2017
Standard deviation(NDVI)	0.01	0.01	0.00	0.01	0.05	0.03	0.02
Pearson Correlation (NDVI $ Soil Moisture)	0.24	0.69	0.55	-0.64	0.65	0.93	0.88
Pearson Correlation(NDVI $ Evapotranspiration)	0.69	0.91	0.68	0.82	0.96	0.92	0.90

Table 5: Statistical values for BWhI

Cross correlation and lag

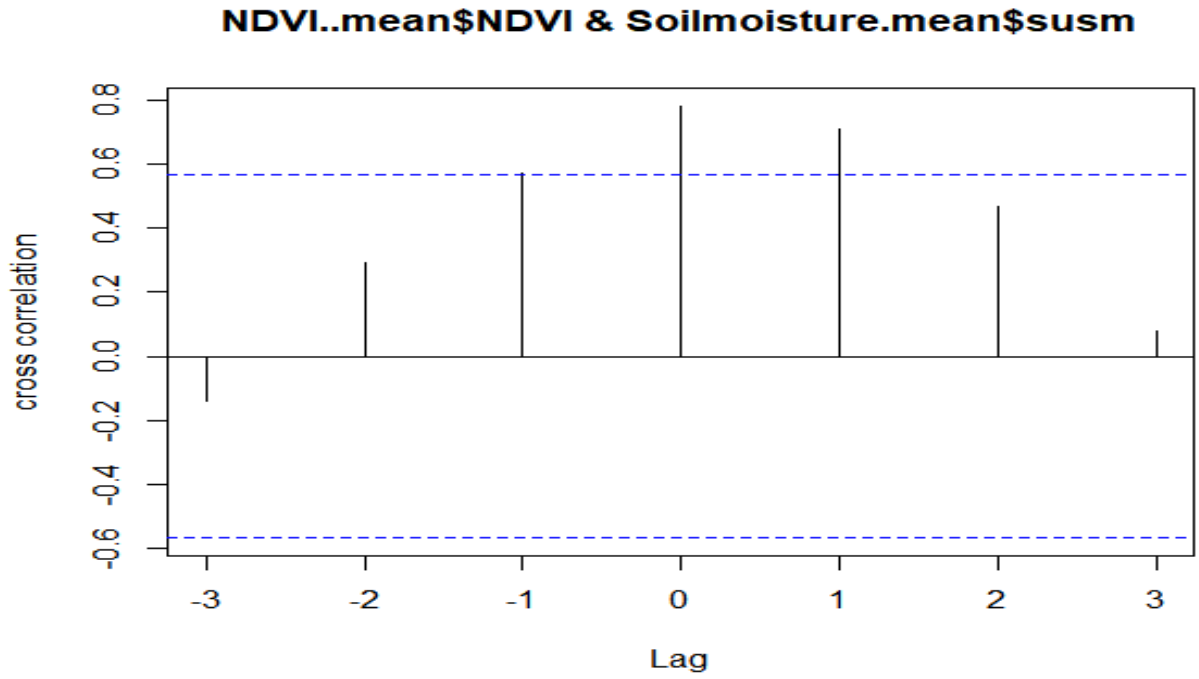

Figure 16: Cross correlation between monthly mean NDVI and Soil moisture

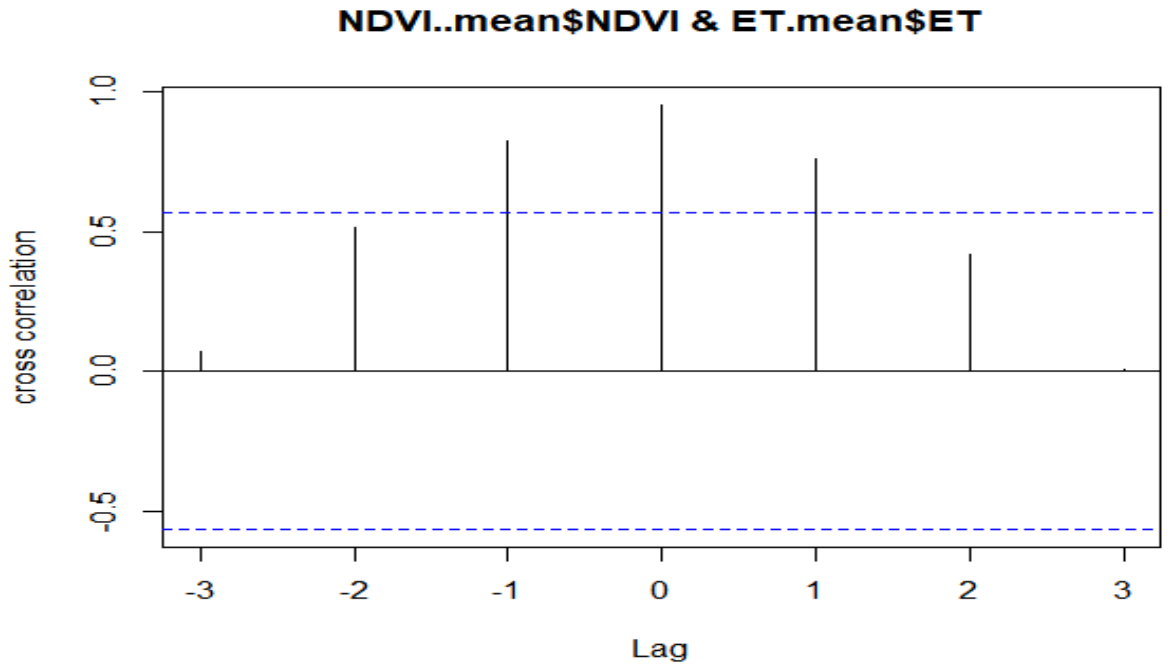

Figure 17: Cross correlation between monthly mean NDVI and evapotranspiration

Map of vegetation dynamics

In this representative case study, cartographic representation of vegetation has been done on yearly basis. Generally, the small multiple static maps here depict high NDVI values corresponding to dense vegetation. However, some years depict an anomaly compared to others. As observed from figure 18, the yearly maps of 2015, 2018 and 2019 have majority of their pixels between -0.1 and 0.2.

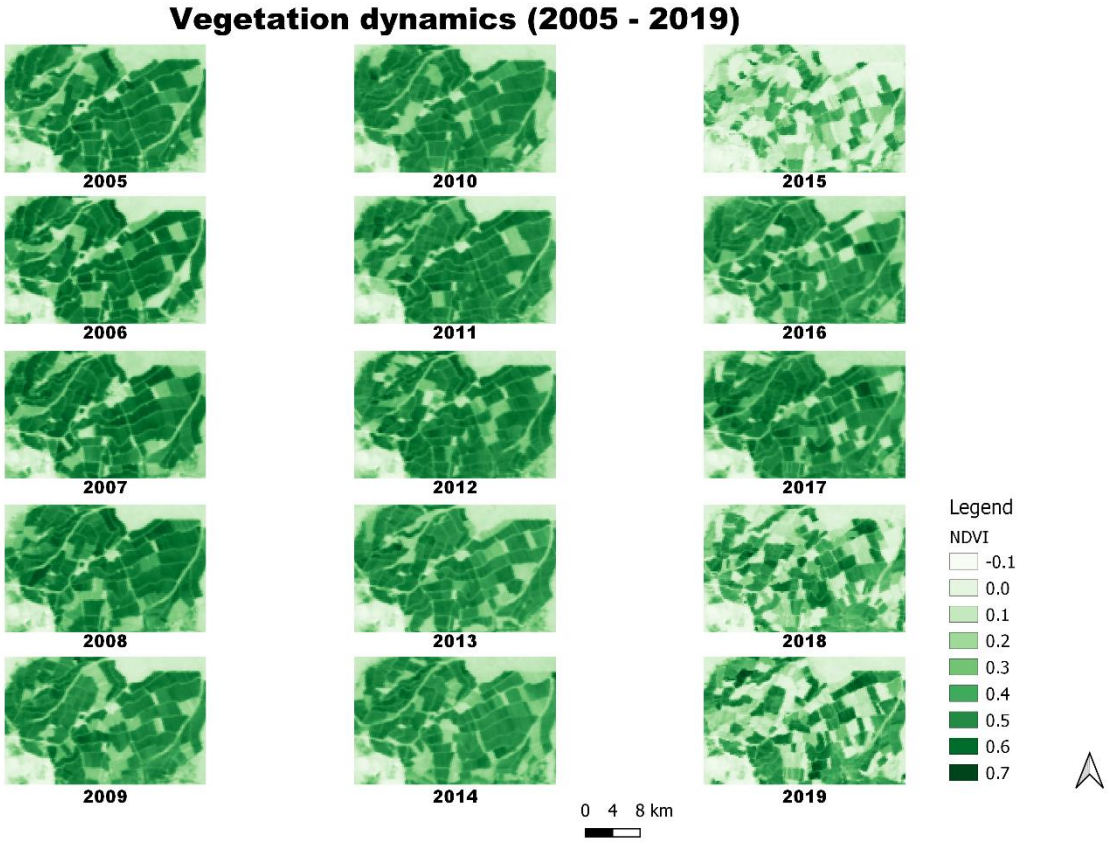

Figure 18: Yearly static maps of vegetation dynamics in BWhI

6.1.2. BWhII

Quantitative changes in vegetation dynamics

From figure 19, the mean inter-annual NDVI from 2005 to 2019 follows a cascading trend. As exhibited by the times series line graph shown by figure 19, no monotonic trend can be found. Rather, from one mean annual NDVI to the other, there is a rise and fall in values. From figure 19, these trends can be observed; increasing-decreasing, gentle increase and gradual decreasing trends. For the long term, the standard deviation of the dataset is 0.01 which implies that all the NDVI values within the stipulated period are clustered around the mean such that there is not enough difference between the values recorded. The highest NDVI value recorded was 0.46 in 2018 while the lowest was 0.40 recorded in 2015. The standard deviation in the NDVI dataset for the long term is similar for the various breakpoints as indicated in table 6. A standard deviation of 0.00, 0.00 and 0.01 corresponding to 2005-2009, 2010-2014 and 2015-2019 respectively were recorded. On seasonal basis, standard deviations of 0.07, 0.02 and 0.05 were for 2012, 2015 and 2017 were recorded. Interestingly, the linear regression line across the NDVI values depicts an overall increasing trend because the NDVI values are not entirely different from each other except for an outlier recorded in the year 2015.

Correlation

The relationship between NDVI and other controlling factors especially soil moisture and evapotranspiration is important in vegetation studies. In the context of this thesis, the correlation was determined based on the Pearson correlation coefficients. For the long term, there was a weak negative correlation of -0.47 between NDVI and soil moisture. However, for the break points, a weak positive correlation was recorded for 2005-2009; r= 0.12 while for 2010-2014, a strong negative correlation; r= - 0.73 as well as a weak negative correlation; r= -0.46 for 2015-2019 were recorded respectively. This negative correlations give a different twist for the relationship between NDVI and soil moisture during the two consecutive break points which succinctly suggests that increase or decrease in NDVI values during these breakpoints

are independent of soil moisture. On seasonal basis, the correlation between NDVI and soil moisture is positive. Out of the three seasons sampled, only 2012 season has a correlation coefficient of 0.61 while the remaining two seasons of 2015 and 2017 recorded weak positive correlation of 0.42 and 0.35 respectively.

The relationship between NDVI and evapotranspiration as estimated by Pearson correlation coefficient (PCC) depicts positive correlation for the long term, break points as well as for the seasons. From table 6, there is a strong positive correlation of 0.66 between NDVI and evapotranspiration for the long term. For the break points, there was a weak negative correlation of -0.03 for 2010-2014 while 2005-2009 and 2015-2019 depicted significantly strong positive correlations of 0.60 and 0.94. For the seasonal trajectories, there was a perfect or strong significant positive correlation between NDVI and evapotranspiration. For the three seasons, the correlation coefficients are 0.99, 0.70 and 0.99 for 2012, 2015 and 2017 respectively. These range of correlation coefficients depicts a strong positive relationship between the two variables, NDVI and evapotranspiration.

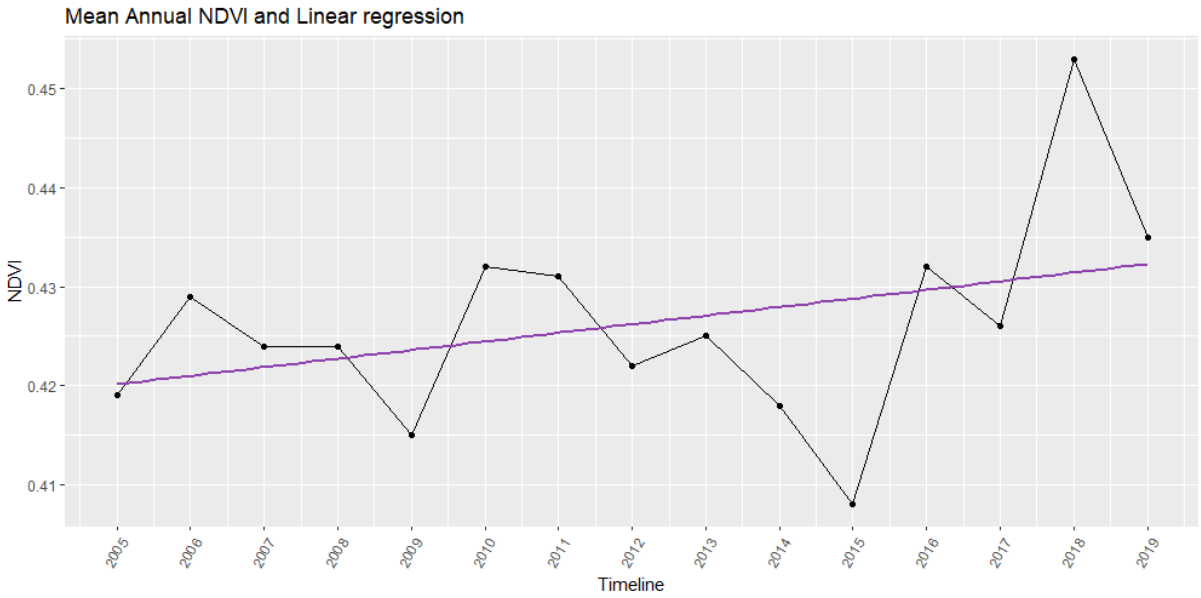

Figure 19: Mean annual NDVI values and linear regression line at BWhII

	Long term	Break Points			Seasonal		
	2005 - 2019	2005-2009	2010 -2014	2015-2019	2012	2015	2017
Standard deviation(NDVI)	0.01	0.00	0.00	0.01	0.07	0.02	0.05
Pearson Correlation (NDVI $ Soil Moisture)	-0.47	0.12	-0.73	-0.46	0.61	0.42	0.35
Pearson Correlation(NDVI $ Evapotranspiration)	0.66	0.60	-0.03	0.94	0.99	0.70	0.99

Table 6: Statistical values at BWhII

Cross-correlation and lag

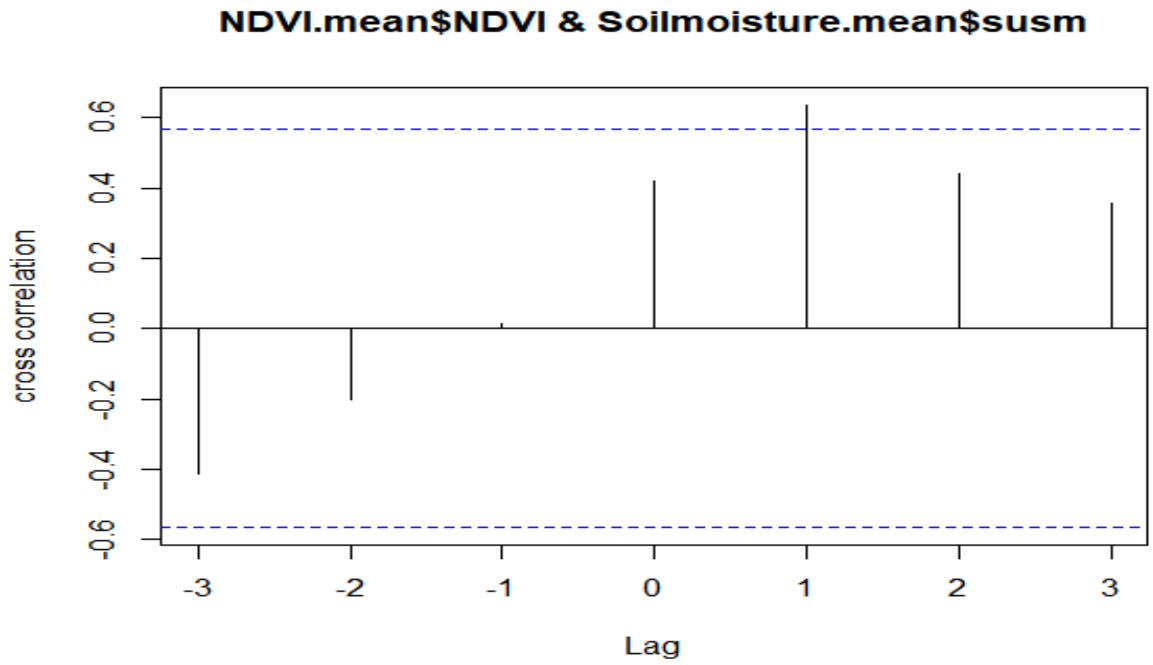

Figure 20: Cross correlation between monthly mean NDVI and soil moisture at BWhII

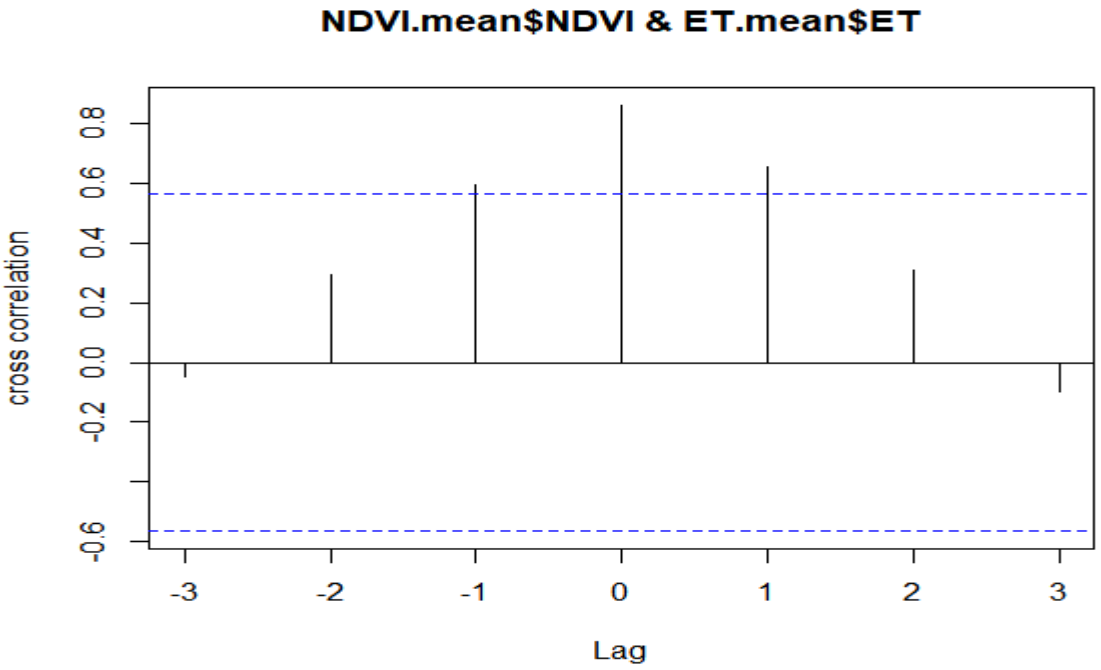

Figure 21: Cross correlation between monthly mean NDVI and evapotranspiration at BWhII

Map of vegetation dynamics

Vegetation dynamics in the context of this representative case study is cartographically represented based on the rainy season. The climate zone within which this area falls has a rainy season from July to September, hence, the monthly vegetation maps from July to September. From figure 22, the monthly vegetation maps of 2015 season are comparatively the same compared to that of 2017. Similarly, in 2017, August recorded high NDVI values compared to July and September.

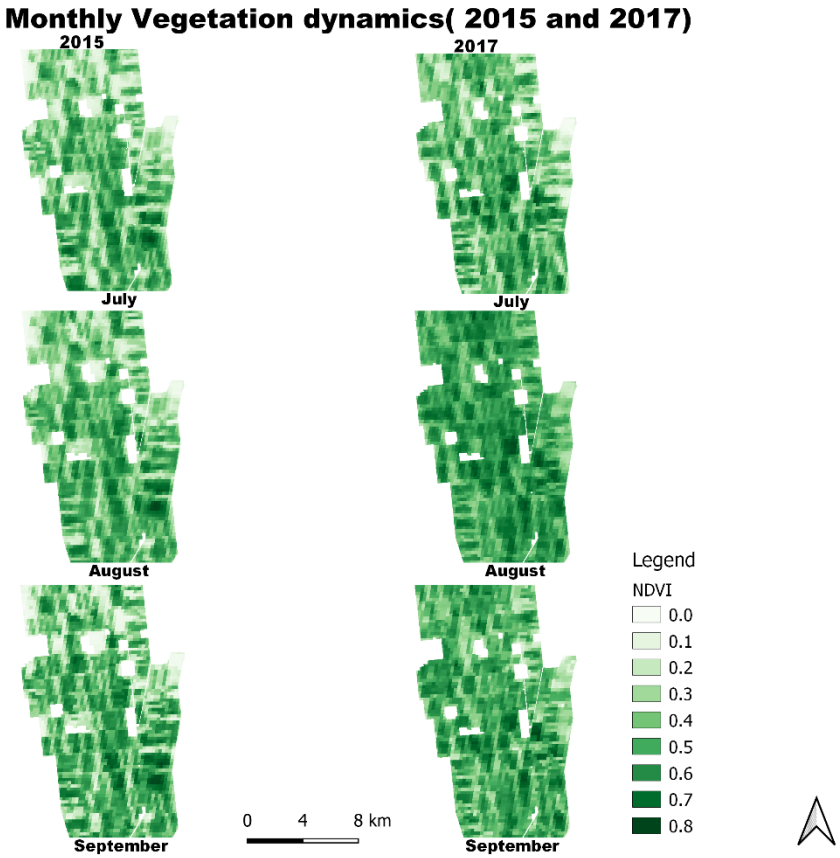

Figure 22: Monthly static maps of vegetation dynamics at BWhII

6.1.3. BWhIII

Quantitative changes in vegetation

In figure 23, the mean inter-annual NDVI from 2005 to 2019 were presented. From figure 23, the trend follows an upward and downward trend. From one mean annual NDVI to the other, a "cascading trend" can be seen. For the long term, the standard deviation of the dataset is 0.01 which implies that all the NDVI values within the stipulated period are clustered around the mean such that there is not enough difference between the values recorded. The standard deviation in the NDVI dataset is the same for the various breakpoints as indicated in table 7. A standard deviation of 0.01 has been recorded for all the breakpoints. On Seasonal basis, standard deviations of 0.06, 0.04 and 0.03 were recorded in 2012, 2015 and 2017 respectively. Interestingly, the linear regression line across the NDVI values as shown in figure 23, points out a general decreasing trend.

Correlation

In the context of this thesis, the correlation between NDVI and soil moisture was computed based on the Pearson correlation coefficients. For the long term, there was a weak positive correlation of 0.34 between NDVI and soil moisture. This correlation coefficient, although it is positive but it is insignificant. However, for the break points, an uphill positive correlation of 0.90 was recorded for the 2005-2009 period while the succeeding periods; 2010-2014 and 2015-2019 NDVI were negatively correlated with soil moisture with coefficients; -0.77 and -0.80 respectively. On seasonal basis, the correlation between NDVI and soil moisture were positively correlated. All the three seasons sampled have a correlation coefficient of 0.81, 0.99 and 0.82 respectively.

The relationship between NDVI and evapotranspiration as estimated by Pearson correlation coefficient (PCC) depicts positive correlation for the long term, break points as well as for the seasons. From table 7, there is a strong positive correlation of 0.82 between NDVI and evapotranspiration for the long term. Similarly, all the break points recorded strong positive correlations of 0.97, 0.84 and 0.98 respectively. For the seasonal trajectories, there were perfect or strong significant positive correlation between NDVI and evapotranspiration. The correlation coefficients of these three seasons are 0.90, 0.98 and 0.99 for 2012, 2015 and 2017 respectively. These correlation coefficients aptly show a strong positive relationship between the two variables, NDVI and evapotranspiration during the seasons.

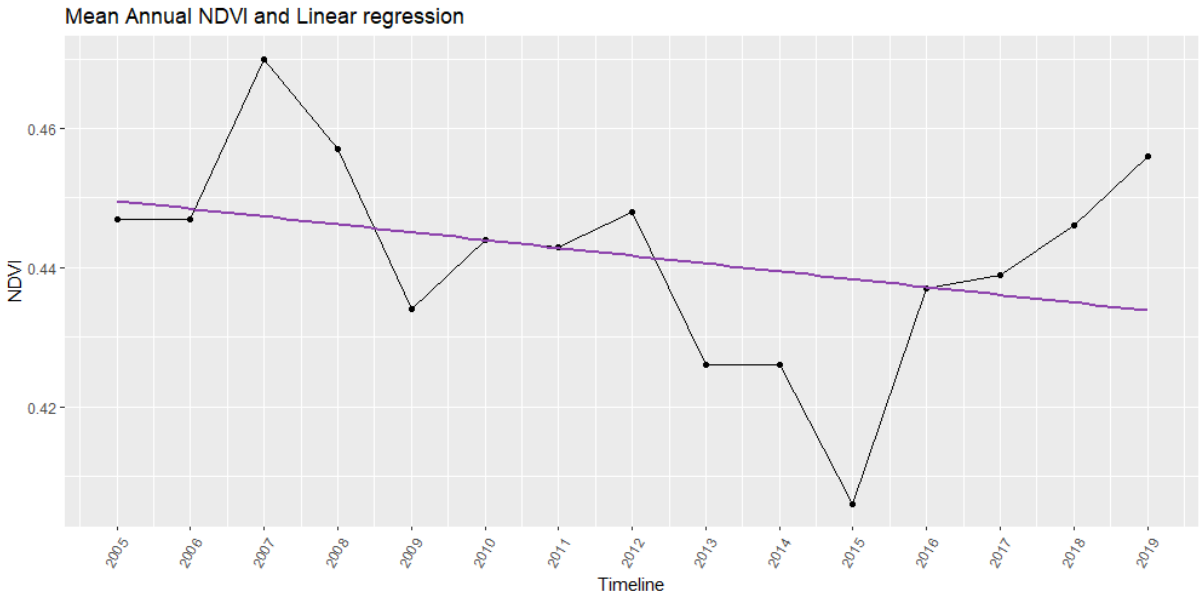

Figure 23: Mean annual NDVI and linear regression at BWhIII

	Long term	Break Points			Seasonal		
	2005 - 2019	2005-2009	2010 -2014	2015-2019	2012	2015	2017
Standard deviation(NDVI)	0.01	0.01	0.01	0.01	0.06	0.043	0.03
Pearson Correlation (NDVI $ Soil Moisture)	0.34	0.90	-0.77	-0.80	0.81	0.99	0.82
Pearson Correlation(NDVI $ Evapotranspiration)	0.82	0.97	0.84	0.98	0.90	0.98	0.99

Table 7: Statistical values at BWhIII

Cross correlation and lag

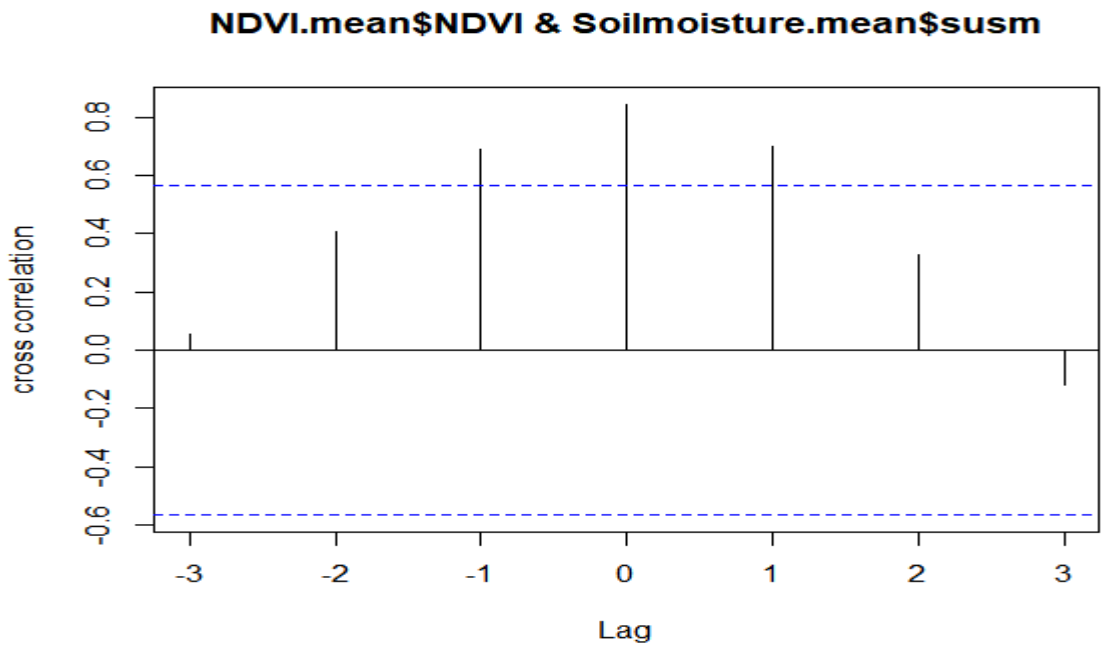

Figure 24: Cross correlation between mean monthly NDVI and soil moisture at BWhIII

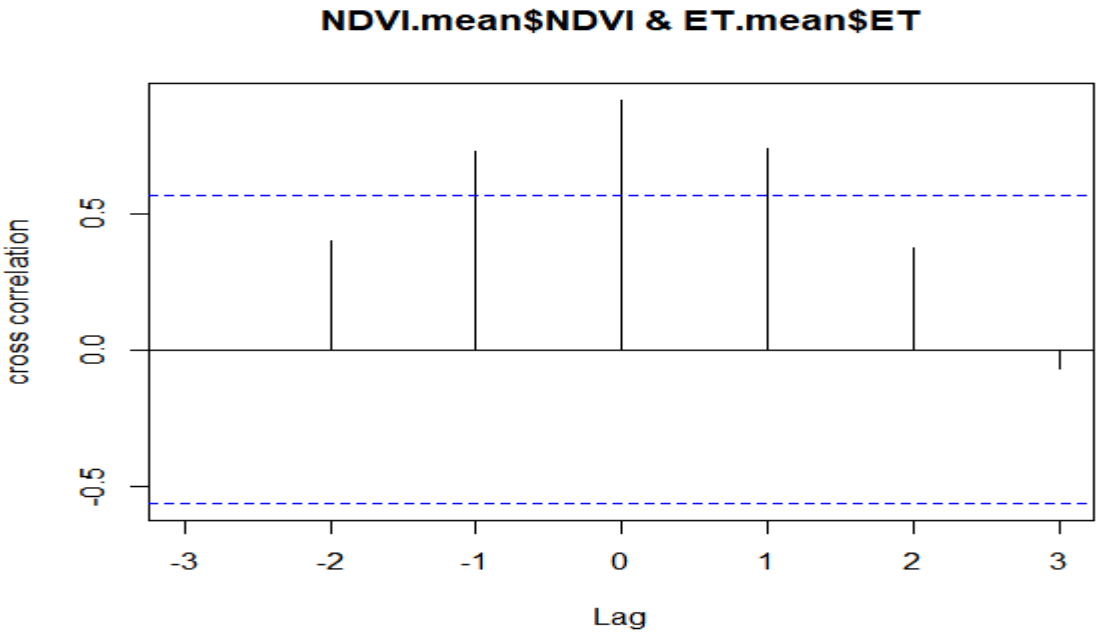

Figure 25: Cross correlation between monthly mean NDVI and evapotranspiration at BWhIII

Map of vegetation dynamics

In figure 26 below, the yearly vegetation maps have been depicted as small multiples. As observed from the maps, there are no significant variations in vegetation for the years covered. As shown in the maps, only minor variations can be seen. For example, in the years 2006, 2007, 2011 and 2012 few pixels of the area covered depicts low NDVI representing vegetation minor decline.

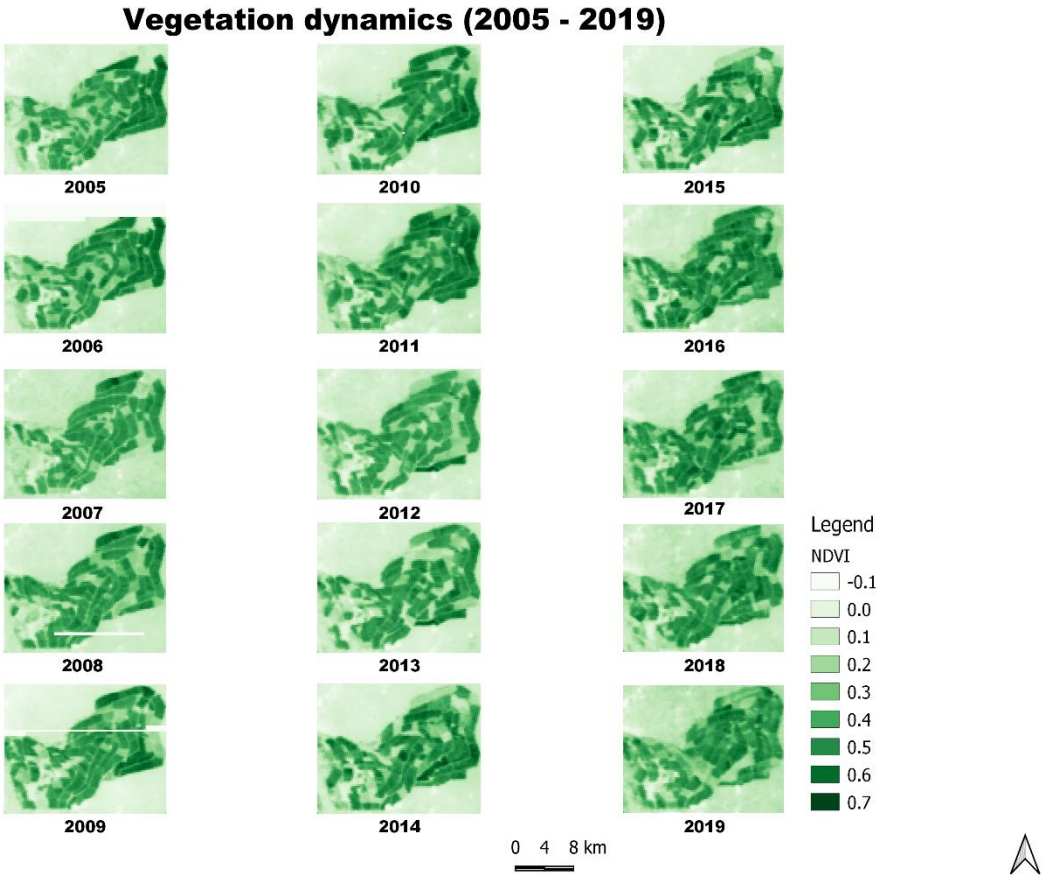

Figure 26: Yearly static maps of vegetation dynamics in BWhIII

6.2. Hot semi-arid climate (BSh)

6.2.1. BShI

Quantitative changes in vegetation

As shown in figure 27 below, the mean inter-annual NDVI from 2005 to 2019 follows a continuously changing trend. Significantly, no monotonic trend can be found. Rather, from one mean annual NDVI to the other, “decreasing-increasing” were recognized in most cases. From table 8, the standard deviation for the long term is 0.02 which implies that all the NDVI values within the stipulated period are clustered around the mean such that there is not enough difference between the values recorded. A standard deviation of 0.01, 0.01 and 0.04 corresponding to 2005-2009, 2010-2014 and 2015-2019 were recorded. On Seasonal basis, the low standard deviations of 0.1, 0.15 and 0.12 were recorded in 2012, 2015 and 2017 seasons. Generally, the linear regression line across the NDVI values as shown in figure 27 depicts an overall increasing trend.

Correlation

Assessing the relationship between NDVI and other controlling factors especially soil moisture and evapotranspiration plays a key role in mapping vegetation dynamics and analysing the results. In the context of this thesis, the correlation was calculated based on the Pearson correlation coefficients. For the long term, there was a weak positive correlation of 0.31 between NDVI and soil moisture. This correlation coefficient, although positive, shows a weak relationship between NDVI and evapotranspiration. However, for the break points, an uphill positive correlation was recorded for two periods; r= 0.77 and 0.96 for 2005-2009 and 2015-2019 respectively. However, for 2010-2014, a weak positive correlation of r = 0.48 was recorded. On seasonal basis, positive correlations were recorded as presented in table 8.

The relationship between NDVI and evapotranspiration as estimated by Pearson correlation coefficient (PCC) depicts positive correlation for the long term, break points as well as for the seasons. From table 8, there is a strong positive correlation of 0.89 between NDVI

and evapotranspiration for the long term. While all the break points recorded positive correlation, the period from 2005-2009 depicted a weak positive correlation, while the relationship between NDVI and evapotranspiration for 2010-2014 and 2015-2019 showed significantly strong positive correlations of 0.91 and 0.98. For the seasonal trajectories, there was a perfect or strong significant positive correlation between NDVI and evapotranspiration from 0.94 to 0.96.

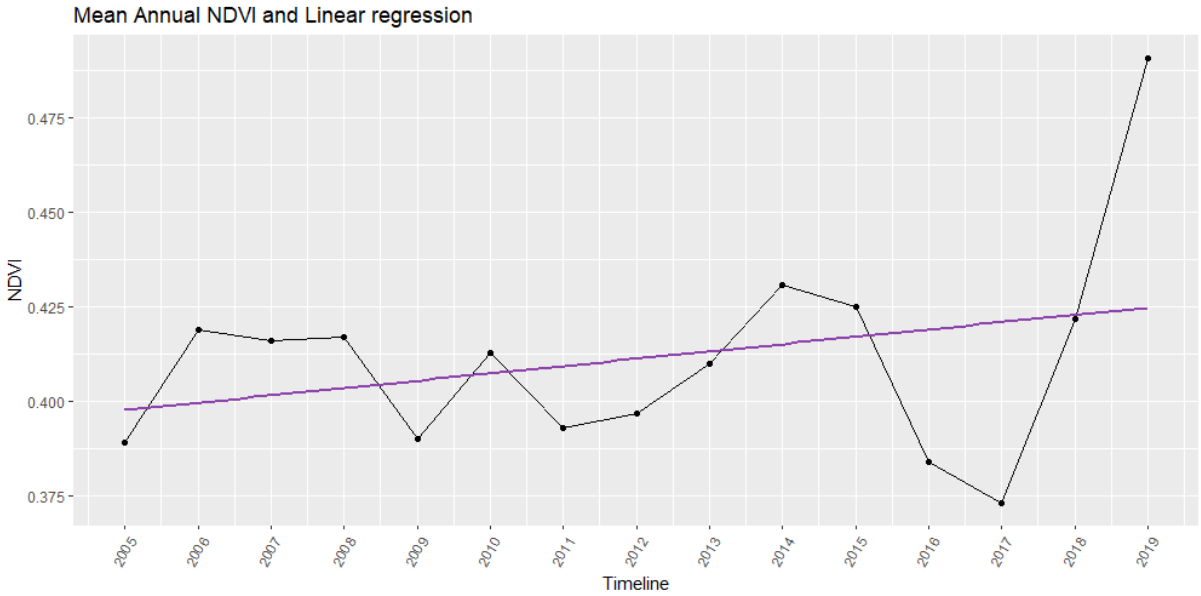

Figure 27: Mean annual NDVI and linear regression at BShI

	Long term	Break Points			Seasonal		
	2005 - 2019	2005-2009	2010 -2014	2015-2019	2012	2015	2017
Standard deviation(NDVI)	0.02	0.01	0.01	0.04	0.13	0.15	0.12
Pearson Correlation (NDVI $ Soil Moisture)	0.31	0.77	0.48	0.96	0.90	0.95	0.88
Pearson Correlation(NDVI $ Evapotranspiration)	0.89	0.44	0.91	0.98	0.94	0.94	0.96

Table 8: Statistical values at BShI

Cross correlation and lag

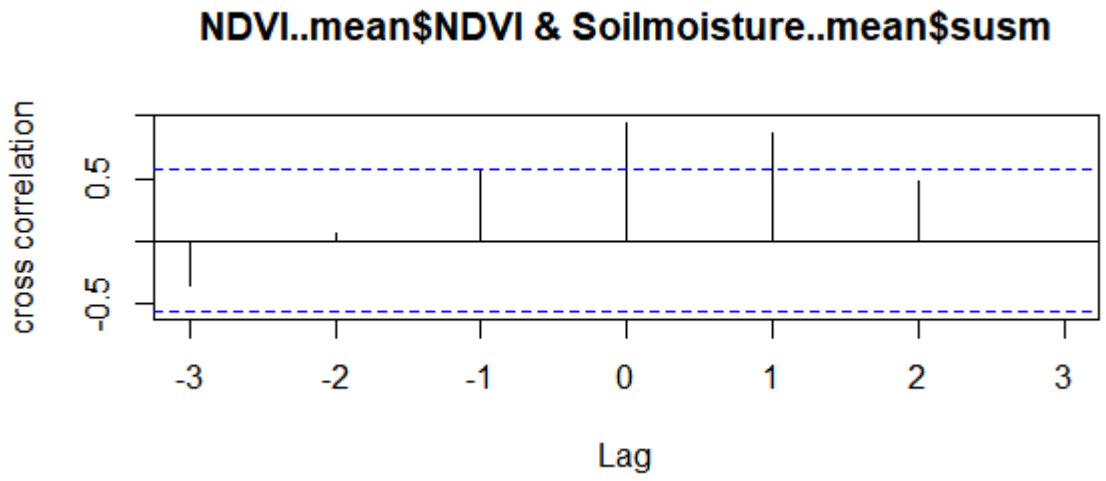

Figure 28: Cross correlation between monthly mean NDVI and soil moisture at BShI

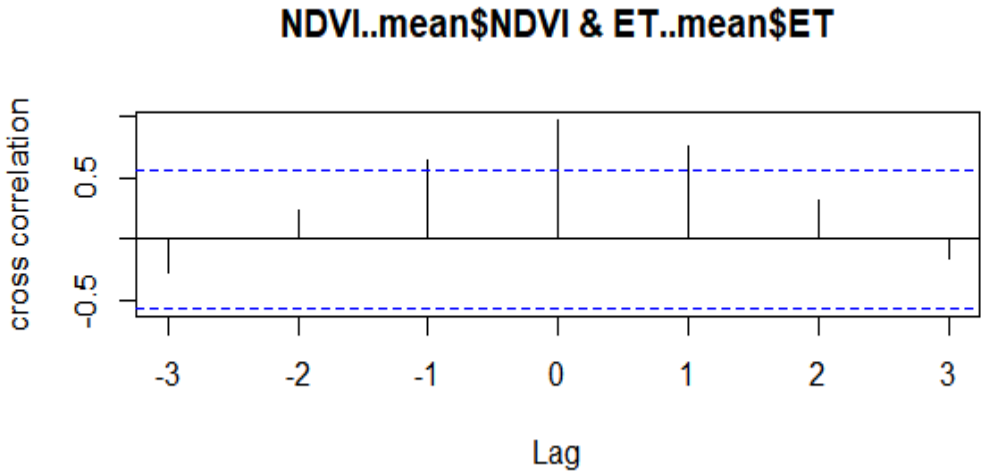

Figure 29: Cross correlation between monthly mean NDVI and evapotranspiration at BShI

Map of vegetation dynamics

To understand and visualize the dynamics of seasonal vegetation change, the case study delineated on the Nuba mountains take into account the seasonal trajectory of two years; 2015 and 2017. This seasonal trajectory has been disaggregated into months that make up the rainy season. In figure 30 and 31, the monthly vegetation maps for the 2015 and 2017 rainy seasons were depicted. Generally, the maps show moderate to dense vegetation from May to October. However, from figure 31 it can be observed that both June and July have more pixels with NDVI values between 0.2 and 0.4. It is worth noting that although 2015 and 2017 are years where drought was reported in Sudan, the monthly vegetation as shown in the maps were proportionally high.

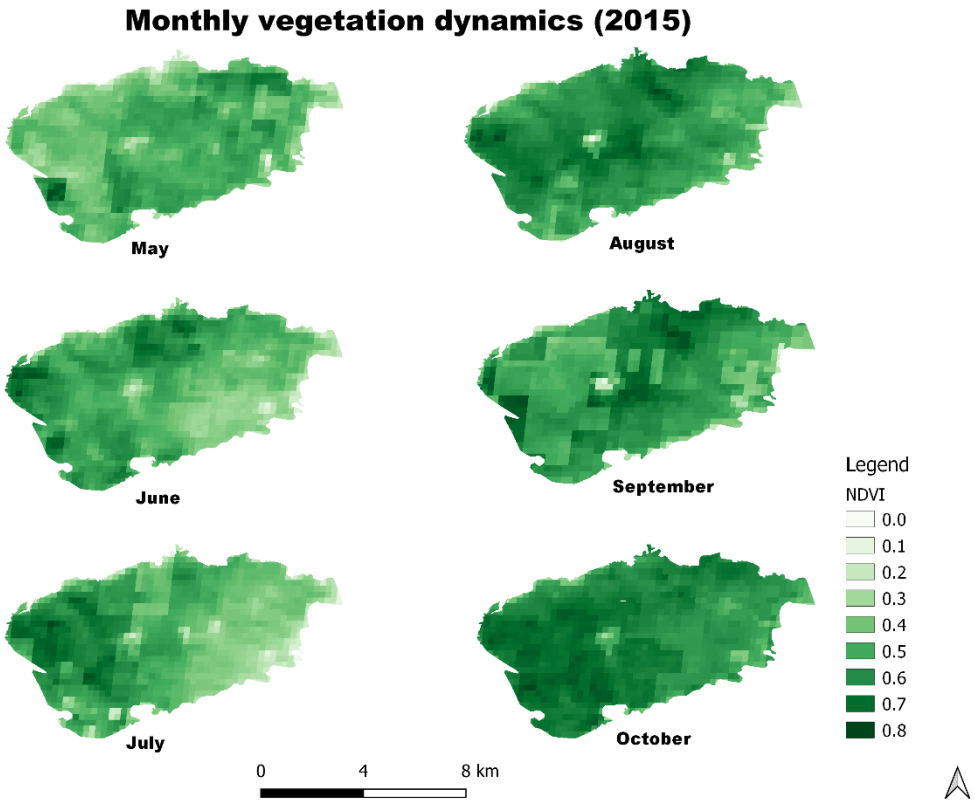

Figure 30: Monthly vegetation dynamics at BShI, 2015 (May - October)

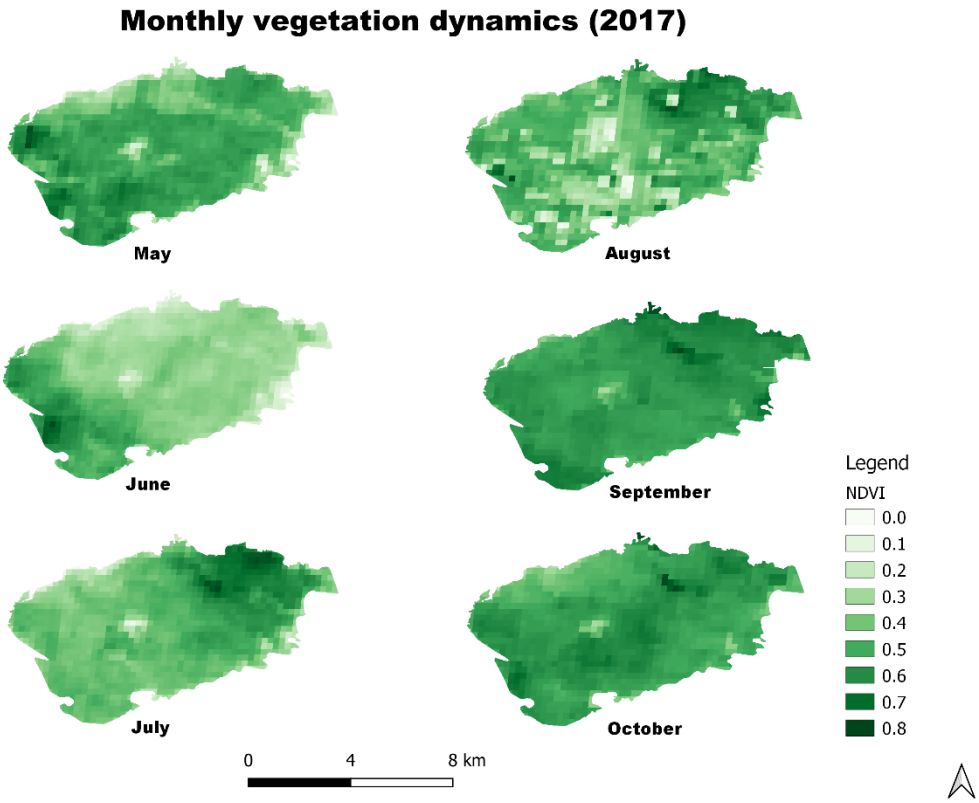

Figure 31: Monthly vegetation dynamics at BShI, 2017 (May - October)

6.2.2. BShII

Quantitative changes in vegetation

As shown in figure 32 below, the mean inter-annual NDVI from 2005 to 2019 follows an erratic trend similar to the other representative case studies. From figure 32, no monotonic trend can be found. Rather, from one mean annual NDVI to the other, there are sharp increases and decreases. The mean NDVI values are generally low in this representative case study such that the highest value recorded in 2018 is below 0.3. For the long term, the standard deviation of the dataset is 0.02. On seasonal basis, the concentration of NDVI values around the mean

remains fairly the same as shown by the standard deviations of 0.16, 0.10 and 0.09 for 2012, 2015 and 2017 seasons. Although the NDVI values in this representative case study are generally low, the linear regression line across the NDVI values depicts an overall increasing trend as can be seen in figure 32.

Correlation

In this climate zone, the relationship between NDVI and other controlling factors especially soil moisture and evapotranspiration is vital for assessing how vegetation changes over time. In the context of this thesis, the relationship was calculated using the Pearson correlation. For the long term, there was a weak negative correlation of -0.40 between NDVI and soil moisture. However, for the break points, positive correlation was recorded for 2005-2009 and 2010-2014 respectively. However, there is negative correlation of r = -0.46 for the period from 2015-2019. On seasonal basis, the correlation between NDVI and soil moisture were positive for 2015 and 2017 but negative for the year 2012.

The relationship between NDVI and evapotranspiration as estimated by Pearson correlation coefficient (PCC) depicts a positive correlation for the long term, break points as well as for the seasons. From table 9, there is a strong positive correlation of 0.88 between NDVI and evapotranspiration for the long term. Similarly, all the break points recorded positive correlation of 0.95, 0.94 and 0.93. For the seasonal trajectories, there were positive correlations recorded as well as shown in table 9.

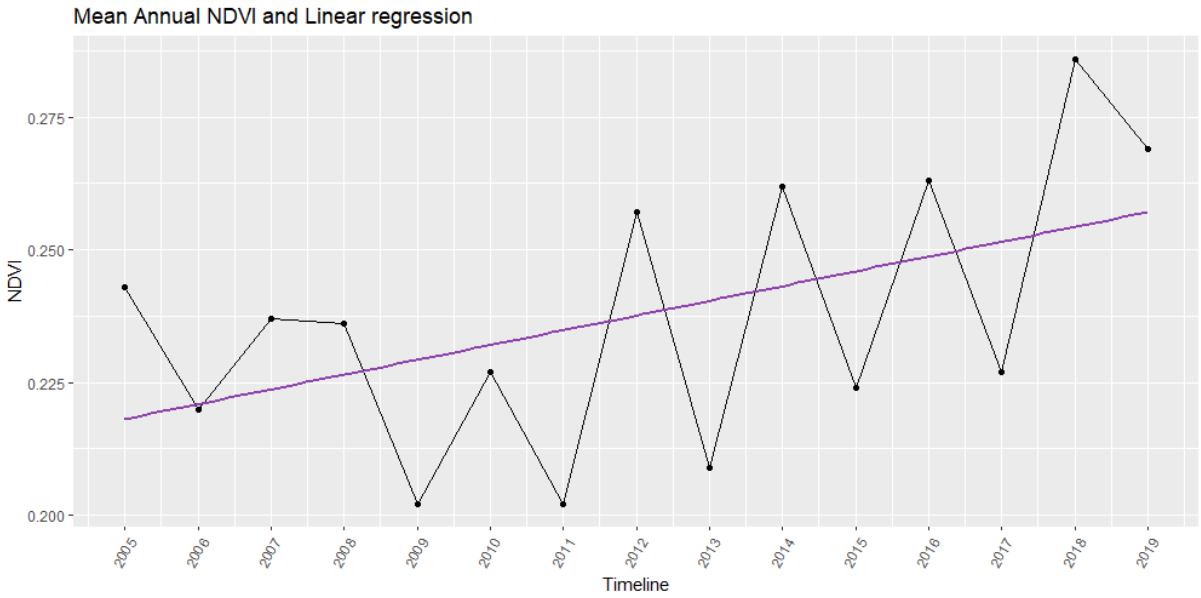

Figure 32: Mean annual NDVI and linear regression at BShII

	Long term	Break Points			Seasonal		
	2005 - 2019	2005-2009	2010 -2014	2015-2019	2012	2015	2017
Standard deviation(NDVI)	0.02	0.01	0.02	0.02	0.16	0.10	0.09
Pearson Correlation (NDVI $ Soil Moisture)	-0.40	0.65	0.49	-0.46	0.48	0.61	0.50
Pearson Correlation(NDVI $ Evapotranspiration)	0.88	0.95	0.94	0.93	0.81	0.86	0.74

Table 9: Statistical values at BShII

Cross correlation and lag

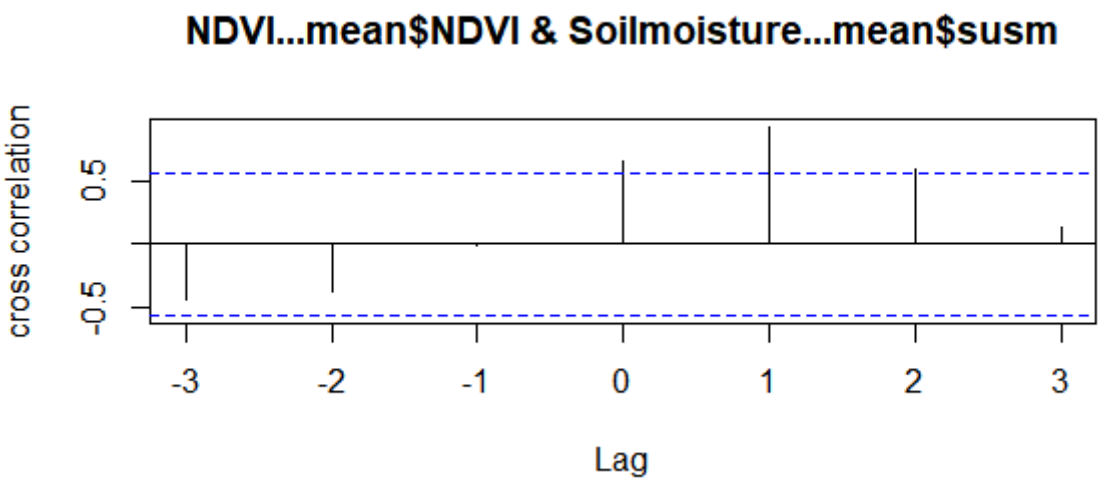

Figure 33: Cross correlation between monthly mean NDVI and soil moisture in BShII

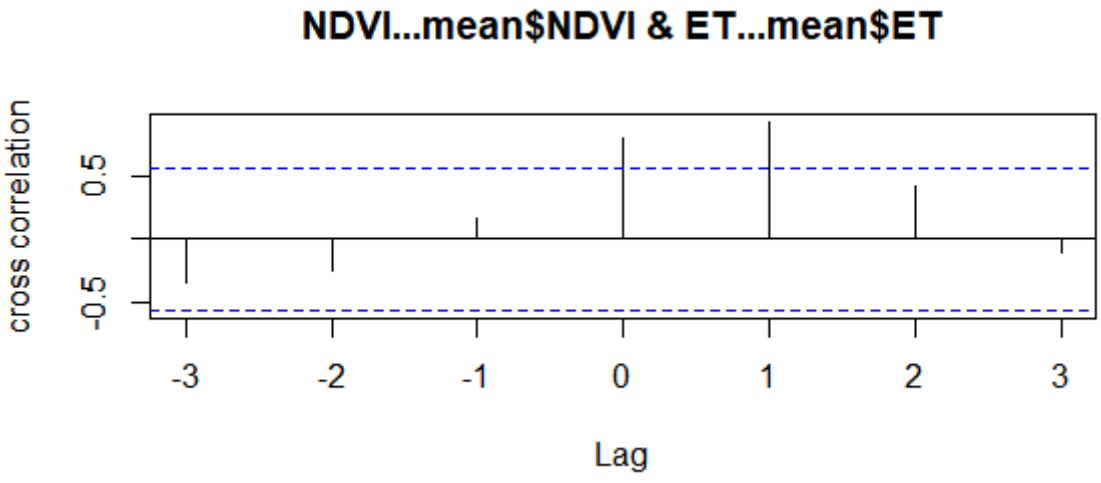

Figure 34: Cross correlation between mean monthly NDVI and evapotranspiration

Map of vegetation dynamics

Figure 35 below shows the yearly vegetation maps of BShII, a popular rain-fed farming site in Al- Qadarif. From the maps, vegetation across this case study is generally low. The maps depict NDVI values within a range of -0.1 to 0.2. Besides the NDVI range generally shown in the maps, a greater part of the area disproportionately show vegetation decline over the years. This arguably is as a result of continuous farming taking place in the site which is mostly dependent on rainfall. Also, the farm area is continuously cleared of natural vegetation "weeds" and the fields prepared for farming. Hence, this area is generally expected to show low NDVI values.

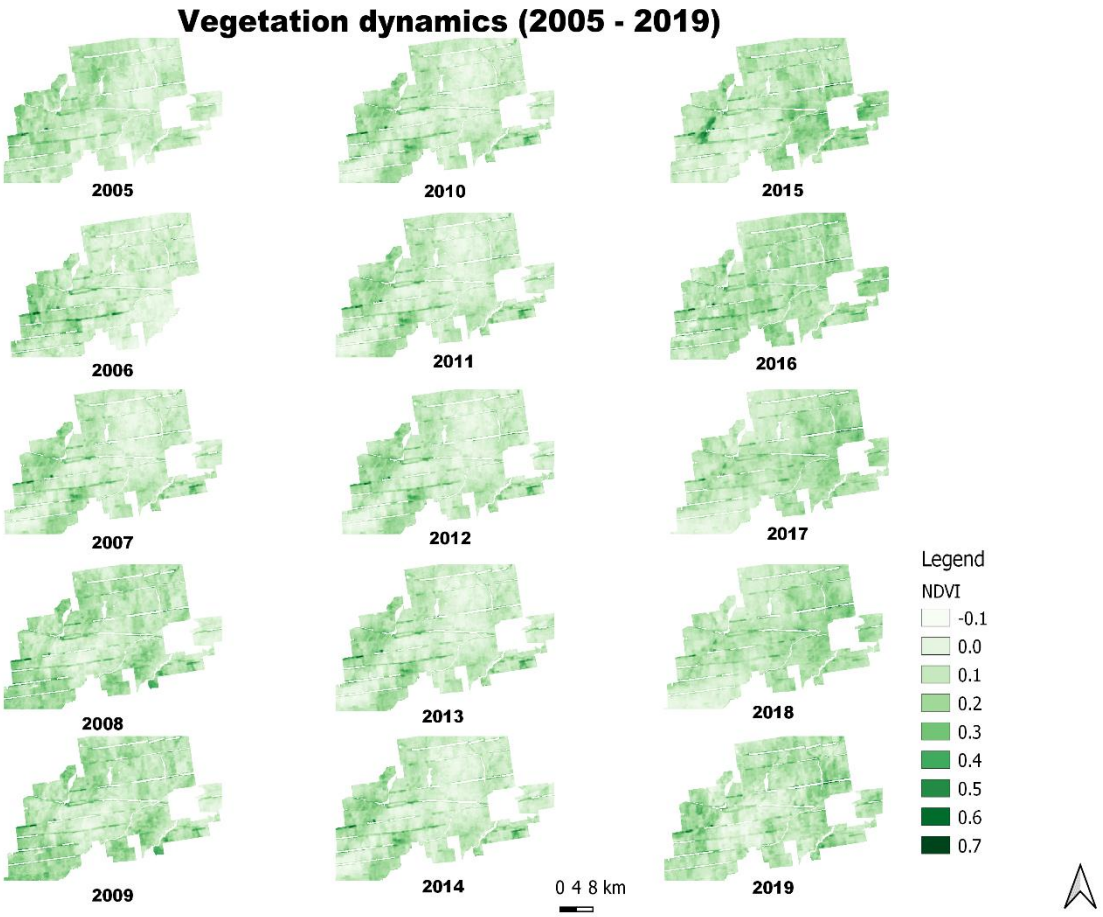

Figure 35: Yearly static maps of vegetation dynamics in BShII

6.2.3. BShIII

Quantitative changes in vegetation dynamics

In figure 36, the mean inter-annual NDVI from 2005 to 2019 has been graphically depicted. From figure 36, no monotonic trend can be found. Rather, from one mean annual NDVI to the other, "changing trends" have been observed. For the long term, the standard deviation of the dataset is 0.03. A standard deviation of 0.03, 0.03 and 0.02 corresponding to 2005-2009, 2010-2014 and 2015-2019 respectively were obtained. Generally, the linear regression line across the NDVI values shows an overall increasing trend.

Correlation

In the context of this thesis, the correlation between NDVI and other controlling factors have been calculated based on Pearson correlation coefficients. For the long term, there was a weak negative correlation of -0.18 between NDVI and soil moisture. In the case of the break points, moderate positive correlations were recorded. On seasonal basis, the correlation between NDVI and soil moisture were positively significant as well. Out of the three seasons sampled, 2012 and 2015 seasons had strong positive coefficient while 2017 season had a moderate positive correlation.

The relationship between NDVI and evapotranspiration as estimated by Pearson correlation coefficient (PCC) did not deviate from the earlier results obtained in other representative case studies. From table 10, positive correlations were recorded between NDVI and evapotranspiration for the long term, break points and the sampled seasons. However, for the 2010-2014 and 2015-2019 breakpoints, the correlations were very weak.

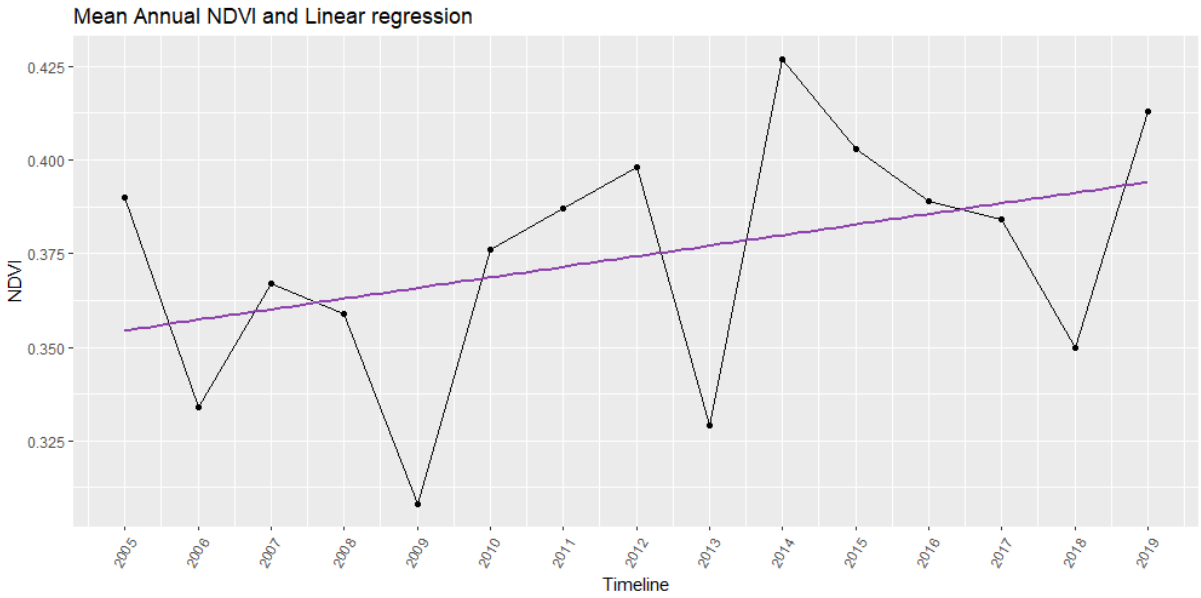

Figure 36: Mean Annual NDVI and linear regression at BShII

	Long term	Break Points			Seasonal		
	2005 - 2019	2005-2009	2010 -2014	2015-2019	2012	2015	2017
Standard deviation(NDVI)	0.03	0.03	0.03	0.02	0.18	0.21	0.24
Pearson Correlation (NDVI $ Soil Moisture)	-0.18	0.50	0.65	0.69	0.96	0.79	0.67
Pearson Correlation(NDVI $ Evapotranspiration)	0.59	0.71	0.33	0.20	0.95	0.87	0.97

Table 10: Statistical values at BShIII

Cross correlation and lag

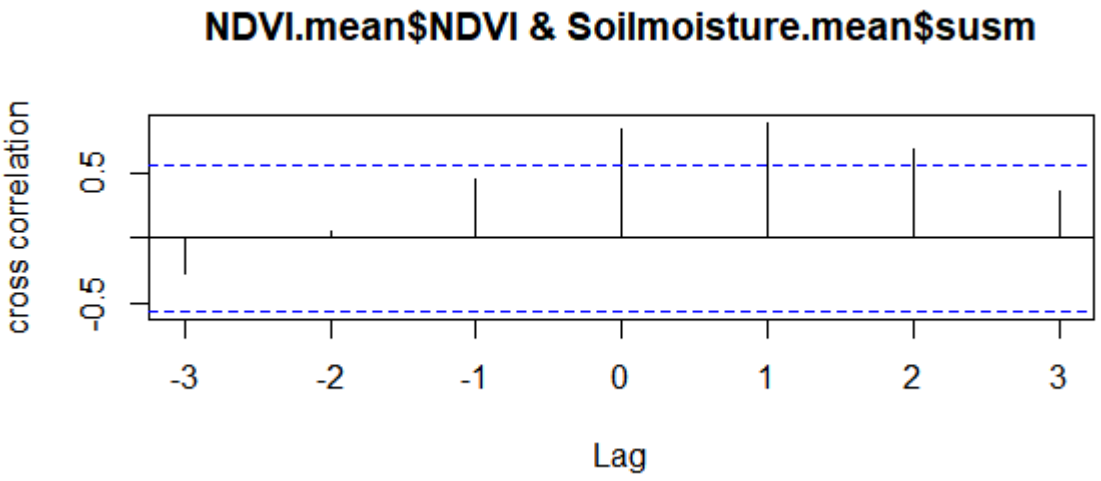

Figure 37: Cross correlation between mean monthly NDVI and soil moisture at BShIII

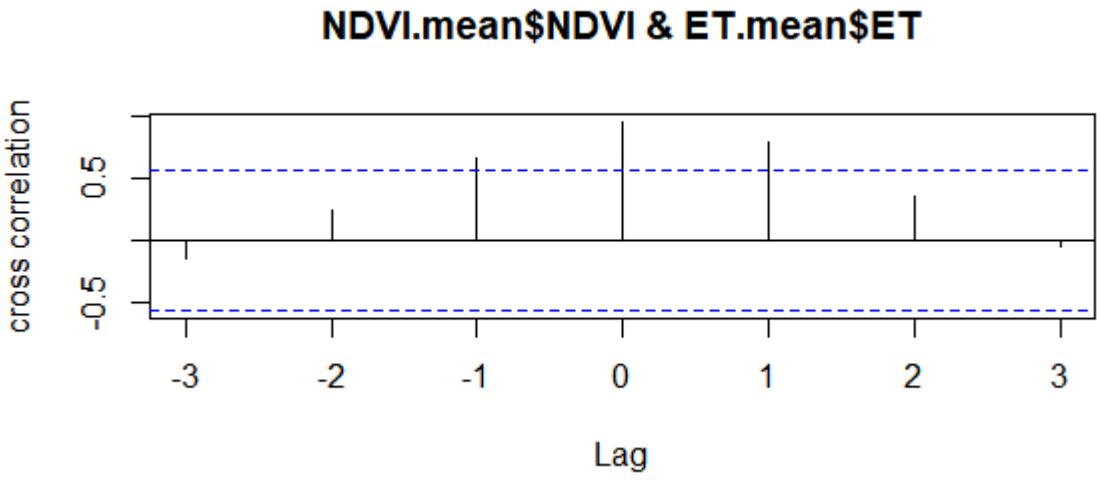

Figure 38: Cross correlation between mean monthly NDVI and evapotranspiration at BShIII

Map of vegetation dynamics

Monthly vegetation maps covering the rainy season are presented to depict vegetation change in this representative case study. Figure 39 and 40 show the maps for 2015 and 2017 seasons respectively. In figure 39, "greener" pixels representing dense vegetation are dominant in the months of August, September and October. However, a clearer visual exploration shows that vegetation is dense in the month of August and October in figure 39, while in figure 40, vegetation is dense in the month of August only. Juxtaposing the two rainy seasons representing 2015 and 2017, the months of May, June and July generally recorded low NDVI values as depicted by the maps in figure 39 and 40 accordingly.

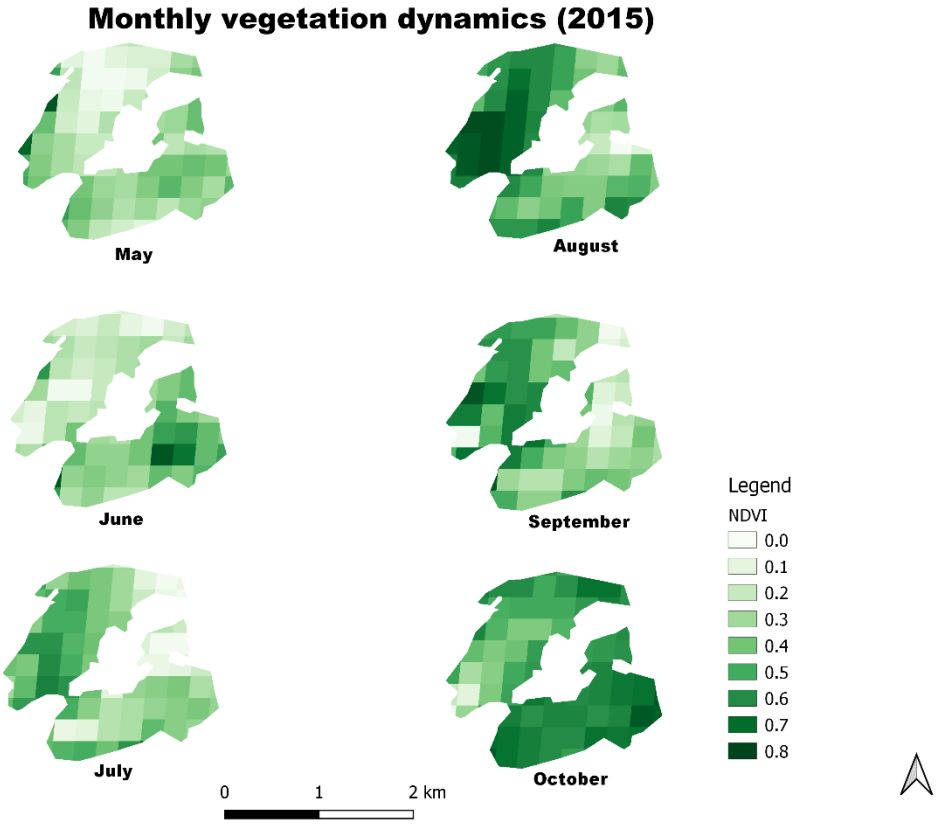

Figure 39: Monthly vegetation dynamics at BShIII, 2015 (May-October)

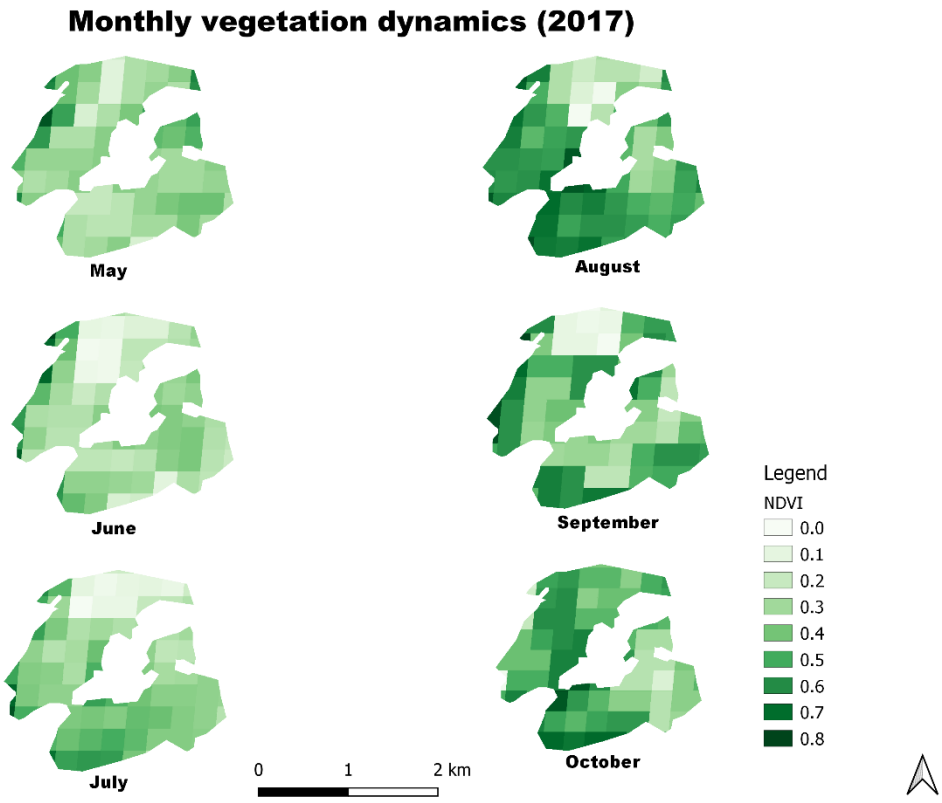

Figure 40: Monthly vegetation dynamics at BShIII, 2017 (May-October)

6.3. Tropical savannah climate (Aw)

6.3.1. AwI

Quantitative changes in vegetation dynamics

In figure 41, the mean inter-annual NDVI values from 2005 to 2019 depicts a cascading trend. The trajectory of the time series begins with a fairly low NDVI value then increases to a higher value and then drops to a lower value for two consecutive years before depicting a cascading pattern. The distribution of the mean NDVI is characterized by a low standard deviation of 0.02 to the long term similar to that of the breakpoints. Interestingly, the highest NDVI value recorded during the entire period is a little above 0.5 in the year 2019. On Seasonal basis, standard deviations of 0.19, 0.19 and 0.15 were obtained. To the long term, the linear regression line across the NDVI values as seen in figure 41 shows an overall increasing trend.

Correlation

Soil moisture and NDVI have weak correlation to the long term as revealed by the correlation coefficient of 0.04 in table 11. The weak correlation has been recorded for the two break points as well although there were all positive. However, the period from 2015 to 2019 recorded a moderate positive correlation were obtained as seen in table 11. The seasonal trajectories however, revealed strong positive correlations with coefficients of 0.97, 0.95 and 0.88 respectively as shown in table 11.

To the long term, a moderate positive correlation was observed between NDVI and evapotranspiration. In terms of the segregated periods; a weak negative correlation of -0.14 was obtained for the period from 2010-2014 while the remaining two depicted moderate to strong positive correlation. On seasonal trajectories, an uphill of strong positive correlation was recorded for the three seasons sampled.

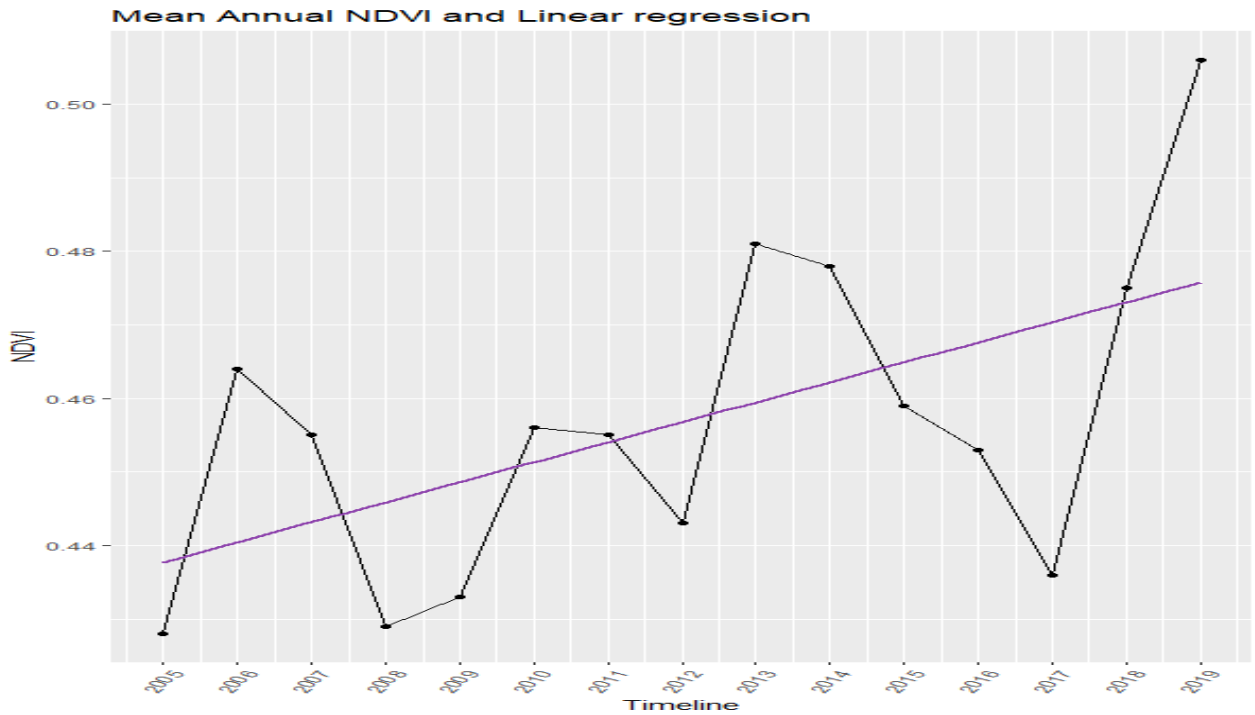

Figure 41: Mean annual NDVI and linear regression at Awl

	Long term	Break points			Seasonal		
	2005 - 2019	2005-2009	2010 -2014	2015-2019	2012	2015	2017
Standard deviation(NDVI)	0.02	0.01	0.01	0.02	0.19	0.19	0.15
Pearson Correlation (NDVI $ Soil Moisture)	0.04	0.47	-0.30	0.62	0.97	0.95	0.88
Pearson Correlation(NDVI $ Evapotranspiration)	0.66	0.69	-0.14	0.93	0.94	0.88	0.90

Table 11: Statistical values at Awl

Cross correlation and lag

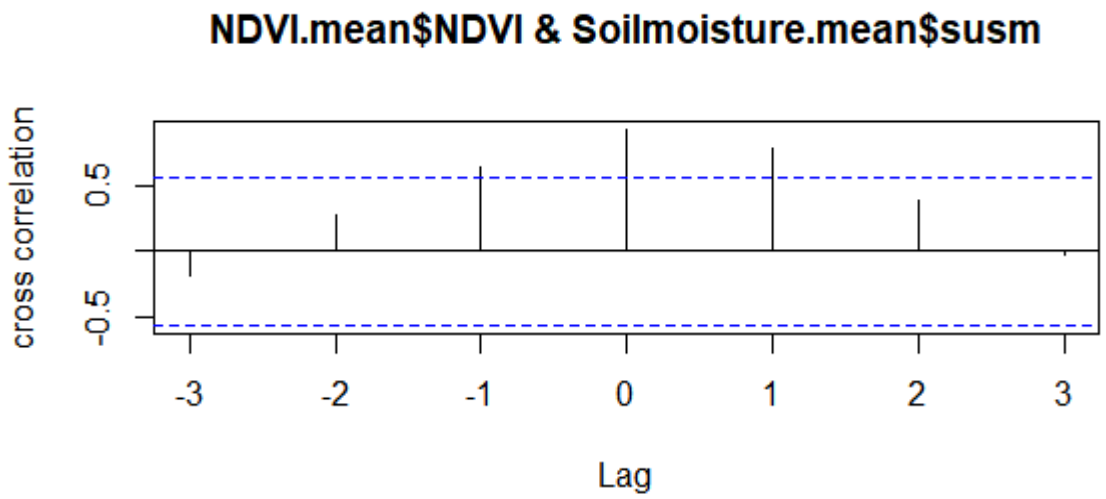

Figure 42: Cross correlation between mean monthly NDVI and soil moisture at AwI

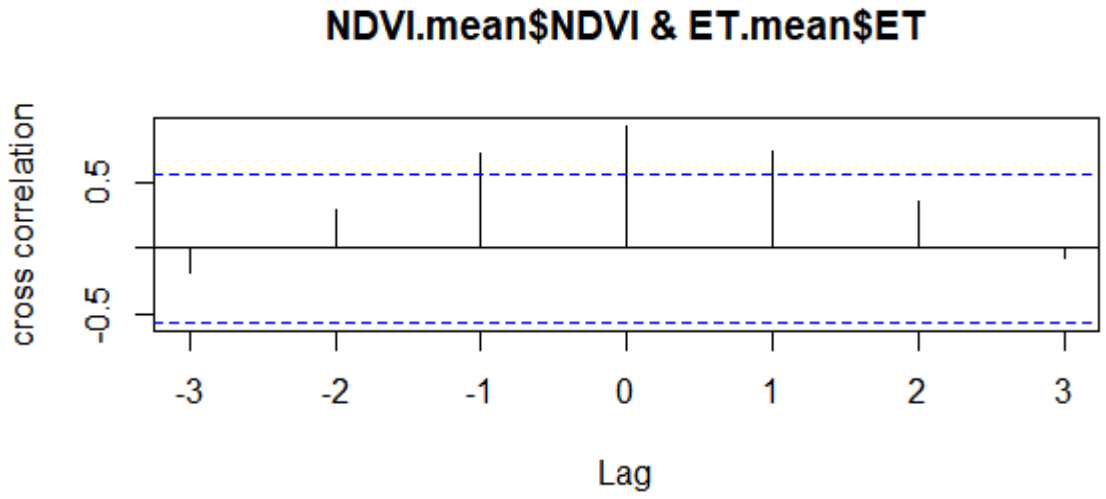

Figure 43: Cross correlation between mean monthly NDVI and evapotranspiration at AwI

Map of vegetation dynamics

In figure 44, yearly static maps showing vegetation change for a period of 15 years have been presented. From figure 44, it can be observed that most of the maps depict low NDVI values representing low or less dense vegetation. While 12 years recorded NDVI values between -0.1 to 0.3, three years: 2006, 2007 and 2011 recorded moderate to high NDVI values of 0.4 to 0.6 compared to the other years.

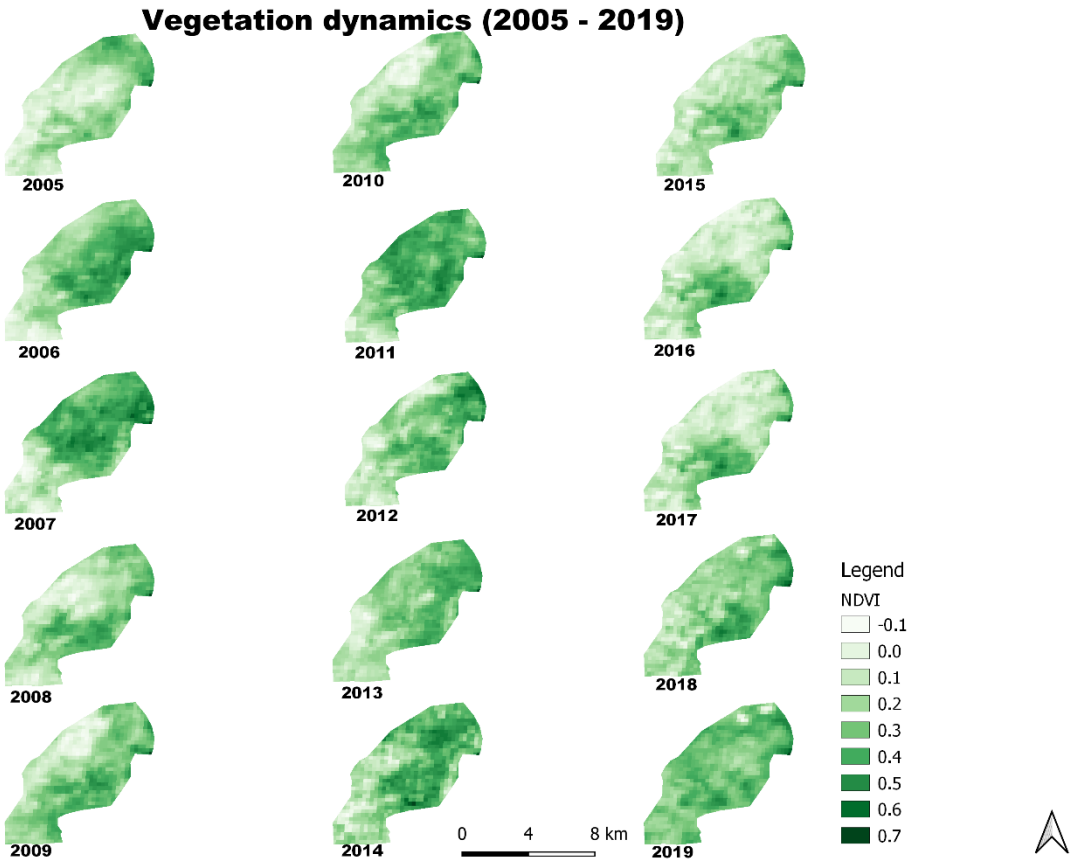

Figure 44: Yearly static maps of vegetation dynamics in Awi

6.3.2. AwII

Quantitative changes in vegetation dynamics

As observed in other case studies, the mean inter-annual NDVI from 2005 to 2019 follows a non-predictable trend as can be seen in figure 45. The series started with a low NDVI value then increases, it then decreases before becoming stable from 2011 to 2015. A downward trend was then recorded thereafter until the year 2017 where it reaches its lowest value for the entire period. For the long term, a standard deviation of 0.02 was obtained. Overall, the linear regression line across the NDVI values shows a decreasing trend.

Correlation

The relationship between NDVI and soil moisture in moderately positive to the long term. For the entire duration of the study, correlation of 0.64 was obtained as indicated in table 12. However, for two of the segregated periods, weak positive correlations were recorded, while the other period recorded a strong positive correlation. On seasonal basis, NDVI is strongly correlated with soil moisture. Of the three seasons sampled, the least coefficient is 0.89 as indicated in table 12.

The relationship between NDVI and evapotranspiration as estimated by Pearson correlation coefficient (PCC) depicts positive correlation for the long term, break points as well as for the seasons. From table 12, a weak positive correlation of 0.43 between NDVI and evapotranspiration for the long term was obtained. Similarly, two of the break points recorded weak positive correlations. Significantly, strong positive correlations were obtained for all the three seasons sampled.

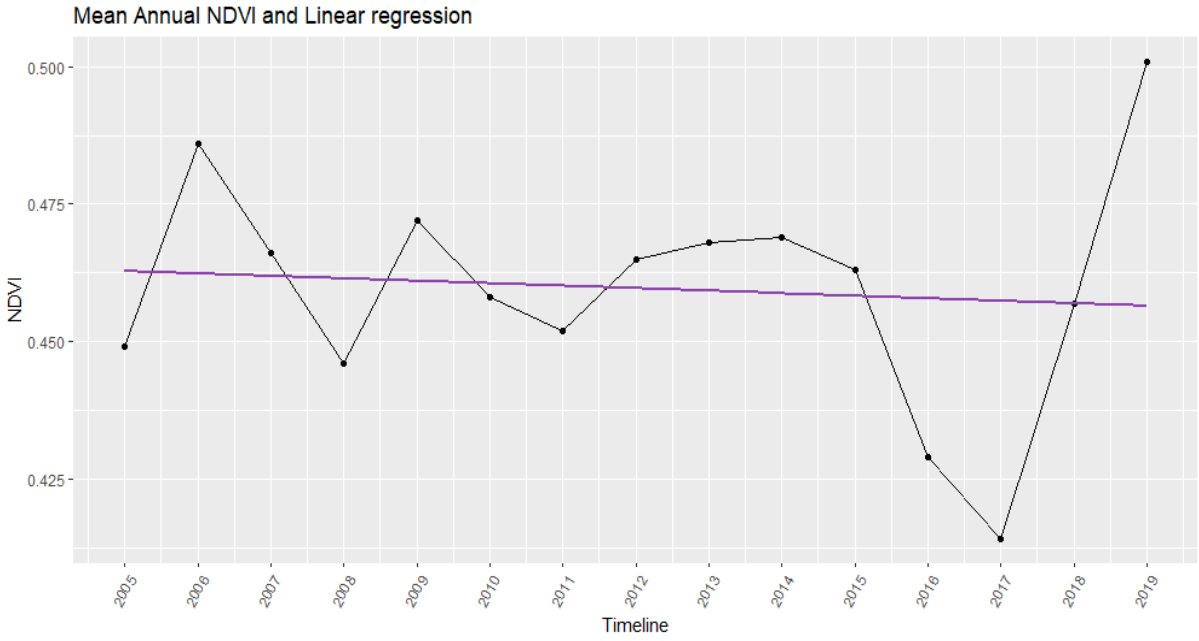

Figure 45: Mean annual NDVI and linear regression at AwII

	Long term	Break points			Seasonal		
	2005 - 2019	2005-2009	2010 -2014	2015-2019	2012	2015	2017
Standard deviation(NDVI)	0.02	0.01	0.00	0.03	0.17	0.16	0.16
Pearson Correlation (NDVI $ Soil Moisture)	0.64	0.21	0.30	0.85	0.89	0.91	0.90
Pearson Correlation(NDVI $ Evapotranspiration)	0.43	0.06	0.46	0.99	0.93	0.91	0.94

Table 12: Statistical values at AwII

Cross correlation and lag

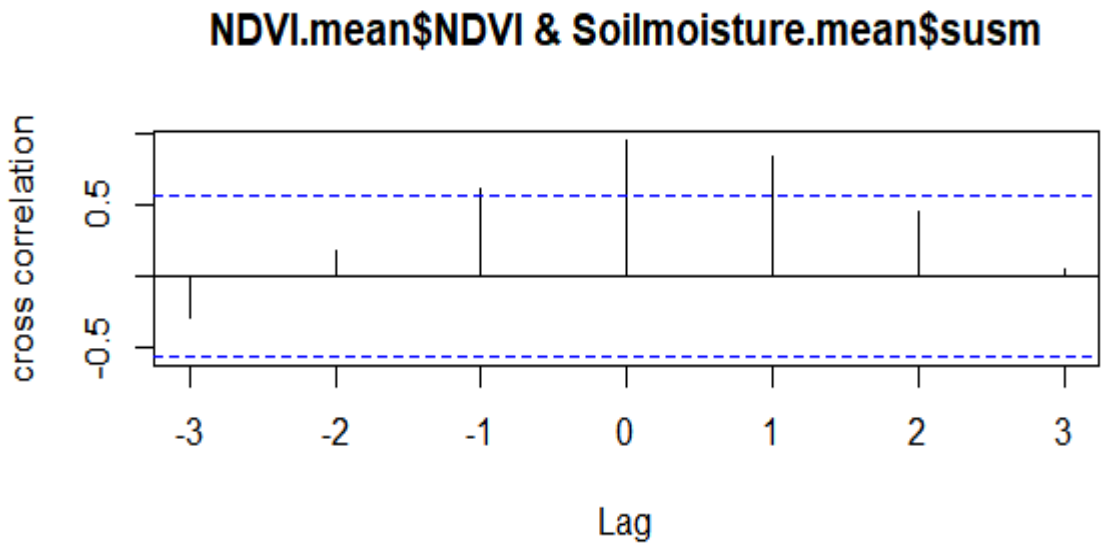

Figure 46: Cross correlation between mean monthly NDVI and soil moisture at AwII

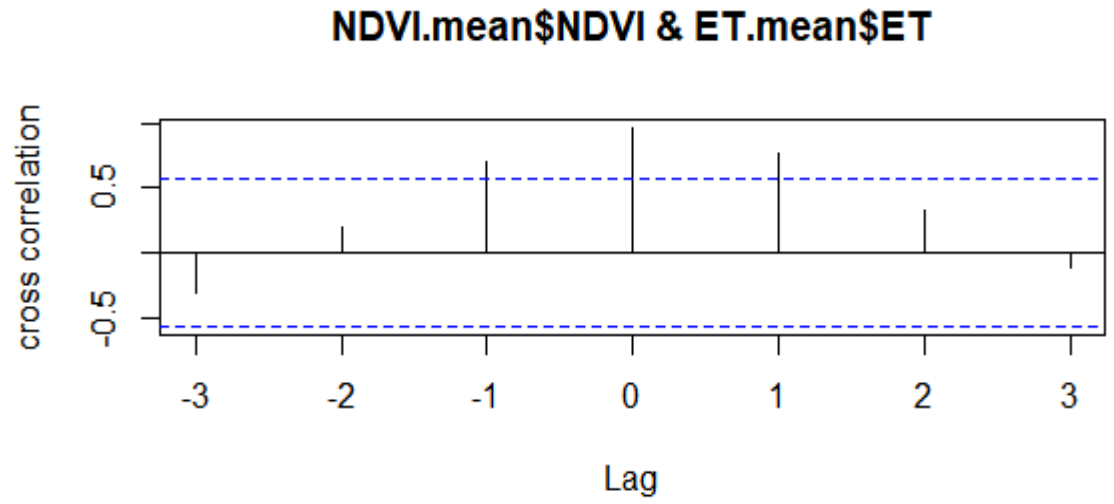

Figure 47: Cross correlation between mean monthly NDVI and evapotranspiration at AwII

Map of vegetation dynamics

Vegetation dynamics in this case study has been visualized on monthly basis spanning the rainy season as defined in the preceding paragraph. The rainy season for two years; 2015 and 2017 were taken into account. In figure 48 and 49, the monthly vegetation maps for 2015 and 2017 were shown respectively. The maps clearly show healthy vegetation in the months of July, August and September. However, in May, June and October, the maps depict low NDVI values corresponding to less dense vegetation.

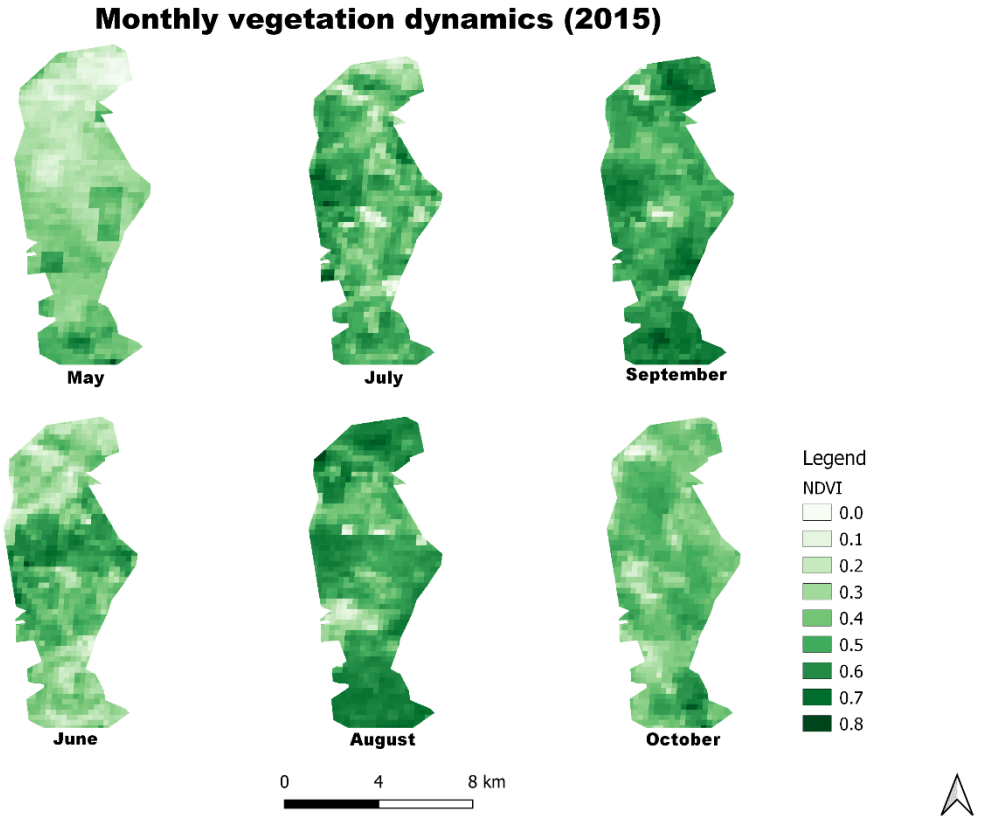

Figure 48: Monthly vegetation dynamics at AwII, 2015 (May-October)

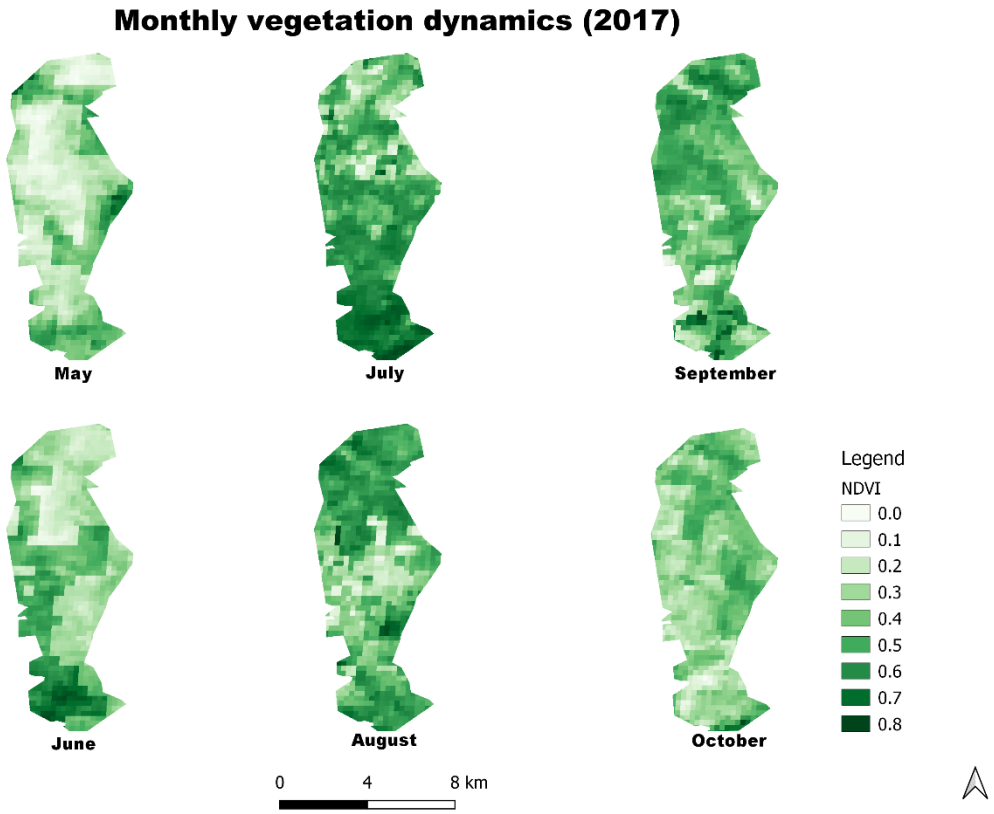

Figure 49: Monthly vegetation dynamics at AwII, 2017 (May-October)

6.3.3. AwIII

Quantitative changes in vegetation

As shown in figure 50 below, the mean inter-annual NDVI from 2005 to 2019 follows an erratic trend. From figure 50, these trends can be observed; increasing-decreasing, moderate increase and a gradual decreasing trends. For the long term, the standard deviation of the dataset is 0.02. The highest NDVI value was recorded in the year 2019. A standard deviation of 0.02, 0.3 and 0.02 corresponding to 2005-2009, 2010-2014 and 2015-2019 were obtained. Taking the entire period into consideration, the linear regression line shows an overall trend as shown in figure 50.

Correlation

There exist a weak negative correlation between NDVI and soil moisture taking the whole study period into consideration. Similarly, two of the breakpoints recorded weak negative correlation as well. However, on seasonal basis, all the three seasons recorded strong positive correlations. For the relationship between NDVI and evapotranspiration, a positive correlation of 0.75 was recorded, similarly the segregated periods also recorded strong positive correlations as well as the seasonal trajectories. These correlation coefficients are provided in table 13.

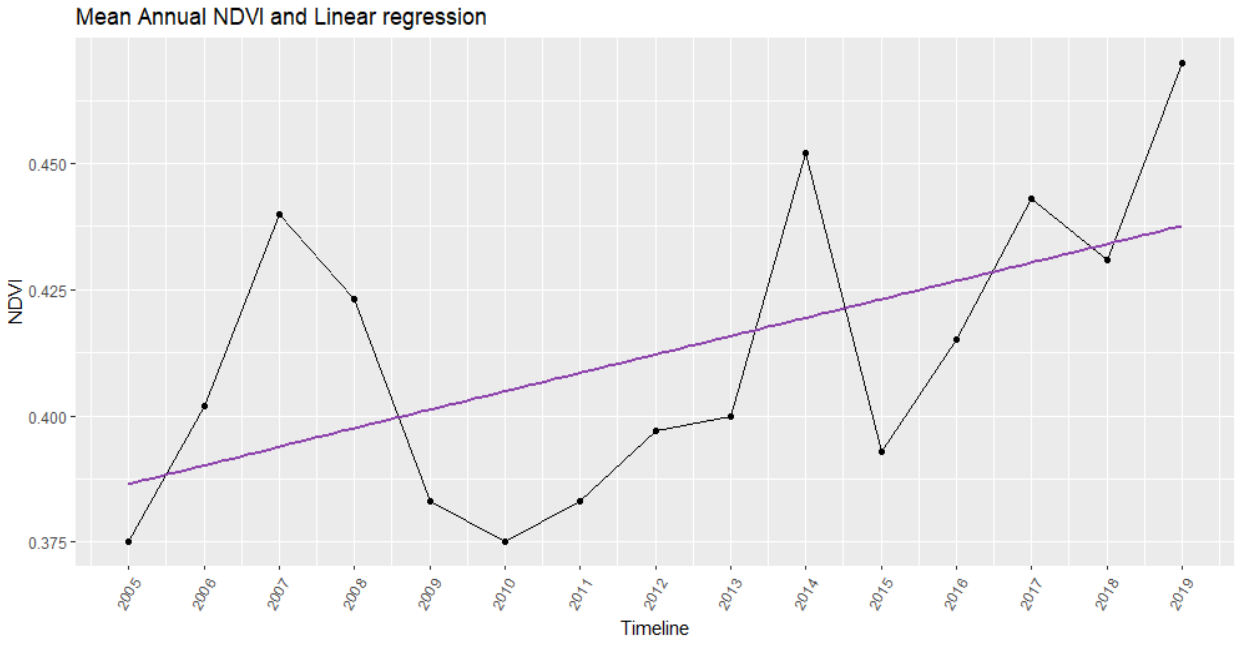

Figure 50: Mean annual NDVI and linear regression at AwIII

	Long term	Break points			Seasonal		
	2005 - 2019	2005-2009	2010 -2014	2015-2019	2012	2015	2017
Standard deviation(NDVI)	0.02	0.02	0.03	0.02	0.16	0.13	0.15
Pearson Correlation (NDVI $ Soil Moisture)	-0.40	0.33	-0.43	-0.50	0.92	0.92	0.74
Pearson Correlation(NDVI $ Evapotranspiration)	0.75	0.70	0.92	0.93	0.94	0.94	0.96

Table 13: Statistical values at AwIII

Cross correlation and lag

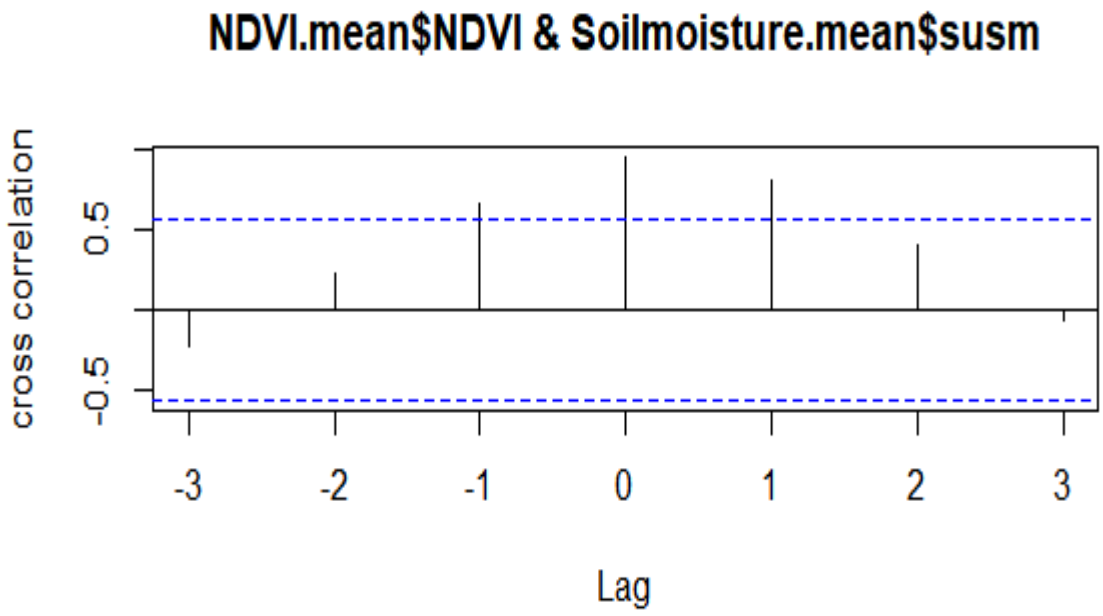

Figure 51: Cross correlation between mean monthly NDVI and soil moisture at AwIII

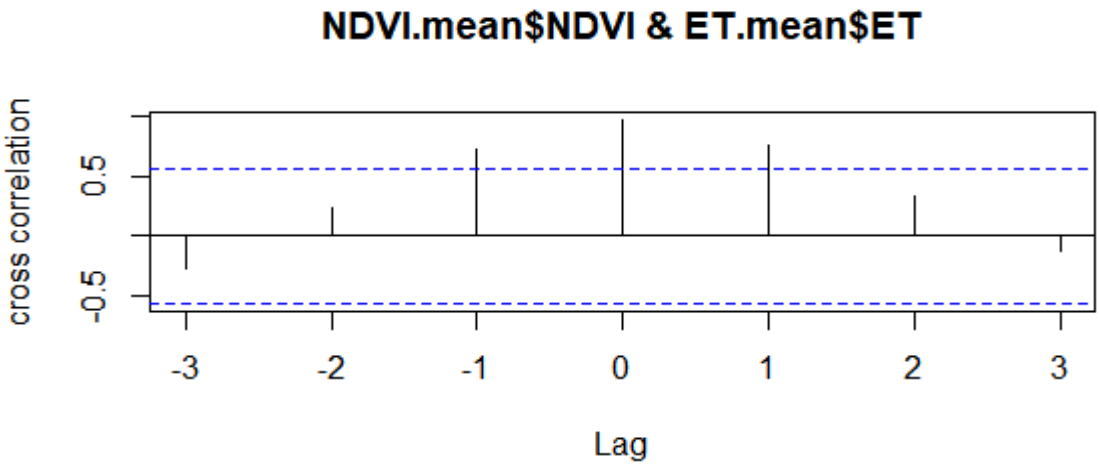

Figure 52: Cross correlation between mean monthly NDVI and evapotranspiration at AwIII

Map of vegetation dynamics

Vegetation dynamics in the context of this thesis has been visualized based on small static maps. Figure 53 below shows the yearly mean NDVI values as observed from remote sensing data across the delineated area. As shown in figure 53, vegetation in this area is generally low. All the static maps depict vegetation corresponding to values between 0.0 and 0.3.

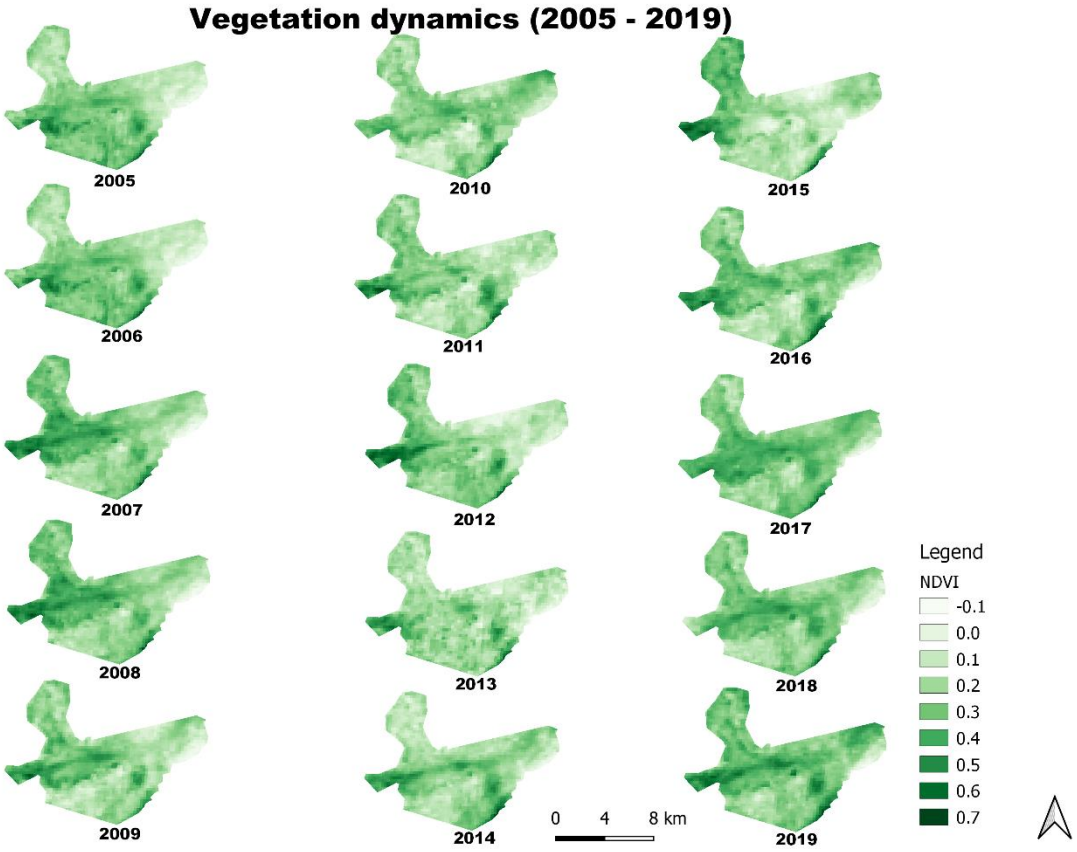

Figure 53: Yearly static maps of vegetation dynamics in AwIII

7. Conclusion and Outlook

This thesis has investigated mapping vegetation dynamics from remote sensing time series. The vegetation dynamics over the study area(s) in the Republic of Sudan was assessed using quantitative methods such as the annual mean NDVI and estimates of standard deviation. The long term trend of vegetation change has been calculated based on linear regression, as shown by the "purple" trend lines in the NDVI graphs (see figures 15,19,23,27,32,36,41,45 and 50).The estimates of standard deviation show minimal or insignificant variations in NDVI values for the long term, breakpoints, and on a seasonal basis. Vegetation change, whether abruptly or gradually, do not occur in a vacuum. Vegetation change studies usually characterize NDVI, the proxy for vegetation as a dependent variable, which is controlled by independent variables such as temperature, precipitation, evapotranspiration, and soil moisture. As a result, this thesis has explored the relationship between NDVI (vegetation) and a series of controlling factors: soil moisture and evapotranspiration for the long term, breakpoints, and in the seasonal context. This relationship has been estimated based on the Pearson correlation coefficient. A weaker positive correlation between NDVI and soil moisture was observed for the long term. However, on a seasonal basis, strong positive correlations were recorded in all representative case studies. The relationship between NDVI and evapotranspiration has been investigated as well, where moderate positive correlations were observed. Likewise, strong positive correlations characterized the seasonal trajectories. A cross-correlation between NDVI, soil moisture, and evapotranspiration determines the "delay" or lag in response between the dependent variable (NDVI) and independent variables. The results, as depicted by the cross-correlation graphs in (figures 16-17,20-21, 24-25,28-29,33-34,37-38,42-43, 46-47 and 51-52), show no significant lags in response.

Going beyond the quantitative assessment, this thesis explored visualization techniques that can be used for the representation of vegetation dynamics. One aspect of this thesis is to use

diagrams, charts, and tables to depict trends, changes, and dynamics of vegetation change. As observed from the results chapter, line charts and graphs dominated the graphical presentation of results. Similarly, cartographic representation of vegetation dynamics in this thesis have been carried out in the form of "small multiple" static maps. These small multiple static maps depict both the yearly and seasonal vegetation changes. These small static maps make it easier for the user to easily identify changes in vegetation within the spatio-temporal context. For example, figure 30 and 31 were a combination of small static maps used to depict the monthly vegetation maps for covering the rainy season. However, other techniques for visualizing various dimensions, **trend, change, and dynamics** of vegetation have been explored and presented as prototypes of visualization techniques, which can serve as alternatives for the line chart.

Aside from the results obtained, this thesis has laid the foundation for other dimensions to be explored presented in the **outlook** below:

- The relationship between NDVI, temperature, and precipitation needs to be examined for the long term, breakpoints, seasonal, and on a daily basis in order to compare and contrast the actual daily changes in vegetation.
- The lag between dependent and independent variables need to be computed daily since the monthly cross-correlation shows no significant lags.
- Although the traditional ways for vegetation dynamics visualization, such as line charts and graphs are powerful to convey information, alternative techniques can also be adapted and tested. Along with line charts for visualizing trends, area charts are also suitable to visualize trends. Another technique explored is isopleth maps for visualizing vegetation change. Not only are isopleth maps suitable for visualizing change, but they can also aptly support visual exploration and spatial analysis of the presented dataset. Besides, visualizing dynamics can be revealed through the chronological or sequential

changes using animation as a visualization technique. This approach shows the sequential changes in vegetation over time and also allows the user to interact with the process. Similarly, animation applied along with individual static maps can depict the sequential process of vegetation dynamics.

References

Abdel-Kader, F. H. (2019). Assessment and monitoring of land degradation in the northwest coast region, Egypt using Earth observations data. *Egyptian Journal of Remote Sensing and Space Science*, *22*(2), 165–173. https://doi.org/10.1016/j.ejrs.2018.02.001

Adrienko, N., & Andrienko, G. (2011). Spatial generalization and aggregation of massive movement data. *IEEE Transactions on Visualization and Computer Graphics*. https://doi.org/10.1109/TVCG.2010.44

Ahmed, M., Else, B., Eklundh, L., Ardö, J., & Seaquist, J. (2017). Dynamic response of ndvi to soil moisture variations during different hydrological regimes in the sahel region. *International Journal of Remote Sensing*. https://doi.org/10.1080/01431161.2017.1339920

Aigner, W., Miksch, S., Müller, W., Schumann, H., & Tominski, C. (2007). Visualizing time-oriented data-A systematic view. *Computers and Graphics (Pergamon)*. https://doi.org/10.1016/j.cag.2007.01.030

Alan, M. M. (2001). An evolving cognitive-semiotic approach to geographic visualization and knowledge construction. *Information Design Journal*.

Andrienko, N., Andrienko, G., & Gatalsky, P. (2000). Towards Exploratory Visualization of Spatio-Temporal Data. *Time*.

Andrienko, N., Andrienko, G., & Gatalsky, P. (2003). Exploratory spatio-temporal visualization: An analytical review. *Journal of Visual Languages and Computing*. https://doi.org/10.1016/S1045-926X(03)00046-6

Appiah, D. O., Schröder, D., Forkuo, E. K., & Bugri, J. T. (2015). Application of geo-information techniques in land use and land cover change analysis in a peri-urban district of Ghana. *ISPRS International Journal of Geo-Information*. https://doi.org/10.3390/ijgi4031265

Assal, T. J., Anderson, P. J., & Sibold, J. (2016). Spatial and temporal trends of drought effects in a heterogeneous semi-arid forest ecosystem. *Forest Ecology and Management*. https://doi.org/10.1016/j.foreco.2016.01.017

Berger, A., Ettlin, G., Quincke, C., & Rodríguez-bocca, P. (2018). Predicting the Normalized Di ff erence Vegetation Index (NDVI) by training a crop growth model with historical data. *Computers and Electronics in Agriculture*, (December 2017), 0–1.

https://doi.org/10.1016/j.compag.2018.04.028

Beygi Heidarlou, H., Banj Shafiei, A., Erfanian, M., Tayyebi, A., & Alijanpour, A. (2019). Effects of preservation policy on land use changes in Iranian Northern Zagros forests. *Land Use Policy*. https://doi.org/10.1016/j.landusepol.2018.10.036

Bin, W., Ming, L., Dan, J., Suju, L., Qiang, C., Chao, W., … Jun, Z. (2019). A METHOD OF AUTOMATICALLY EXTRACTING FOREST FIRE BURNED AREAS USING GF-1 REMOTE SENSING IMAGES 1 . DongFangHong Satellite Corporation Limited , Beijing , China 100094 2 . National Disaster Reduction Center of China , Beijing , China 100124 NDVI □ Nir □ R . *IGARSS 2019 - 2019 IEEE International Geoscience and Remote Sensing Symposium*, 9953–9955.

Bing.com. (2020). No Title. Retrieved 15 March 2020, from https://www.bing.com/images/search?view=detailV2&id=1B498DF0B6160CC27172F48D6EDE7D72031BE2E8&thid=OIP.6Kj2ocrBaW4nrH3MnKbQfAHaEj&mediaurl=http%3A%2F%2Fdsparks.files.wordpress.com%2F2012%2F07%2F2008-cces-ideological-self-placement-leveled-copy.png%3Fw%3D500&exph=307&expw=500&q=What+Is+an+Isopleth+Map&selectedindex=44&ajaxhist=0&vt=0&eim=0,1,2,5,6&ccid=6Kj2ocrB&simid=608047362998272041&sim=11

Blok, C. A. (2005). Dynamic visualization variables in animation to support monitoring of spatial phenomena.

Blok, C., Köbben, B., Cheng, T., & Kuterema, A. A. (1999). Visualization of relationships between spatial patterns in time by cartographic animation. *Cartography and Geographic Information Science*. https://doi.org/10.1559/152304099782330716

Boegh, E., Soegaard, H., Broge, N., Schelde, K., Thomsen, A., Hasager, C. B., & Jensen, N. O. (2002). Airborne multispectral data for quantifying leaf area index, nitrogen concentration, and photosynthetic efficiency in agriculture. *Remote Sensing of Environment*. https://doi.org/10.1016/S0034-4257(01)00342-X

Borak, J. S., Lambin, E. F., & Strahler, A. H. (2000). The use of temporal metrics for land cover change detection at coarse spatial scales. *International Journal of Remote Sensing*. https://doi.org/10.1080/014311600210245

Boyd, D. S., & Danson, F. M. (2005). Satellite remote sensing of forest resources: Three decades of research development. *Progress in Physical Geography*. https://doi.org/10.1191/0309133305pp432ra

Bradley, B. A., Jacob, R. W., Hermance, J. F., & Mustard, J. F. (2007). A curve fitting procedure to derive inter-annual phenologies from time series of noisy satellite NDVI data. *Remote Sensing of Environment*. https://doi.org/10.1016/j.rse.2006.08.002

Brandt, M., Rasmussen, K., Peñuelas, J., Tian, F., Schurgers, G., Verger, A., … Fensholt, R. (2017). Human population growth offsets climate-driven increase in woody vegetation in sub-Saharan Africa. *Nature Ecology and Evolution*, *1*(4), 4–9. https://doi.org/10.1038/s41559-017-0081

Broge, N. H., & Mortensen, J. V. (2002). Deriving green crop area index and canopy chlorophyll density of winter wheat from spectral reflectance data. *Remote Sensing of Environment*. https://doi.org/10.1016/S0034-4257(01)00332-7

Bruzzone, L., Smits, P. C., & Tilton, J. C. (2003). Foreword - Special Issue on Analysis of Multitemporal Remote Sensing Images. *IEEE Transactions on Geoscience and Remote Sensing*. https://doi.org/10.1109/TGRS.2003.820004

Cai, Z., Jönsson, P., Jin, H., & Eklundh, L. (2017). Performance of smoothing methods for reconstructing NDVI time-series and estimating vegetation phenology from MODIS data. *Remote Sensing*, *9*(12), 20–22. https://doi.org/10.3390/rs9121271

Campbell, G. S. (1974). A simple method for determining unsaturated conductivity from moisture retention data. *Soil Science*. https://doi.org/10.1097/00010694-197406000-00001

Chakraborty, S., Banerjee, A., Gupta, S., Papandreou-suppappola, A., & Christensen, P. (2017). *ESTIMATION OF DYNAMIC PARAMETERS OF MODIS NDVI TIME SERIES NONLINEAR School of Computing , Informatics , and Decision Systems Engineering , ASU School of Electrical Computer and Energy Engineering , ASU School of Earth and Space Exploration , ASU*. 1091–1094.

Chen, H., Liu, X., Ding, C., & Huang, F. (2018). Phenology-Based Residual Trend Analysis of MODIS-NDVI Time Series for Assessing Human-Induced Land Degradation. *Sensors (Basel, Switzerland)*. https://doi.org/10.3390/s18113676

Chen, T., de Jeu, R. A. M., Liu, Y. Y., van der Werf, G. R., & Dolman, A. J. (2014). Using satellite based soil moisture to quantify the water driven variability in NDVI: A case study over mainland Australia. *Remote Sensing of Environment*. https://doi.org/10.1016/j.rse.2013.08.022

Choudhary, K., Shi, W., Singh, M., & Corgne, S. (2019). *Agriculture Phenology Monitoring Using NDVI Time Series Based on Remote Sensing Satellites : A Case Study of Guangdong , China*. *28*(3), 204–214. https://doi.org/10.3103/S1060992X19030093

Cliamte-Data.org. (2018). No Title. Retrieved from https://en.climate-data.org/africa/sudan/an-nil-al-azraq/al-kurumuk-717345/

Climate-Data.org. (2019). No Title.

Climate-Data.org. (2020a). No Title. Retrieved 14 March 2020, from https://en.climate-

data.org/africa/sudan/kassala/kassala-3713/]

Climate-Data.org. (2020b). No Title.

Colombo, R., Bellingeri, D., Fasolini, D., & Marino, C. M. (2003). Retrieval of leaf area index in different vegetation types using high resolution satellite data. *Remote Sensing of Environment*. https://doi.org/10.1016/S0034-4257(03)00094-4

Cowling, S. A., & Field, C. B. (2003). Environmental control of leaf area production: Implications for vegetation and land-surface modeling. *Global Biogeochemical Cycles*. https://doi.org/10.1029/2002gb001915

David, A., & J M Tauro, C. (2015). Web 3D Data Visualization of Spatio Temporal Data using Data Driven Document (D3js). *International Journal of Computer Applications*, *111*(4), 42–46. https://doi.org/10.5120/19529-1169

Dawson, T. P., Cutler, M. E. J., & Brown, C. (2016). The role of remote sensing in the development of SMART indicators for ecosystem services assessment. *Biodiversity*, *17*(4), 136–148. https://doi.org/10.1080/14888386.2016.1246384

De Beurs, K. M., & Henebry, G. M. (2005). A statistical framework for the analysis of long image time series. *International Journal of Remote Sensing*. https://doi.org/10.1080/01431160512331326657

de Jong, R., Verbesselt, J., Schaepman, M. E., & de Bruin, S. (2012). Trend changes in global greening and browning: Contribution of short-term trends to longer-term change. *Global Change Biology*, *18*(2), 642–655. https://doi.org/10.1111/j.1365-2486.2011.02578.x

De Koninck, R. (2012). Mayhew, Susan et Penny, Anne (1992) The Concise Oxford Dictionary of Geography. Oxford and New York, Oxford University Press, 250 p. *Cahiers de Géographie Du Québec*. https://doi.org/10.7202/022335ar

Didan, K. (2015a). MOD13C1 MODIS/Terra Vegetation Indices 16-Day L3 Global 0.05Deg CMG V006. *EOSDIS Land Processes DAAC*.

Didan, K. (2015b). No Title. Retrieved 15 January 2020, from https://doi.org/10.5067/MODIS/MOD13Q1.006

Dong, C., Id, G. Z., Qin, Y., & Wan, H. (2019). *Area extraction and spatiotemporal characteristics of winter wheat – summer maize in Shandong Province using NDVI time series*. 1–19. https://doi.org/10.1371/journal.pone.0226508

Easdale, M. H., Bruzzone, O., Mapfumo, P., & Tittonell, P. (2018). Phases or regimes? Revisiting NDVI trends as proxies for land degradation. *Land Degradation and Development*, *29*(3), 433–445. https://doi.org/10.1002/ldr.2871

Easterling, D. R., Evans, J. L., Groisman, P. Y., Karl, T. R., Kunkel, K. E., & Ambenje, P.

(2000). Observed variability and trends in extreme climate events: A brief review. *Bulletin of the American Meteorological Society*. https://doi.org/10.1175/1520-0477(2000)081<0417:OVATIE>2.3.CO;2

Engine, G. E. (2020). No Title. Retrieved 15 February 2020, from https://code.earthengine.google.com/?scriptPath=users%2Faedwinhilarysk%2FAll%3AAnimationMockup

Eugster, W., Rouse, W. R., Pielke, R. A., Mcfadden, J. P., Baldocchi, D. D., Kittel, T. G. F., … Chambers, S. (2000). Land-atmosphere energy exchange in Arctic tundra and boreal forest: Available data and feedbacks to climate. *Global Change Biology*. https://doi.org/10.1046/j.1365-2486.2000.06015.x

Falloon, P., Jones, C. D., Ades, M., & Paul, K. (2011). Direct soil moisture controls of future global soil carbon changes: An important source of uncertainty. *Global Biogeochemical Cycles*. https://doi.org/10.1029/2010GB003938

Fang, H.-Y., & Daniels, J. L. (2006). Introductory Geotechnical Engineering. In *Introductory Geotechnical Engineering*. https://doi.org/10.4324/9780203403525

FAO. (2020). No Title. Retrieved 15 March 2020, from http://www.fao.org/3/x0490e/x0490e04.htm

Fatikhunnada, A., Solahudin, M., Buono, A., Kato, T., & Boro, K. (2020). Remote Sensing Applications : Society and Environment Assessment of pre-treatment and classification methods for Java paddy field cropping pattern detection on MODIS images. *Remote Sensing Applications: Society and Environment*, *17*(December 2019), 100281. https://doi.org/10.1016/j.rsase.2019.100281

Fensholt, R., & Proud, S. R. (2012). Evaluation of Earth Observation based global long term vegetation trends - Comparing GIMMS and MODIS global NDVI time series. *Remote Sensing of Environment*, *119*, 131–147. https://doi.org/10.1016/j.rse.2011.12.015

Fensholt, R., Rasmussen, K., Theis, T., & Mbow, C. (2009). Remote Sensing of Environment Evaluation of earth observation based long term vegetation trends — Intercomparing NDVI time series trend analysis consistency of Sahel from AVHRR GIMMS , Terra MODIS and SPOT VGT data. *Remote Sensing of Environment*, *113*(9), 1886–1898. https://doi.org/10.1016/j.rse.2009.04.004

Function, W. D., Method, F., Series, T., & Set, D. (n.d.). *Weighted Double-Logistic Function Fitting Method for Reconstructing the High-Quality Sentinel-2 NDVI Time Series Data Set*.

Gago, J., Douthe, C., Coopman, R. E., Gallego, P. P., Ribas-Carbo, M., Flexas, J., … Medrano, H. (2015). UAVs challenge to assess water stress for sustainable agriculture.

Agricultural Water Management. https://doi.org/10.1016/j.agwat.2015.01.020

Gorelick, N., Hancher, M., Dixon, M., Ilyushchenko, S., Thau, D., & Moore, R. (2017). Google Earth Engine: Planetary-scale geospatial analysis for everyone. *Remote Sensing of Environment*. https://doi.org/10.1016/j.rse.2017.06.031

Graser, A., Schmidt, J., Roth, F., & Brändle, N. (2019). Untangling origin-destination flows in geographic information systems. *Information Visualization*, *18*(1), 153–172. https://doi.org/10.1177/1473871617738122

Guo, D., Chen, J., MacEachren, A. M., & Liao, K. (2006). A Visualization System for Space-Time and Multivariate Patterns (VIS-STAMP). *IEEE Transactions on Visualization and Computer Graphics*. https://doi.org/10.1109/TVCG.2006.84

Guo, X., Zhang, H., Yuan, T., Zhao, J., & Xue, Z. (2015). Detecting the temporal scaling behavior of the normalized difference vegetation index time series in China using a detrended fluctuation analysis. *Remote Sensing*, *7*(10), 12942–12960. https://doi.org/10.3390/rs71012942

Hall-Beyer, M. (2003). Comparison of Single-Year and Multiyear NDVI Time Series Principal Components in Cold Temperate Biomes. *IEEE Transactions on Geoscience and Remote Sensing*. https://doi.org/10.1109/TGRS.2003.817274

Handavu, F., Chirwa, P. W. C., & Syampungani, S. (2019). Socio-economic factors influencing land-use and land-cover changes in the miombo woodlands of the Copperbelt province in Zambia. *Forest Policy and Economics*. https://doi.org/10.1016/j.forpol.2018.10.010

HILLEL, D. (1980). The Task of Soil Physics. In *Fundamentals of Soil Physics*. https://doi.org/10.1016/b978-0-08-091870-9.50006-6

Hou, Z., Mehtätalo, L., McRoberts, R. E., Ståhl, G., Tokola, T., Rana, P., … Xu, Q. (2019). Remote sensing-assisted data assimilation and simultaneous inference for forest inventory. *Remote Sensing of Environment*, *234*(September), 111431. https://doi.org/10.1016/j.rse.2019.111431

Howell, T. A. (2001). Enhancing water use efficiency in irrigated agriculture. *Agronomy Journal*. https://doi.org/10.2134/agronj2001.932281x

Hua, A. K. (2017). Land Use Land Cover Changes in Detection of Water Quality: A Study Based on Remote Sensing and Multivariate Statistics. *Journal of Environmental and Public Health*, *2017*, 5–7. https://doi.org/10.1155/2017/7515130

Huete, A., Justice, C., & Liu, H. (1994). *Development of Vegetation and Soil Indices for MODIS-EOS*. *234*, 224–234.

Huiling, L., Xiaobing, L., Yun, B., Lingmei, H., & Zhongfei, L. (2010). Time LAG analysis

between vegetation and climate change in inner Mongolia. *International Geoscience and Remote Sensing Symposium (IGARSS)*. https://doi.org/10.1109/IGARSS.2010.5652806

Jia, Q.-S., Wang, H., Lei, Y., Zhao, Q., & Guan, X. (2014). A Decentralized Stay-Time Based Occupant Distribution Estimation Method for Buildings. *IEEE Transactions on Automation Science and Engineering*, *12*(4), 1482–1491. https://doi.org/10.1109/tase.2014.2361122

Johnston, R. J. (1981). The dictionary of human geography. *The Dictionary of Human Geography*. https://doi.org/10.2307/633383

Jung, M., & Lee, S.-H. (2019). Land-cover Monitoring Using Time Series of Satellite Images Based on Harmonic Analysis. *DEStech Transactions on Engineering and Technology Research*, (cemms), 162–167. https://doi.org/10.12783/dtetr/cemms2019/32029

Kan, C., & Kan, C. (2017). *Real-time Animation of Vegetation : Novel 2D Approach and Interactive Authoring Interface by Real-time Animation of Vegetation : Novel 2D Approach and Interactive Authoring Interface by*.

Kessler, F. (2011). Book Review: Cartography: Visualization of Spatial Data (3rd ed.), Menno-Jan Kraak and Ferjan Ormeling. Pearson, Harlow England, 2010. *Applied Spatial Analysis and Policy*. https://doi.org/10.1007/s12061-010-9052-6

Kim, S., Jeong, S., Woo, I., Jang, Y., Maciejewski, R., & Ebert, D. S. (2018). Data Flow Analysis and Visualization for Spatiotemporal Statistical Data without Trajectory Information. *IEEE Transactions on Visualization and Computer Graphics*, *24*(3), 1287–1300. https://doi.org/10.1109/TVCG.2017.2666146

Kim, Y. S., Walls, L. A., Krafft, P., & Hullman, J. (2019). A Bayesian cognition approach to improve data visualization. *Conference on Human Factors in Computing Systems - Proceedings*, 1–14. https://doi.org/10.1145/3290605.3300912

Laio, F., Porporato, A., Ridolfi, L., & Rodriguez-Iturbe, I. (2002). On the seasonal dynamics of mean soil moisture. *Journal of Geophysical Research Atmospheres*.

Landmann, T., Eidmann, D., Cornish, N., Franke, J., & Siebert, S. (2019). Optimizing harmonics from Landsat time series data: the case of mapping rainfed and irrigated agriculture in Zimbabwe. *Remote Sensing Letters*, *10*(11), 1038–1046. https://doi.org/10.1080/2150704X.2019.1648901

Latifi, H., & Heurich, M. (2019). Multi-scale remote sensing-assisted forest inventory: A glimpse of the state-of-the-art and future prospects. *Remote Sensing*, *11*(11), 3–6. https://doi.org/10.3390/rs11111260

Lippitt, C. D., Stow, D. A., & Riggan, P. J. (2016). Application of the remote-sensing communication model to a time-sensitive wildfire remote-sensing system. *International*

Journal of Remote Sensing, *37*(14), 3272–3292. https://doi.org/10.1080/01431161.2016.1196840

Lu, Y., Coops, N. C., & Hermosilla, T. (2017). ISPRS Journal of Photogrammetry and Remote Sensing Estimating urban vegetation fraction across 25 cities in pan-Pacific using Landsat time series data. *ISPRS Journal of Photogrammetry and Remote Sensing*, *126*, 11–23. https://doi.org/10.1016/j.isprsjprs.2016.12.014

Maceachren, A. M. (1995). How maps work: representation, visualization and design. *How Maps Work: Representation, Visualization and Design*. https://doi.org/10.14714/cp24.757

MacEachren, A. M., & Kraak, M.-J. (2001). Research Challenges in Geovisualization. *Cartography and Geographic Information Science*. https://doi.org/10.1559/152304001782173970

Maneta, M., Camps-valls, G., Martino, L., Robinson, N., Allred, B., & Running, S. W. (2018). *Alvaro Numerical Terradynamic Simulation Group (NTSG), University of Montana , USA , Department of Geosciences , University of Montana , USA , Image Processing Laboratory (IPL), Universitat de Val ` Dep . Signal Processing and Communications , Univers*. 349–352.

Measho, S., Chen, B., Trisurat, Y., Pellikka, P., Guo, L., Arunyawat, S., … Yemane, T. (2019). Spatio-Temporal Analysis of Vegetation Dynamics as a Response to Climate Variability and Drought Patterns in the Semiarid Region, Eritrea. *Remote Sensing*, *11*(6), 724. https://doi.org/10.3390/rs11060724

Meyfroidt, P., van Noordwijk, M., Minang, P., Dewi, S., Lambin, E. (2011). Drivers and consequences of tropical forest transitions: options to bypass land degradation? *Policy Briefs*.

Mohammadi, A., Costelloe, J. F., & Ryu, D. (2017). Application of time series of remotely sensed normalized difference water, vegetation and moisture indices in characterizing flood dynamics of large-scale arid zone floodplains. *Remote Sensing of Environment*, *190*, 70–82. https://doi.org/10.1016/j.rse.2016.12.003

Na-U-Dom, T., Mo, X., & García, M. (2017). Assessing the Climatic Effects on Vegetation Dynamics in the Mekong River Basin. *Environments*. https://doi.org/10.3390/environments4010017

NASA_USDA. (2020). NASA-USDA Global Soil Moisture Data. Retrieved 15 March 2020, from Google Earth Engine Developers website: https://developers.google.com/earth-engine/datasets/catalog/NASA_USDA_HSL_soil_moisture

NASA. (n.d.). No Title. Retrieved 14 March 2020, from Google Earth Engine Developers

website: https://developers.google.com/earth-engine/datasets/catalog/NASA_GLDAS_V021_NOAH_G025_T3H

NASA. (2005). No Title. Retrieved from MODIS Image website: https://commons.wikimedia.org/w/index.php?curid=9565093

Nicolai-Shaw, N., Zscheischler, J., Hirschi, M., Gudmundsson, L., & Seneviratne, S. I. (2017). A drought event composite analysis using satellite remote-sensing based soil moisture. *Remote Sensing of Environment*. https://doi.org/10.1016/j.rse.2017.06.014

O'Sullivan, D., & Unwin, D. J. (2010). Geographic Information Analysis: Second Edition. In *Geographic Information Analysis: Second Edition*. https://doi.org/10.1002/9780470549094

Padhee, S. K., & Dutta, S. (2019). Spatio-Temporal Reconstruction of MODIS NDVI by Regional Land Surface Phenology and Harmonic Analysis of Time-Series. *GIScience and Remote Sensing*, *56*(8), 1261–1288. https://doi.org/10.1080/15481603.2019.1646977

Pang, G., Wang, X., & Yang, M. (2017). Using the NDVI to identify variations in, and responses of, vegetation to climate change on the Tibetan Plateau from 1982 to 2012. *Quaternary International*, *444*, 87–96. https://doi.org/10.1016/j.quaint.2016.08.038

Pettorelli, N., Vik, J. O., Mysterud, A., Gaillard, J. M., Tucker, C. J., & Stenseth, N. C. (2005). Using the satellite-derived NDVI to assess ecological responses to environmental change. *Trends in Ecology and Evolution*. https://doi.org/10.1016/j.tree.2005.05.011

Rahman, M. S., & Di, L. (2017). The state of the art of spaceborne remote sensing in flood management. *Natural Hazards*, *85*(2), 1223–1248. https://doi.org/10.1007/s11069-016-2601-9

Ramakrishna, A., Chang, Y. H., & Maheswaran, R. (2013). An interactive web based spatio-temporal visualization system. *Lecture Notes in Computer Science (Including Subseries Lecture Notes in Artificial Intelligence and Lecture Notes in Bioinformatics)*. https://doi.org/10.1007/978-3-642-41939-3_66

Raziq, A., Xu, A., & Li, Y. (2016). Monitoring of Land Use/Land Cover Changes and Urban Sprawl in Peshawar City in Khyber Pakhtunkhwa: An Application of Geo- Information Techniques Using of Multi-Temporal Satellite Data. *Journal of Remote Sensing & GIS*, *05*(04). https://doi.org/10.4172/2469-4134.1000174

Reddy, D. S., & Prasad, P. R. C. (2018). Prediction of vegetation dynamics using NDVI time series data and LSTM. *Modeling Earth Systems and Environment*, *4*(1), 409–419. https://doi.org/10.1007/s40808-018-0431-3

Rees, M., Condit, R., Crawley, M., Pacala, S., & Tilman, D. (2001). Long-term studies of vegetation dynamics. *Science*. https://doi.org/10.1126/science.1062586

Richardson, A. J., & Wiegand, C. L. (1977). Distinguishing vegetation from soil background information. *Photogrammetric Engineering and Remote Sensing*.

Rimal, B. (2011). Application of remote sensing and gis, land use/land cover change in Kathmandu Metropolitan City, Nepal. *Journal of Theoretical and Applied Information Technology*.

Robinson, D. A., Campbell, C. S., Hopmans, J. W., Hornbuckle, B. K., Jones, S. B., Knight, R., … Wendroth, O. (2008). Soil Moisture Measurement for Ecological and Hydrological Watershed-Scale Observatories: A Review. *Vadose Zone Journal*. https://doi.org/10.2136/vzj2007.0143

Rodriguez-Iturbe, I. (2000). Ecohydrology: A hydrologic perspective of climate-soil-vegetation dynamics. *Water Resources Research*. https://doi.org/10.1029/1999WR900210

Roth, R. E. (2011). Interacting With Maps : the Science and Practice of Cartographic Interaction. *Cartography*.

Roy, D. P. (1997). Investigation of the maximum Normalized Difference Vegetation Index (NDVI) and the maximum surface temperature (Ts) AVHRR compositing procedures for the extraction of NDVI and Ts over forest. *International Journal of Remote Sensing*. https://doi.org/10.1080/014311697217675

Roy, D. P., & Yan, L. (2020). Robust Landsat-based crop time series modelling. *Remote Sensing of Environment*, *238*(March), 0–1. https://doi.org/10.1016/j.rse.2018.06.038

Running, S., Mu, Q., Zhao, M. (2017). *No Title*. Retrieved from lpdaac.usgs.gov/products/mod16a2v006/#citation

Saatchi, S., Asefi-Najafabady, S., Malhi, Y., Aragão, L. E. O. C., Anderson, L. O., Myneni, R. B., & Nemani, R. (2013). Persistent effects of a severe drought on Amazonian forest canopy. *Proceedings of the National Academy of Sciences of the United States of America*. https://doi.org/10.1073/pnas.1204651110

Scheepens, R., Willems, N., Van De Wetering, H., Andrienko, G., Andrienko, N., & Van Wijk, J. J. (2011). Composite density maps for multivariate trajectories. *IEEE Transactions on Visualization and Computer Graphics*. https://doi.org/10.1109/TVCG.2011.181

Schucknecht, A., Erasmi, S., Niemeyer, I., & Matschullat, J. (2013). Assessing vegetation variability and trends in north-eastern Brazil using AVHRR and MODIS NDVI time series. *European Journal of Remote Sensing*, *46*(1), 40–59.

https://doi.org/10.5721/EuJRS20134603

Schurman, J. S., Trotsiuk, V., Bače, R., Čada, V., Fraver, S., Janda, P., … Svoboda, M. (2018). Large-scale disturbance legacies and the climate sensitivity of primary Picea abies forests. *Global Change Biology*. https://doi.org/10.1111/gcb.14041

Sharma, I., Ueranantasun, A., Tongkumchum, P., Campus, P., & Rd, C. (2018). *Jurnal Teknologi M ODELING OF SATELLITE DATA TO IDENTIFY THE S EASONAL PATTERNS AND TRENDS OF VEGETATION INDEX IN K ATHMANDU V ALLEY , N EPAL FROM 2000 TO 2015*. *4*, 125–133.

Siddig, K., Stepanyan, D., Wiebelt, M., Grethe, H., & Zhu, T. (2020). Climate change and agriculture in the Sudan: Impact pathways beyond changes in mean rainfall and temperature. *Ecological Economics*, *169*(October 2018), 106566. https://doi.org/10.1016/j.ecolecon.2019.106566

Solomon, S., D., Qin, M., Manning, Z., Chen, M., Marquis, K. B., Averyt, M. T., … Miller, H. L. (2007). Summary for Policymakers. In: Climate Change 2007: The Physical Science Basis. Contribution of Working Group I to the Fourth Assessment Report of the Intergovernmental Panel on Climate Change. *D Qin M Manning Z Chen M Marquis K Averyt M Tignor and HL Miller New York Cambridge University Press Pp*. https://doi.org/10.1038/446727a

Song, J., Wesely, M. L., Coulter, R. L., & Brandes, E. A. (2000). Estimating watershed evapotranspiration with PASS. Part I: Inferring root-zone moisture conditions using satellite data. *Journal of Hydrometeorology*. https://doi.org/10.1175/1525-7541(2000)001<0447:EWEWPP>2.0.CO;2

Spalding, A. K. (2017). Exploring the evolution of land tenure and land use change in Panama: Linking land policy with development outcomes. *Land Use Policy*. https://doi.org/10.1016/j.landusepol.2016.11.023

Sun, G., Liu, Y., Wu, W., Liang, R., & Qu, H. (2014). Embedding temporal display into maps for occlusion-free visualization of spatio-Temporal data. *IEEE Pacific Visualization Symposium*, 185–192. https://doi.org/10.1109/PacificVis.2014.56

Suzuki, R., Masuda, K., & G. Dye, D. (2007). Interannual covariability between actual evapotranspiration and PAL and GIMMS NDVIs of northern Asia. *Remote Sensing of Environment*. https://doi.org/10.1016/j.rse.2006.10.016

Szpakowski, D. M., & Jensen, J. L. R. (2019). A review of the applications of remote sensing in fire ecology. *Remote Sensing*, *11*(22). https://doi.org/10.3390/rs11222638

Tominski, C., Abello, J., & Schumann, H. (2004). Axes-based visualizations with radial layouts. *Proceedings of the ACM Symposium on Applied Computing*.

https://doi.org/10.1145/967900.968153

Tominski, C., Schulze-Wollgast, P., & Schumann, H. (2005). 3D information visualization for time dependent data on maps. *Proceedings of the International Conference on Information Visualisation*. https://doi.org/10.1109/IV.2005.3

Townshend, J., Justice, C., Li, W., Gurney, C., & McManus, J. (1991). Global land cover classification by remote sensing: present capabilities and future possibilities. *Remote Sensing of Environment*. https://doi.org/10.1016/0034-4257(91)90016-Y

USTIN, S. L., ROBERTS, D. A., GAMON, J. A., ASNER, G. P., & GREEN, R. O. (2004). Using Imaging Spectroscopy to Study Ecosystem Processes and Properties. *BioScience*. https://doi.org/10.1641/0006-3568(2004)054[0523:uistse]2.0.co;2

Van Wijk, J. J. (2002). Image based flow visualization. *Proceedings of the 29th Annual Conference on Computer Graphics and Interactive Techniques, SIGGRAPH '02*. https://doi.org/10.1145/566570.566646

Vargas, L., Willemen, L., & Hein, L. (2019). Assessing the Capacity of Ecosystems to Supply Ecosystem Services Using Remote Sensing and An Ecosystem Accounting Approach. *Environmental Management*, *63*(1), 1–15. https://doi.org/10.1007/s00267-018-1110-x

Viña, A., Gitelson, A. A., Nguy-Robertson, A. L., & Peng, Y. (2011). Comparison of different vegetation indices for the remote assessment of green leaf area index of crops. *Remote Sensing of Environment*. https://doi.org/10.1016/j.rse.2011.08.010

Von Buttlar, J., Zscheischler, J., Rammig, A., Sippel, S., Reichstein, M., Knohl, A., … Mahecha, M. D. (2018). Impacts of droughts and extreme-temperature events on gross primary production and ecosystem respiration: A systematic assessment across ecosystems and climate zones. *Biogeosciences*. https://doi.org/10.5194/bg-15-1293-2018

Wang, R., Gamon, J. A., Emmerton, C. A., Springer, K. R., Yu, R., & Hmimina, G. (2020). Agricultural and Forest Meteorology Detecting intra- and inter-annual variability in gross primary productivity of a North American grassland using MODIS MAIAC data. *Agricultural and Forest Meteorology*, *281*(November 2019), 107859. https://doi.org/10.1016/j.agrformet.2019.107859

Wang, W. B., Huang, M. L., Nguyen, Q. V., Huang, W., Zhang, K., & Huang, T. H. (2016). Enabling decision trend analysis with interactive scatter plot matrices visualization. *Journal of Visual Languages and Computing*, *33*, 13–23. https://doi.org/10.1016/j.jvlc.2015.11.002

Wang, X., Xie, H., Guan, H., & Zhou, X. (2007). Different responses of MODIS-derived NDVI to root-zone soil moisture in semi-arid and humid regions. *Journal of Hydrology*.

https://doi.org/10.1016/j.jhydrol.2007.03.022

Wang, Yunhai, Han, F., Zhu, L., Deussen, O., & Chen, B. (2018). Line Graph or Scatter Plot? Automatic Selection of Methods for Visualizing Trends in Time Series. *IEEE Transactions on Visualization and Computer Graphics*, *24*(2), 1141–1154. https://doi.org/10.1109/TVCG.2017.2653106

Wang, Yunzhe, Baciu, G., & Li, C. (2019). Visualizing Dynamics of Urban Regions Through a Geo-Semantic Graph-Based Method. *Computer Graphics Forum*, *00*(00). https://doi.org/10.1111/cgf.13882

Weng, Q. (2001). A remote sensing?GIS evaluation of urban expansion and its impact on surface temperature in the Zhujiang Delta, China. *International Journal of Remote Sensing*. https://doi.org/10.1080/713860788

West, H., Quinn, N., & Horswell, M. (2019). Remote sensing for drought monitoring & impact assessment: Progress, past challenges and future opportunities. *Remote Sensing of Environment*, *232*(June), 111291. https://doi.org/10.1016/j.rse.2019.111291

Wheeler, K. I., & Dietze, M. C. (2019). *A Statistical Model for Estimating Midday NDVI from the Geostationary Operational Environmental Satellite (GOES) 16 and 17*. *17*.

Wilson, B. T., Knight, J. F., & McRoberts, R. E. (2018). Harmonic regression of Landsat time series for modeling attributes from national forest inventory data. *ISPRS Journal of Photogrammetry and Remote Sensing*, *137*, 29–46. https://doi.org/10.1016/j.isprsjprs.2018.01.006

Wu, D., Zhao, X., Liang, S., Zhou, T., Huang, K., Tang, B., & Zhao, W. (2015). Time-lag effects of global vegetation responses to climate change. *Global Change Biology*. https://doi.org/10.1111/gcb.12945

Wu, T., Fu, H., Feng, F., & Bai, H. (2019). A new approach to predict normalized difference vegetation index using time-delay neural network in the arid and semi-arid grassland. *International Journal of Remote Sensing*, *40*(23), 9050–9063. https://doi.org/10.1080/01431161.2019.1624870

Xiang, J., Song, X., & Li, J. (2019). Cropland use transitions and their driving factors in poverty-stricken counties of Western Hubei Province, China. *Sustainability (Switzerland)*. https://doi.org/10.3390/su11071997

Xiao, X., He, L., Salas, W., Li, C., Moore, I., Zhao, R., … Boles, S. (2002). Quantitative relationships between field-measured leaf area index and vegetation index derived from VEGETATION images for paddy rice fields. *International Journal of Remote Sensing*. https://doi.org/10.1080/01431160110115799

Xu, C., & Katchova, A. L. (2019). *Predicting Soybean Yield with NDVI Using a Flexible*

Fourier Transform Model. 402–416. https://doi.org/10.1017/aae.2019.5

Xu, T., Gao, J., & Li, Y. (2019). Machine learning-assisted evaluation of land use policies and plans in a rapidly urbanizing district in Chongqing, China. *Land Use Policy*. https://doi.org/10.1016/j.landusepol.2019.104030

Yan, L., He, R., Kašanin-Grubin, M., Luo, G., Peng, H., & Qiu, J. (2017). The dynamic change of vegetation cover and associated driving forces in nanxiong basin, China. *Sustainability (Switzerland)*. https://doi.org/10.3390/su9030443

Yang, Y., & Chen, T. (2019). Analysis and visualization implementation of medical big data resource sharing mechanism based on deep learning. *IEEE Access*, *7*, 156077–156088. https://doi.org/10.1109/ACCESS.2019.2949879

Yue, Y., Wang, K., Zhang, B., Chen, Z., Jiao, Q., Liu, B., & Chen, H. (2010). Exploring the relationship between vegetation spectra and eco-geo-environmental conditions in karst region, Southwest China. *Environmental Monitoring and Assessment*. https://doi.org/10.1007/s10661-008-0665-z

Zhai, H., Zhang, H., Zhang, L., & Li, P. (2018). ISPRS Journal of Photogrammetry and Remote Sensing Cloud / shadow detection based on spectral indices for multi / hyperspectral optical remote sensing imagery. *ISPRS Journal of Photogrammetry and Remote Sensing*, *144*(July), 235–253. https://doi.org/10.1016/j.isprsjprs.2018.07.006

Zhang, W., Brandt, M., Tong, X., Tian, Q., & Fensholt, R. (2017). Impacts of the seasonal distribution of rainfall on vegetation productivity across the Sahel. *Biogeosciences Discussions*, (August), 1–27. https://doi.org/10.5194/bg-2017-331

Zhao, L., Dai, A., & Dong, B. (2018). Changes in global vegetation activity and its driving factors during 1982–2013. *Agricultural and Forest Meteorology*, *249*(November), 198–209. https://doi.org/10.1016/j.agrformet.2017.11.013

Zhao, W., Zhao, X., Zhou, T., Wu, D., Tang, B., & Wei, H. (2017). Climatic factors driving vegetation declines in the 2005 and 2010 Amazon droughts. *PLoS ONE*, *12*(4), 1–19. https://doi.org/10.1371/journal.pone.0175379

Zhou, J., Jia, L., & Menenti, M. (2015). Reconstruction of global MODIS NDVI time series: Performance of Harmonic ANalysis of Time Series (HANTS). *Remote Sensing of Environment*, *163*, 217–228. https://doi.org/10.1016/j.rse.2015.03.018

Zhu, Z. (2017). ISPRS Journal of Photogrammetry and Remote Sensing Change detection using landsat time series : A review of frequencies , preprocessing , algorithms , and applications. *ISPRS Journal of Photogrammetry and Remote Sensing*, *130*, 370–384. https://doi.org/10.1016/j.isprsjprs.2017.06.013